MAP2008-1

GEOSCIENTIFIC MAP

Geology of the Bird River Belt, southeastern Manitoba (parts of NTS 52L5, 6)

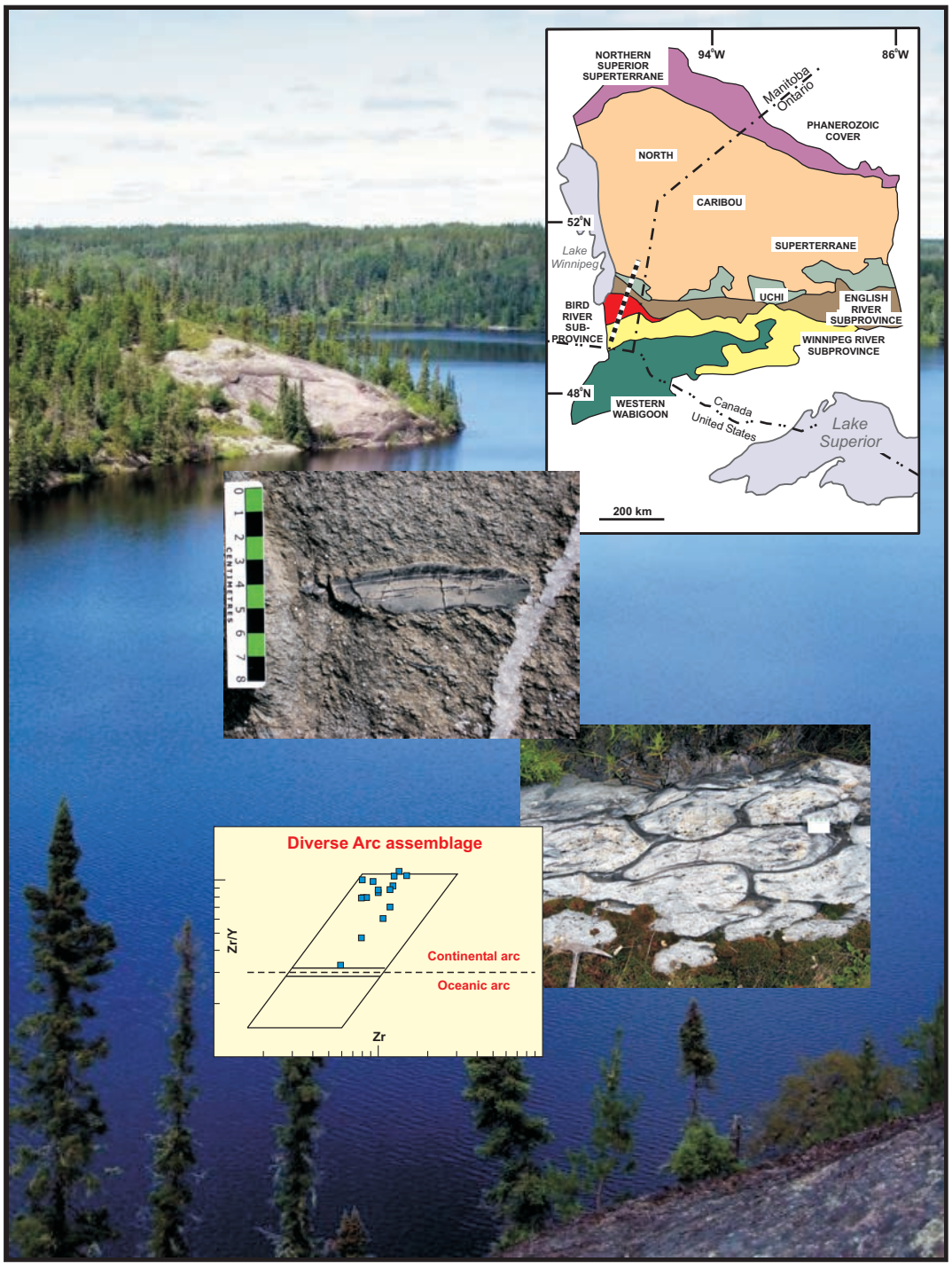

By
H.P. Gilbert, D.W. Davis, M. Duguet,
P.D. Kremer, C.A. Mealin and J. MacDonald

Manitoba

Geoscientific Map MAP2008-1

Geology of the Bird River Belt, southeastern Manitoba (parts of NTS 52L5, 6)

by H.P. Gilbert, D.W. Davis, M. Duguet, P.D. Kremer, C.A. Mealin and J. MacDonald

Winnipeg, 2008

Science, Technology, Energy and Mines

Hon. Jim Rondeau
Minister

John Clarkson
Deputy Minister

Mineral Resources Division

John Fox
Assistant Deputy Minister

Manitoba Geological Survey

E.C. Syme
Director

When using information from this publication in other publications or presentations, due acknowledgment should be given to the Manitoba Geological Survey. The following reference format is recommended:

Gilbert, H.P., Davis, D.W., Duguet, M., Kremer, P.D., Mealin, C.A. and MacDonald, J. 2008: Geology of the Bird River Belt, southeastern Manitoba (parts of NTS 52L5, 6); Manitoba Science, Technology, Energy and Mines, Manitoba Geological Survey, Geoscientific Map MAP2008-1, scale 1:50 000 (plus notes and appendix).

NTS grid: NTS 52L5, 6

Keywords: Manitoba; Bird River Belt; Neoarchean; calc-alkalic composition; tholeiite; back-arc basins; platinum-group elements; rare elements; pegmatite; continental arcs

External author addresses:

D.W. Davis
Department of Geology
University of Toronto
Toronto, ON M5S 3B1
416-946-0365
dond@geology.utoronto.ca

M. Duguet
Ontario Geological Survey
933 Ramsey Lake Road
Sudbury, ON P3E 6B5
705-670-5755
Manuel.Duguet@ontario.ca

C.A. Mealin
Marathon PGM Corporation
330 Bay Street, Suite 1505
Toronto, ON M5H 2S8
705-772-8867
camealin@yahoo.ca

J. MacDonald
Dept. of Earth and Environmental Sciences
University of Waterloo
Waterloo, ON N2L 3G1
519-888-4567
j8macdon@sciborg.uwaterloo.ca

Published by:
Manitoba Science, Technology, Energy and Mines
Manitoba Geological Survey
360-1395 Ellice Avenue
Winnipeg, Manitoba
R3G 3P2 Canada
Telephone: (800) 223-5215 (General Enquiry)
(204) 945-4154 (Publication Sales)
Fax: (204) 945-8427
E-mail: minesinfo@gov.mb.ca
Website: manitoba.ca/minerals

This publication is available to download free of charge at Manitoba.ca/minerals.

Cover photo: The Bird River Belt, located in the southwestern Superior Province, contains Neoarchean supracrustal rocks of continental arc affinity. Diverse volcanic and sedimentary rocks, commonly redeposited as mass flows, are intercalated with extrusive rocks that are locally pillowed and silicified. The landscape view overlooks a granitoid terrane immediately north of the greenstone belt.

Abstract

The Neoarchean Bird River Belt (BRB) in the Bird River Subprovince (southwestern Superior Province) occurs in a transitional oceanic–continental-margin setting between flanking older cratonic blocks — the North Caribou Superterrane to the north and the Winnipeg River Subprovince to the south. The predominant arc-type rocks of the BRB are tectonically distinct from flanking, mid-ocean-ridge basalt (MORB)–type basaltic sequences that may represent a back-arc setting, possibly associated with early arc rifting. The continental-arc magmatism spanned approximately 80 Ma (2.80–2.72 Ga). Two geochemically distinct arc-type sequences are recognized (north and south panels, respectively). The north panel is akin to modern subduction-related rocks at active continental margins, whereas the south panel documents incipient rifting in an extensional tectonic regime. Subsequent to arc volcanism, orogenic sedimentation (2.71–2.70 Ga) resulted in the deposition of turbidites (Booster Lake Formation) and fluvial-alluvial deposits (Flanders Lake Formation). These orogenic sedimentary rocks may be stratigraphically equivalent to epiclastic rocks and metamorphic derivatives in the English River Subprovince, northeast of the BRB.

Early deformation is characterized by northward low-angle thrusting of older formations over relatively younger rocks along the south side of the greenstone belt, whereas subsequent transpressive deformation occurred along steeper faults. Associated metamorphism up to amphibolite-facies grade was followed by greenschist-facies retrogression.

Base-metal mineralization prospects in the BRB include both magmatic types and stratigraphically associated occurrences. The Bird River Sill hosts base-metal and platinum-group-element (PGE) mineralization; elsewhere, base-metal mineralization commonly occurs at lithological contacts within the volcano-sedimentary sequences. The BRB also hosts the TANCO mine at Bernic Lake, wholly owned by the Cabot Corporation. The mine produces Ta, Li and Cs from pegmatite and accounts for approximately 80% of global reserves of Cs.

TABLE OF CONTENTS

Page

ACCOMPANYING NOTES

TABLES

FIGURES

APPENDIX

Introduction

The Neoarchean Bird River Belt (BRB) in southeastern Manitoba is host to both base-metal (Maskwa-Dumbarton mine) and rare-element-bearing pegmatite (TANCO mine) ore deposits, and is currently the focus of several mineral exploration projects. The Manitoba Geological Survey (MGS) initiated a collaborative mapping project in 2005 because the existing geological maps (1952–1981) of the BRB were outdated and of limited value to exploration companies for planning new programs. Concurrent with detailed stratigraphic mapping and geochemical investigations by H.P. Gilbert, post-graduate projects at the University of Waterloo include 1) a post-doctoral research project on the tectonic setting and structural-metamorphic history of the Bird River area by M. Duguet; and 2) M.Sc. studies of the setting of rare-element-bearing pegmatite bodies (P.D. Kremer) and the geology of the PGE-bearing Bird River Sill (C.A. Mealin). Geochronological data have been obtained for key geological units by C. Böhm in collaboration with A. Simonetti (University of Alberta), and by D.W. Davis (University of Toronto). These age data, together with the geochemical, tectonic and metamorphic studies, have led to reappraisals of the stratigraphy, structure and regional setting of the BRB.

New U-Pb age data for 10 volcanic and plutonic rock types, summarized in Table 1, are the result of work carried out by D.W. Davis at the Jack Satterly Geochronology Laboratory (University of Toronto), in collaboration with the University of Waterloo, between 2006 and 2008. A comprehensive description of the U-Pb geochronological data, including methods, interpretation and concordia plots, is provided in the Appendix.

Table 1: Summary of U-Pb geochronology results for 10 igneous rocks from the Bird River Belt (Jack Satterly Geochronology Laboratory, University of Toronto).

	Sample	UTM (NAD 83) easting/northing	Rock type	Mineral	No. of analyses	No. in age[1]	Age (Ma)	Error (Ma; 95%)	Fit	Method	Interpretation
1	MD05-222B	0317997/5590573	Rhyolite, Peterson Creek Formation	zircon	3	3	2731.1	1	84%	ID-TIMS (Ab)	volcanism
2	MD05-1081	0328562/5589555	Dacite, Bernic Lake Formation	zircon	3	3	2724.6	1.1	33%	ID-TIMS (Ab)	volcanism
3	LIN06-2356	0347025/5591840	Marijane Lake pluton (granodiorite)	monazite	5	4	2645.6	1.3	27%	ID-TIMS (Ab)	pluton emplacement
4	MD07-2622	0328697/5606528	Maskwa Lake batholith (tonalite)	zircon	6	2	2852.8	1.1	46%	ID-TIMS (CA)	pluton emplacement
				apatite	1	1	2652	2	--	ID-TIMS	thermal closure, ~500°C
5	MD06-2598	0324844/5597449	Maskwa Lake batholith (granodiorite)	zircon	6	5	2832.3	0.9	44%	ID-TIMS (Ab)	pluton emplacement
6	PK06-1250	0327146/5587712	Birse Lake pluton (granodiorite); 0327146/5587712	zircon	4	4	2723.2	0.7	48%	ID-TIMS (Ab)	pluton emplacement
7	PK06-1197	0325002/5589349	Gabbro pegmatite	zircon	3	3	2723.1	0.8	81%	ID-TIMS (Ab)	pluton emplacement
8	MD07-2679	0329786/5616191	Syn-shear granite	zircon	2	2	2714	13	--	ID-TIMS (CA, Ab)	upper age limit on pluton emplacement
				monazite	7	3	2684.3	0.8	81%	ID-TIMS	lower age limit on pluton emplacement
9	PK05-1050	0330443/5588432	Granitoid pegmatite, shear-zone hosted	columbite	3	2	columbite results combined with PK06-1251 below				
				zircon	3	1	2650.7	0.2	--	TE-TIMS	pluton emplacement
				cassiterite	1	1	2999	9	--	TE-TIMS	inheritance
10	PK06-1251	0325807/5590495	Granitoid pegmatite, post-shear	columbite	6	3	2647.4	1.0	34%	ID-TIMS	pluton emplacement

[1] number of analyses used in age determination

Abbreviations: Ab, abraded; CA, chemical abrasion; ID-TIMS, isotope dilution–thermal ionization mass spectrometry; TE-TIMS, thermal extraction–thermal ionization mass spectrometry

Geoscientific Map MAP2008-1 at 1:50 000 scale is a compilation of 1:20 000 scale mapping by the authors (Gilbert, 2006a, 2007a, b; Duguet et al., 2006, 2007; Kremer and Lin, 2006; Mealin, 2006) and incorporates previously published data in some peripheral parts of the map area (Černý et al., 1981).

Regional setting

The Bird River Belt (BRB), located in the southern part of the Bird River Subprovince, is part of an east-trending supracrustal belt that extends for 150 km from Lac du Bonnet in the west to Separation Lake (Ontario) in the east (Figure 1). The northern part of the Bird River Subprovince consists of a granitoid terrane (Maskwa Lake Batholith) that contains intrusive phases ranging from 2.85 to 2.73 Ga (Table 2). The BRB occurs in a transitional oceanic–continental-margin setting between flanking older cratonic blocks — the North Caribou Superterrane to the north and the Winnipeg River Subprovince to the south. Continental-arc magmatism and orogenic sedimentation in the Bird River Subprovince spanned approximately 100 Ma (2.80–2.70 Ga; Percival et al., 2006a). In contrast, a protracted 300 Ma history of similar magmatism and sedimentation has been documented in the Uchi Subprovince to the north (Figure 1), beginning with ca. 3.0 Ga rifting associated with northward subduction of oceanic lithosphere at the southern margin of the North Caribou Superterrane (Percival et al., 2006a). Early (>2.87 Ga) supracrustal assemblages in the Uchi Subprovince (e.g., Lewis-Storey, Wallace, Garner Lake) have no known counterparts in the Bird River Subprovince. Possible correlations may be made, however, among the younger supracrustal sequences of the two subprovinces: for example, the >2722 Ma (Davis, 1994) Gem assemblage in the Rice Lake greenstone belt of the Uchi Subprovince (Anderson, 2005) and the 2724.6 ±1.1 Ma Bernic Lake Formation in the Bird River Subprovince (Table 2). Volcanic rocks in the Gem assemblage and Bernic Lake Formation are geochemically similar and appear to document incipient rifting of the continental-arc sequences.

Orogenic sedimentation (2713–2704 Ma) subsequent to continental-arc volcanism resulted in deposition of turbidites in both the BRB (Booster Lake Formation) and the Rice Lake greenstone belt (Edmunds assemblage; Anderson, 2005) to the north. The turbidites are penecontemporaneous with fluvial-alluvial deposits (Flanders Lake Formation in the BRB, Table 2; San Antonio Formation in the Rice Lake belt) that are possibly stratigraphically equivalent to the contiguous, but more distal, turbidite strata (Booster Lake Formation and Edmunds assemblage, respectively; Anderson, 2005). The orogenic sedimentary rocks have been widely assumed to be stratigraphically equivalent to epiclastic rocks and metamorphic derivatives in the west- to northwest-trending English River Subprovince, which lies between the Uchi and Bird River subprovinces (Figure 1; Anderson, 2005; Hrabi and Cruden, 2006; Nitescu et al., 2006). The turbidite sequences are invariably fault bounded except in the Rice Lake belt, where the turbidites locally rest unconformably on older volcanic strata. Regional deformation, metamorphism and granitoid plutonism postdated the orogenic sedimentation; five generations of deformation have been documented as postdating this sedimentation within the Rice Lake greenstone belt in the western part of the Uchi Subprovince (Anderson, 2003, 2004). Orogenic sedimentation, subsequent magmatism and deformation mark the end of subduction-related volcanic activity, due to collision of the

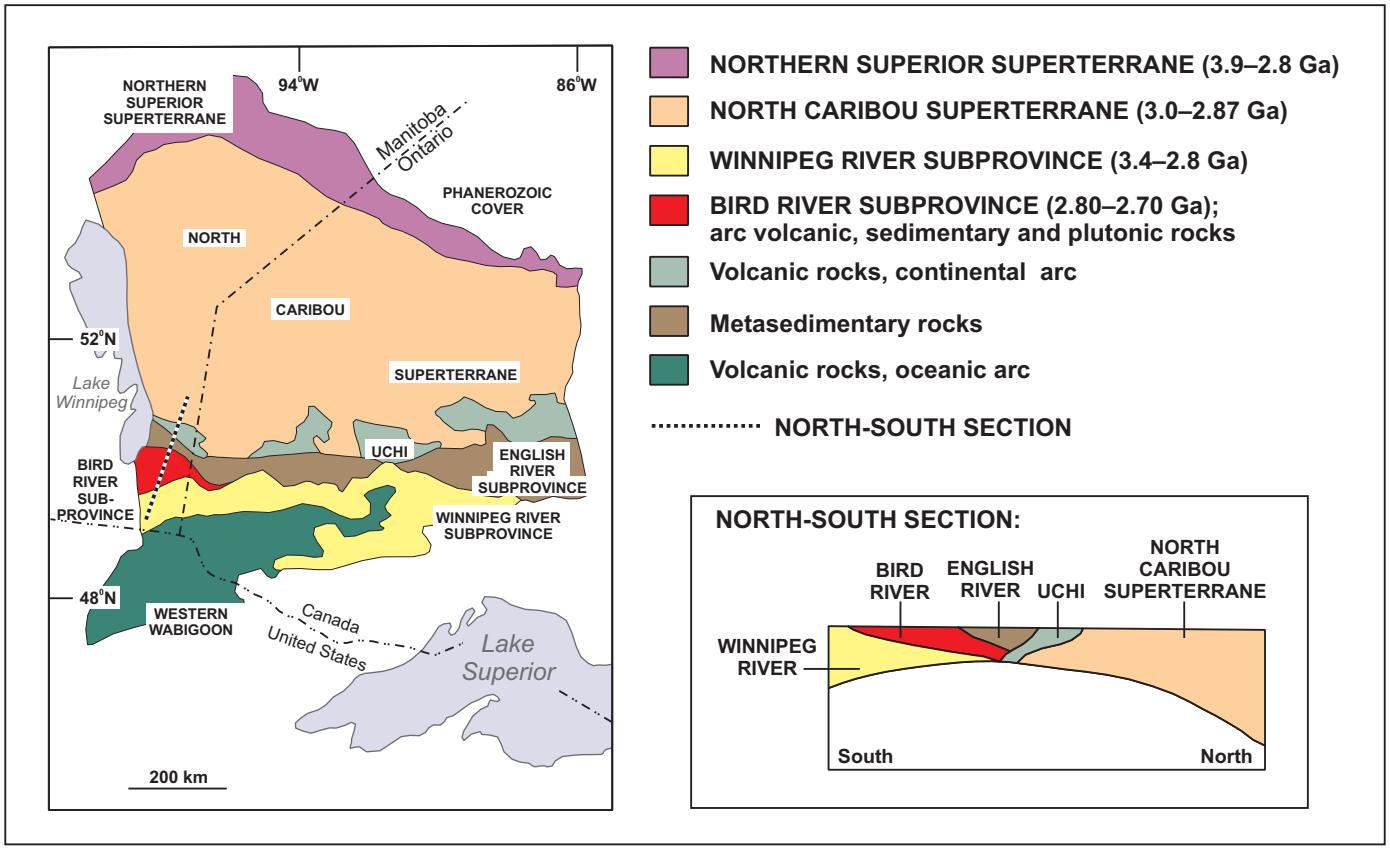

Figure 1: *Geology of the western Superior Province, showing the location of the Bird River Subprovince.*

Table 2: Geological formations, Bird River Belt.

Late intrusive rocks
Granite, pegmatite, granodiorite, tonalite, quartz diorite
(TANCO pegmatite, **2640 ±7 Ma**[1]; Marijane Lake pluton, **2645.6 ±1.3 Ma**; Lac du Bonnet Batholith, **2660 ±3**[2] **Ma**
Sedimentary rocks
FLANDERS LAKE FORMATION **(2697 ±18 Ma3**[3]**)**
Lithic arenite, polymictic conglomerate
========== ***Fault, inferred*** ==========
BOOSTER LAKE FORMATION **(2712 ±17 Ma**[3]**)**
Greywacke-siltstone turbidite, conglomerate
~~ ***Unconformity, inferred*** ~~~~~~~~~~
Intrusive rocks
MISCELLANEOUS INTRUSIONS
Gabbro, diorite, quartz-feldspar porphyry; granodiorite
(Birse Lake pluton, **2723.2 ±0.7 Ma**; Maskwa Lake Batholith II, **2725 ±6 Ma**[2]; Pointe du Bois Batholith, **2729 ±8.7 Ma2**[2])
(TANCO gabbro, **2723.1 ±0.8 Ma**)
Metavolcanic and metasedimentary rocks
BERNIC LAKE FORMATION **(2724.6 ±1.1 Ma)**
Basalt, andesite, dacite and rhyolite (massive to fragmental); related intrusive rocks and heterolithic volcanic fragmental rocks
PETERSON CREEK FORMATION **(2731.1 ±1 Ma)**
Dacite, rhyolite (massive to fragmental); felsic tuff and heterolithic felsic volcanic fragmental rocks
DIVERSE ARC ASSEMBLAGE **(2706 ±23 Ma**[4]**)**
Basalt, andesite, rhyolite, related fragmental and intrusive rocks; heterolithic volcanic fragmental rocks; greywacke-siltstone turbidite, chert, iron-formation; polymictic conglomerate (contains clasts derived from Bird River Sill)
~~ ***Unconformity, inferred*** ~~~~~~~~~~
Intrusive rocks
BIRD RIVER SILL **(2744.7 ±5.2 Ma**[2]**)**
Dunite, peridotite, picrite, anorthosite and gabbro
========== ***Fault, inferred*** ==========
Metavolcanic and metasedimentary rocks
MORB-type VOLCANIC ROCKS
Basalt (aphyric to plagioclase-phyric; locally pillowed, amygdaloidal or megacrystic); related volcanic breccia; oxide-facies iron formation
========== ***Fault, inferred*** ==========
EAGLENEST LAKE FORMATION
Greywacke-siltstone turbidite
Older intrusive rocks
Granodiorite, diorite (Maskwa Lake Batholith I, **2782 ±11 Ma**[2]**, 2852.8 ±1.1 Ma, 2844 ±12 Ma**[2])
References for geochronological data: [1] Baadsgaard and Černý, 1993; [2] Wang, 1993; [3] Gilbert, 2006; [4] Gilbert, unpublished data, 2007

Uchi continental-margin succession with the Winnipeg River Subprovince, which followed 2.72–2.71 Ga convergence of the North Caribou and Winnipeg River cratonic blocks (Lemkow et al., 2006). According to LITHOPROBE seismic-reflection data (Percival et al., 2006b), this collision appears to have resulted in underplating of the BRB by continental lithosphere at the margin of the Winnipeg River Subprovince (Figure 1).

Geology of the Bird River area

The Bird River Belt (BRB) extends more than 50 km from Lac du Bonnet in the west to Flanders Lake in the east (Figure 2). The greenstone belt consists mainly of ca. 2.73 Ga arc-type volcanic rocks divided into north and south panels by the relatively younger, turbiditic Booster Lake Formation (<2712 ±17 Ma; Gilbert, 2006b). Mid-ocean-ridge basalt (MORB)–type volcanic rocks (Lamprey Falls Formation of Černý et al., 1981) extend along both the northern and southern margins of the belt. The regional, east-trending synclinorial structural model for the BRB (Černý et al., 1981), which implies that the north and south panels are stratigraphically equivalent fold limbs, is discounted on the basis of new data that suggest these two components differ both in age and in geochemical composition. A corollary of this revision is that the MORB-type volcanic rocks (former Lamprey Falls Formation) that occur along both the northern and southern margins of the arc-type rocks, although lithologically and geochemically

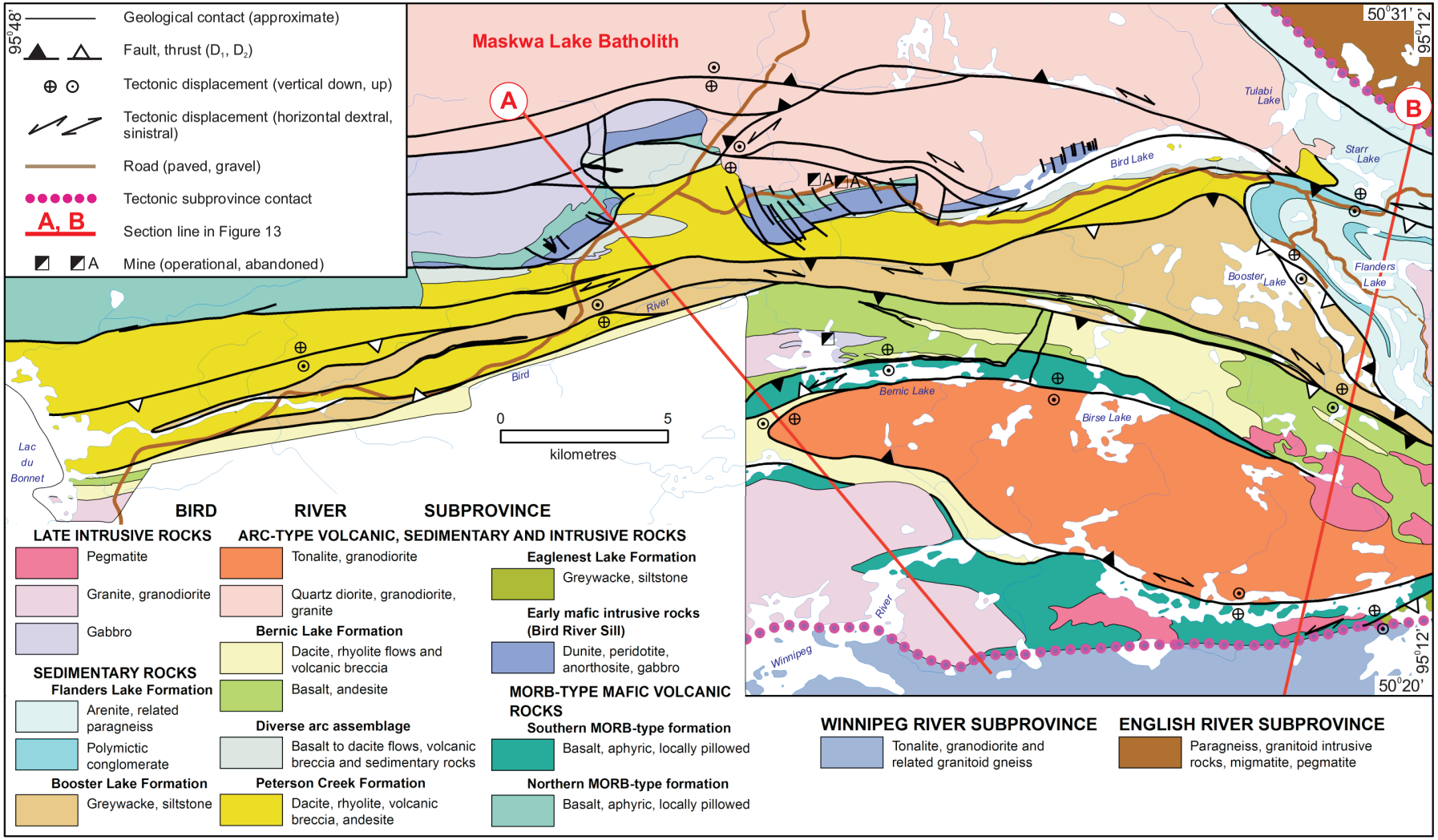

Figure 2: *Geology of the Bird River Belt, showing the main stratigraphic and structural features.*

similar, are unlikely to be parts of the same stratigraphic unit; hence, these basaltic formations are termed 'Northern MORB-type' and 'Southern MORB-type', respectively.

MORB-type formations

Northern MORB-type formation

The Northern MORB-type formation appears to be the oldest supracrustal component in the map area, because it is intruded by the 2745 Ma Bird River Sill (Wang, 1993). A maximum age of 2832.3 ±0.9 Ma (Table 1) may be inferred for the MORB volcanism, this being the intrusive age of a tonalitic phase in the granitoid Maskwa Lake Batholith that is cut by gabbro compositionally similar and possibly coeval with the Northern MORB-type formation. This formation is characterized by relatively juvenile ε_{Nd} values (+1.3 at 2.7 Ga), consistent with its interpreted origin as back-arc basin basalt derived from a primitive, depleted mantle source. Alternatively, the Northern MORB-type formation may represent remnant oceanic lithosphere, most of which was subducted northward at the margin of the North Caribou Superterrane prior to arc magmatism. The Northern MORB-type formation is flanked to the north by granitoid rocks of the Maskwa Lake Batholith (Figure 2). The oldest, 2852.8 ±1.1 Ma part of this multiphase batholith (Table 1) is interpreted to be a remnant of the North Caribou Superterrane that was detached from the main cratonic block and represents continental lithosphere at the site of subduction of oceanic crust. Younger granitoid phases in the same batholith are interpreted to be intrusive into the Northern MORB-type formation.

The 2–3 km wide Northern MORB-type formation is a south-facing, monoclinal sequence of pillowed basalt and extensive, synvolcanic gabbroic intrusions associated with localized base-metal sulphide mineralization (e.g., Coppermine zone; Marathon PGM Corporation, 2007). Basaltic flow-breccia and mafic tuff are subordinate components of the formation. Pillow basalt is generally aphyric (Figure 3a), but a unit of pillowed, plagioclase-megaphyric basalt (>70 m thick) occurs close to the upper (south) margin of the sequence (Figure 3b).

Northern MORB-type basalt exhibits a flat, slightly depleted rare-earth-element (REE) pattern (Figure 4a) except for moderately elevated Th content relative to N-MORB, suggesting that the source mantle magma was partly contaminated by subducted epiclastic detritus or material derived from continental crust (White and Dupré, 1986; Hawkesworth et al., 1994; Stern et al., 1995a). However, the low Zr/Y ratio of Northern MORB-type basalt (Table 3) indicates that it is not affiliated with modern continental-arc rocks, in contrast to the arc-type rocks in the BRB north and south panels (Figure 5a–e; Table 3). The flat REE profile with elevated Th is consistent with a back-arc basin environment of eruption for Northern MORB-type basalt (Sinton and Fryer, 1987; Saunders and Tarney, 1991; Stern et al., 1995b).

Southern MORB-type formation

The Southern MORB-type formation extends along the BRB southern margin in the Winnipeg River–Birse Lake area (Figure 2). These rocks are similar to the Northern MORB-type formation both geochemically and lithologically; aphyric pillowed basalt (Figure 3c) and related gabbro (Figure 3d) account for over 95% of the sequence, which also contains minor siltstone-chert formations (± base-metal sulphide mineralization). The Southern MORB-type formation is interpreted as derived from a juvenile mantle source associated with arc rifting, possibly penecontemporaneous with the onset of the crustal extension suggested for the 2724.6 ±1.1 Ma BRB south panel arc-type sequence (Table 1, Bernic Lake Formation; *see* 'South panel arc-type rocks' below). In this case, the Southern MORB-type rocks would be significantly younger than their northern (>2745 Ma) counterparts. The Birse Lake pluton (2723.2 ±0.7 Ma; Table 1) is emplaced within the Southern MORB-type formation and thus provides a minimum age of extrusion for the basaltic rocks.

The approximately 2.5 km wide Southern MORB-type sequence is predominantly north facing, except for a syncline-anticline fold pair delineated by pillow tops close to the upper (northern) margin of the sequence at the Winnipeg River (Geoscientific Map MAP2008-1). A 65 m wide zone that contains a chert-magnetite iron formation, associated with base-metal sulphide mineralization and alteration, occurs within the basaltic sequence on the south shore of the Winnipeg River (Gilbert, 2006b). Minor (<30 m wide) felsic volcanic units that occur close to the northern margin of the MORB-type sequence at Bernic Lake are interpreted as structural outliers of the Bernic Lake Formation, rather than stratigraphic components within the Southern MORB-type Formation. Southern MORB-type basalt, like its northern counterpart, exhibits a flat, slightly depleted REE pattern relative to N-MORB, with moderately elevated Th content, consistent with a back-arc basin environment of eruption (Figure 4b).

North panel arc-type rocks

The north panel of arc-type rocks consists largely (>75%) of massive and fragmental, intermediate to felsic volcanic rocks of calcalkaline geochemical affinity, associated with subordinate basaltic flows and epiclastic deposits. The abundance of dacite and rhyolite, and various geochemical trace-element indices in the north panel rocks indicate that they have a continental-arc affinity and correlate well with modern arc-type rocks in an 'active continental-margin' (ACM) setting (Figure 6a, b). The ε_{Nd} values (+1.0 to –1.1 at 2.7 Ga) indicate that a limited amount of recycled continental lithosphere was incorporated into the mantle source magma. The incompatible element profiles of north panel rocks (Peterson Creek Formation and Diverse Arc assemblage) also suggest that the mantle source was modified by subduction-zone processes (Figure 4c, d). An interval of at least 14 Ma separated arc volcanism (2731.1 ±1 Ma; Table 1, Peterson Creek Formation) from the cessation of MORB-type extrusion that occurred prior to the emplacement of the Bird River Sill (2744.7 ±5.2 Ma; Wang, 1993).

North panel arc-type rocks are subdivided into the almost exclusively volcanic Peterson Creek Formation and the volcano-sedimentary Diverse Arc assemblage (Gilbert, 2007c). The latter includes a wide variety of mafic to felsic volcanic rocks, reworked volcanic fragmental deposits, epiclastic detritus, sporadic chert and iron formation. The relative age relationship between the Peterson Creek Formation and Diverse Arc

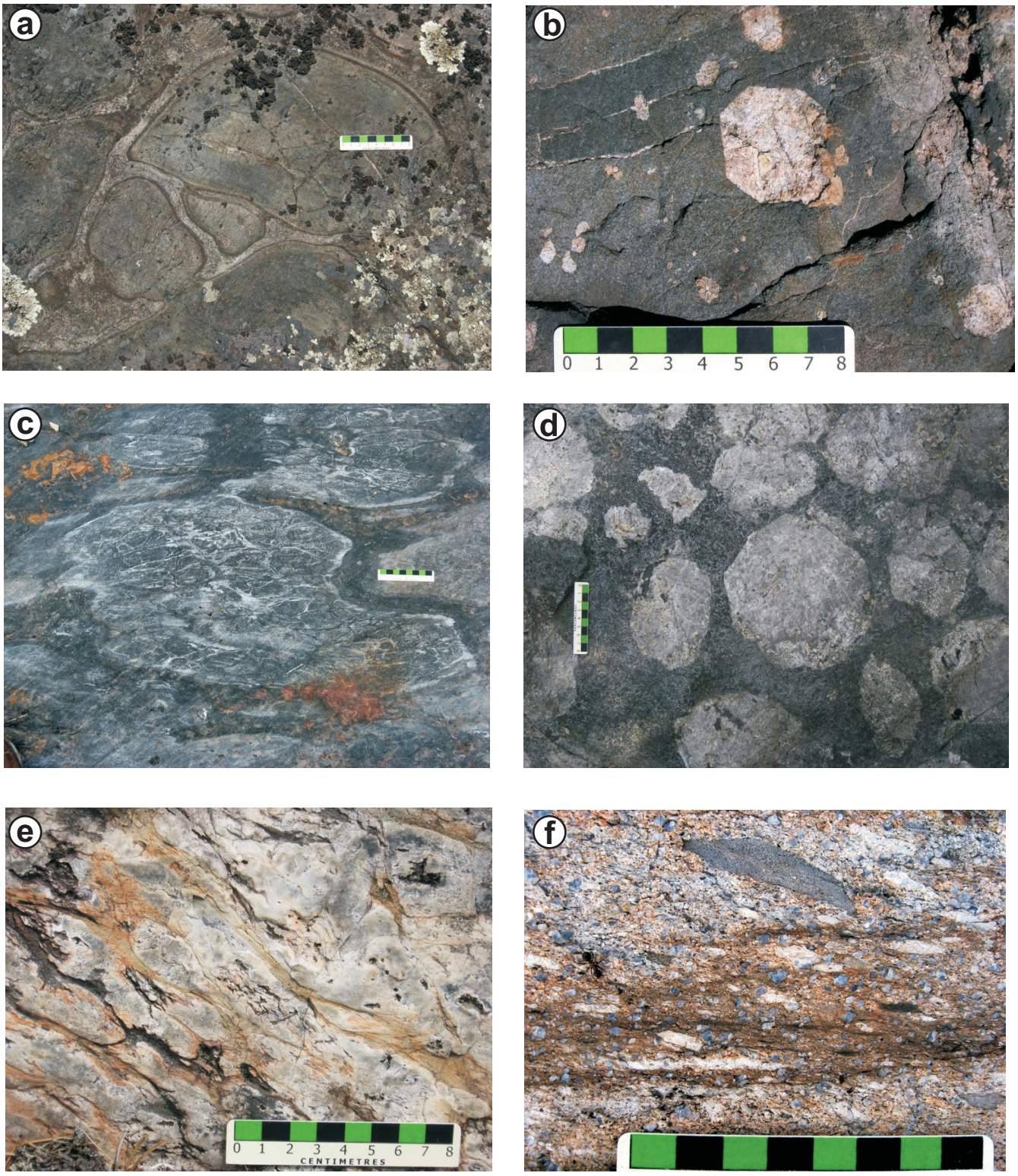

Figure 3: *Outcrop photographs of massive and fragmental volcanic rocks in the north and south panels of the Bird River Belt:* ***a)*** *aphyric pillowed basalt with interpillow hyaloclastite, Northern MORB-type basalt (UTM 318769E, 5593392N)[1]; **b)** plagioclase-megaphyric pillowed basalt, Northern MORB-type basalt (UTM 318638E, 5593286N); **c)** polygonal metasomatic alteration pattern in pillowed basalt, Southern MORB-type basalt (UTM 333091E, 5582191N); **d)** megaphyric 'football' gabbro within Southern MORB-type basalt, interpreted as synvolcanic (UTM 325864E, 5587933N); known at only a single locality, this megaphyric unit contrasts with typically aphyric gabbro sills interlayered with Southern MORB-type basalt elsewhere; **e)** anastomosing fractures attributed to thermal contraction during cooling of a massive rhyolite flow, Peterson Creek Formation (UTM 321639E, 5593256N); **f)** heterolithic crystal-lithic tuff with mainly felsic clast types, Peterson Creek Formation (UTM 309003E, 5587634N).*

[1] All UTM co-ordinates in this report are are Zone 15 (NAD 83).

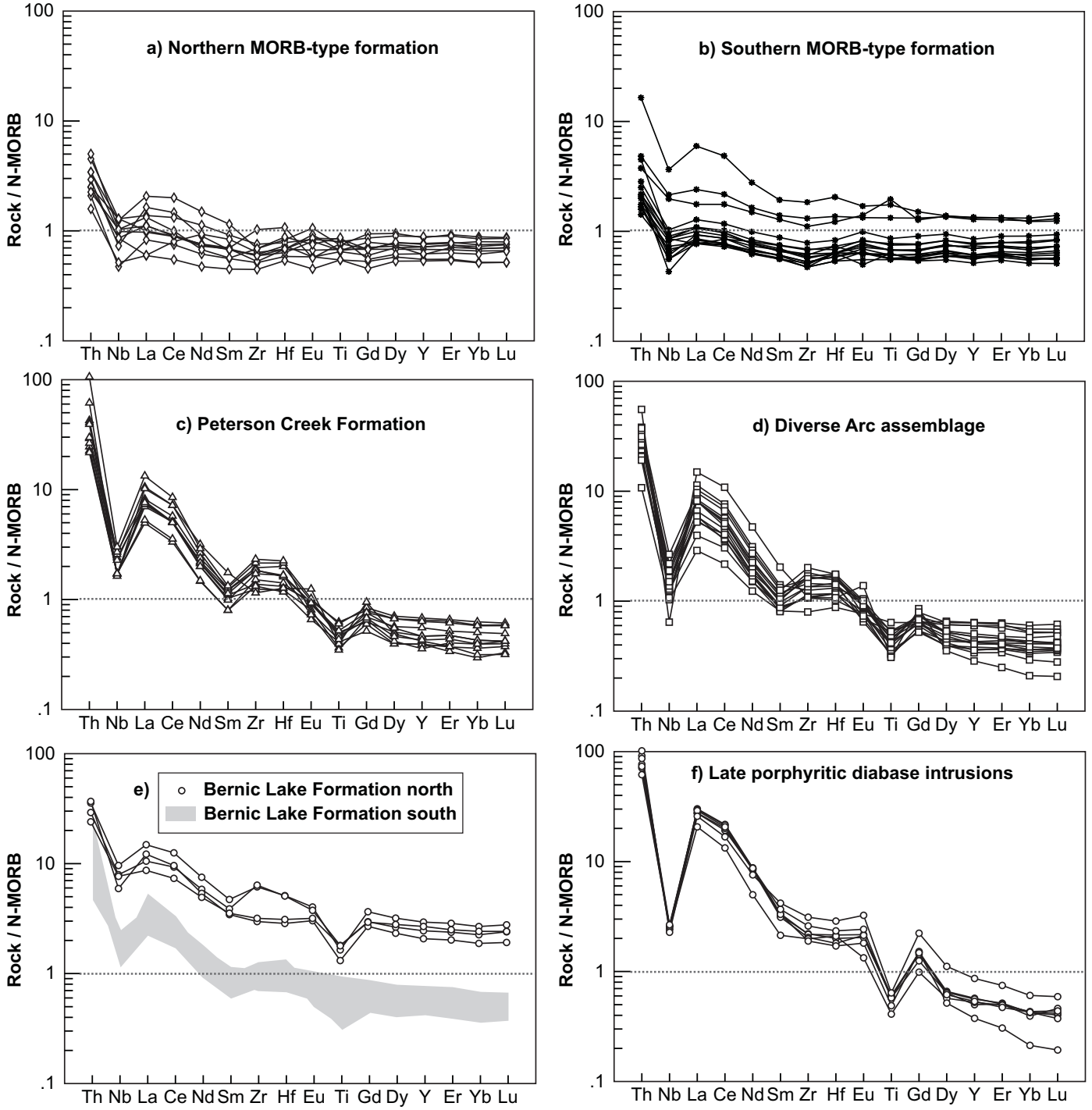

Figure 4: *N-MORB normalized incompatible element plots of mafic to intermediate volcanic rocks from the Bird River Belt (normalizing values from Sun and McDonough, 1989):* ***a)*** *Northern MORB-type formation,* ***b)*** *Southern MORB-type formation,* ***c)*** *Peterson Creek Formation,* ***d)*** *Diverse Arc assemblage,* ***e)*** *Bernic Lake Formation,* ***f)*** *late porphyritic diabase intrusions.*

assemblage is uncertain, but geochemical and geochronological data suggest a younger age for the latter assemblage. A concordant 2706 ±23 Ma age (2σ error) obtained for the youngest detrital zircon grain in greywacke within the Diverse Arc assemblage (Gilbert, unpublished data, 2007) suggests that the volcano-sedimentary north panel spanned at least 25 Ma, and may thus overlap with the age of the turbiditic Booster Lake Formation (2712 ±17 Ma; Gilbert, 2006b). Volcanic and granitoid rocks with ages between 2785 and 2725 Ma appear to be the predominant detrital source for the greywacke.

Peterson Creek Formation

The Peterson Creek Formation is an intermediate to felsic volcanic sequence that extends through the BRB north panel for more than 40 km; it is up to 2.7 km wide, although the true thickness of the section may be less due to possible structural repetition. Massive and brecciated, aphyric and porphyritic dacite to rhyolite flows are the predominant facies type (Figure 3e); the flows are associated with felsic to heterolithic tuff and volcanic breccia (Figure 3f) that constitute up to 40% of the Peterson Creek Formation in the western part of the BRB. The

Table 3: Selected analytical data (average values and ranges) for mafic to intermediate volcanic rocks in the Bird River Belt.

GEOLOGICAL FORMATION	Average (range)	SiO_2 (%)	FeO_{total} (%)	MgO (%)	TiO_2 (%)	Cr (ppm)	Ni (ppm)	Zr (ppm)	Rb (ppm)	Nb (ppm)
Peterson Creek	Average	59.8	7.3	5.3	0.6	314	123	118	39	4.8
	(range)	54.3 - 61.7	5.4 - 9.3	1.5 - 8.8	0.5 - 0.8	28 - 700	35 - 220	85 - 159	11 - 97	3.8 - 6.3
Diverse arc assemblage	Average	58.0	8.0	6.1	0.5	291	153	99	18	3.3
	(range)	50.3 - 61.5	5.8 - 13.2	4.7 - 10.0	0.4 - 0.8	120 - 460	90 - 200	59 - 134	0 - 68	1.5 -5.1
Bernic Lake north	Average	57.5	13.5	2.1	2.1	< 20	< 20	342	58	18.0
	(range)	55.4 - 60.6	10.1 - 16.7	1.7 - 2.6	1.7 - 2.3	-	-	218 - 467	2 - 133	13.7 - 22.2
Bernic Lake south	Average	54.5	12.6	3.8	1.5	77	51	146	25	8.1
	(range)	45.7 - 59.4	7.9 - 18.2	2.0 - 6.7	0.8 - 2.4	<20 - 110	<20 - 100	101 - 189	7 - 77	5.4 - 11.8
Northern MORB-type	Average	49.2	13.5	7.1	0.9	238	127	48	7	2.2
	(range)	47.7 - 51.4	11.7 - 16.2	4.9 - 9.2	0.7 - 1.1	160 - 390	70 - 200	33 - 76	0 - 30	1.1 - 3.0
Southern MORB-type	Average	49.8	13.4	6.6	1.1	287	143	53	2	2.5
	(range)	46.4 - 54.9	9.1 - 21.6	3.9 - 8.6	0.7 - 2.5	<20 - 380	<20 - 190	35 - 136	1 - 5	1 - 8.5
Late porphyritic diabase	Average	56.9	7.1	6.0	0.7	158	101	169	58	5.8
	(range)	52.6 - 62.8	4.6 - 9.7	3.5 - 9.7	0.5 - 0.8	53 - 400	70 - 150	140 - 231	22 - 102	5.3 - 6.2

GEOLOGICAL FORMATION	Average (range)	La (ppm)	Yb (ppm)	Th (ppm)	$(La/Yb)_{ch}$	Zr/Y	Ta/Yb	Th/Ta	Mg#	No. of analyses
Peterson Creek	Average	19.1	1.4	4.0	10.7	8.6	0.30	10.8	57	9
	(range)	12.4 - 26.4	0.9 - 1.9	2.6 - 7.4	6.8 - 19.1	6.6 - 13.6	0.22 - 0.42	6.3 - 29.4	36 - 74	
Diverse arc assemblage	Average	18.9	1.3	3.6	12.6	8.1	0.26	13.2	61	15
	(range)	7.2 - 37.3	0.64 - 1.84	1.3 - 6.6	2.8 - 41.8	3.3 - 11.2	0.10 - 0.38	6.8 - 51.1	48 - 73	
Bernic Lake north	Average	28.7	7.0	3.7	3.0	4.8	0.18	3.0	24	4
	(range)	21.5 - 36.8	5.7 - 8.1	2.9 - 4.4	2.1 - 3.8	3.1 - 6.9	0.17 - 0.19	2.3 - 4.2	21 - 28	
Bernic Lake south	Average	19.0	3.0	3.5	4.8	4.9	0.22	5.6	38	12
	(range)	11.1 - 27.0	2.2 - 4.1	1.2 - 5.8	2.3 - 8.7	3.2 - 6.6	0.13 - 0.31	2.1 - 8.5	19 - 53	
Northern MORB-type	Average	2.9	2.1	0.4	1.0	2.4	0.08	2.5	52	11
	(range)	1.5 - 5.2	1.6 - 2.7	0.2 - 0.6	0.5 - 1.4	2.1 - 3.5	0.05 - 0.20	0.7 - 3.5	41 - 62	
Southern MORB-type	Average	3.4	2.3	0.4	1.0	2.4	0.07	2.1	50	17
	(range)	1.9 - 14.9	1.6 - 4.0	0.2 - 2.0	0.6 - 3.0	2.1 - 3.7	0.05 - 0.16	1.4 - 3.9	29 - 59	
Late porphyritic diabase	Average	68.1	1.3	9.6	42.2	11.2	0.38	22.2	63	7
	(range)	51.7 - 75.4	0.7 - 1.9	7.4 - 12.2	25.0 - 80.2	9.3 - 18.3	0.19 - 0.69	17.6 - 34.9	57 - 69	

fragmental rocks are interpreted to be mostly reworked mass flows derived from volcanic fragmental deposits (Figure 7a), but a pyroclastic origin can be inferred for some units (Figure 7b). Two distinct lithological types are distinguished on the basis of aphyric/porphyritic texture: a coarsely plagioclase+quartz–phyric phase with up to 35% phenocrysts (1–5 mm) and an aphyric to sparsely porphyritic phase with up to 10% phenocrysts (1–2 mm). These textural types occur both as massive, extrusive/intrusive felsic units and as reworked volcanic fragmental rocks. Sporadic deposits of epiclastic rocks within the felsic volcanic sequence are locally associated with alteration and porphyroblastesis.

Iron formations (oxide-, sulphide- and carbonate-facies types), locally associated with conspicuous aeromagnetic anomalies, occur toward the south margin of the Peterson Creek Formation in both the eastern and western parts of the BRB (Figure 7c). Base-metal mineralization is locally associated with these iron formations; a chert-magnetite-sulphide–bearing iron formation that occurs in the eastern part of the Peterson Creek Formation has been the focus of exploration drilling (Owyhee property; Mustang Minerals Corp., 2007a).

The Peterson Creek Formation consists of calcalkaline andesite, dacite and rhyolite[2] (Figure 8a) that display REE patterns characteristic of modern arc-type rocks, with elevated light REE and depleted heavy REE contents compared to N-MORB (Figure 4c). Peterson Creek Formation rocks are, furthermore, comparable with modern volcanic rocks at active continental margins (Figure 6a). Chondrite-normalized REE

[2] Volcanic rocks are classified according to SiO_2 content (volatile-free basis): basalt, 46–54% (mafic); andesite, 54–62% (intermediate); dacite, 62–70%; and rhyolite, 70–80% (felsic)

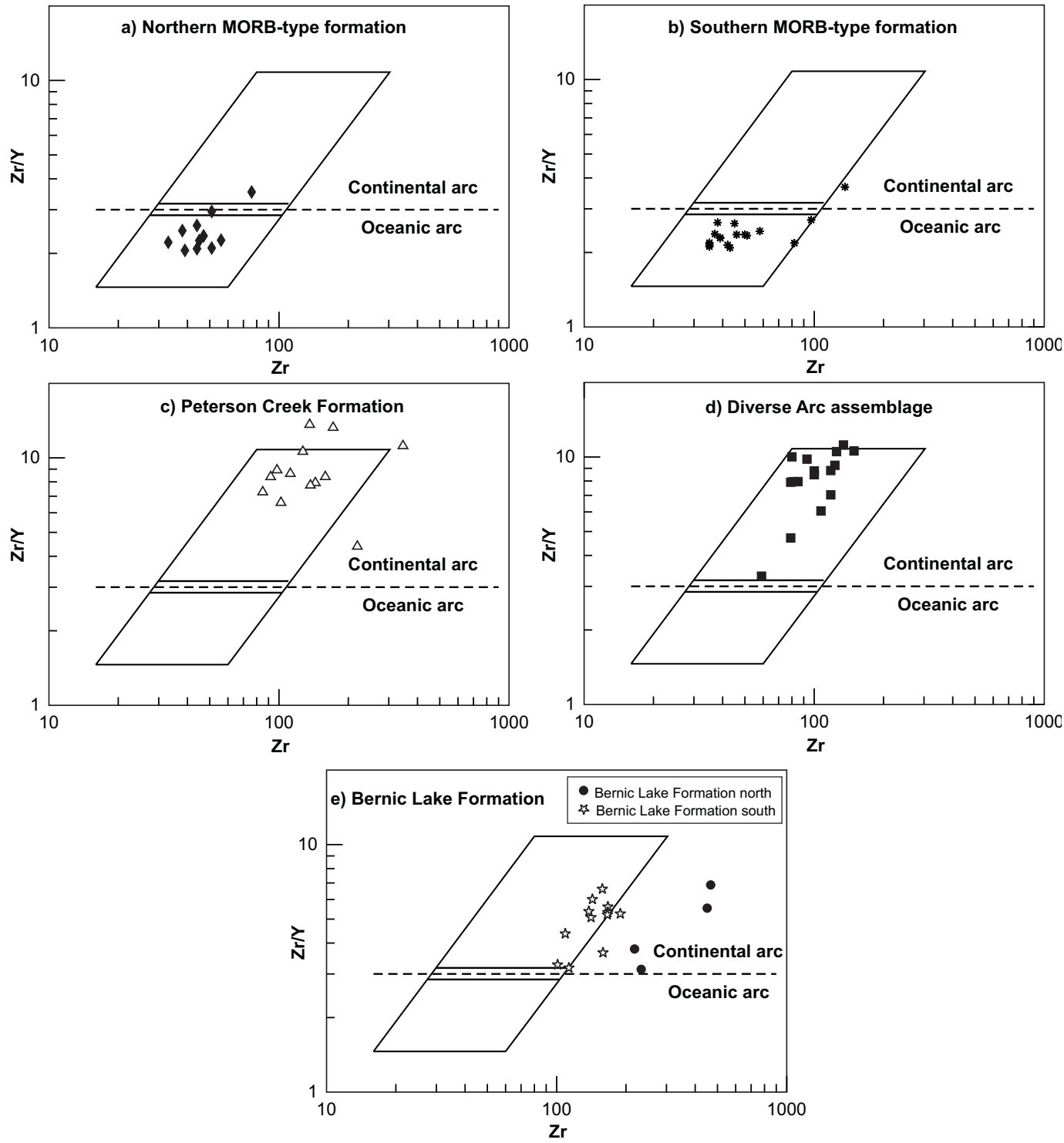

Figure 5: *Zr/Y versus Zr diagram of mafic to intermediate volcanic rocks (Pearce, 1983) from the Bird River Belt:* ***a)*** *Northern MORB-type formation,* ***b)*** *Southern MORB-type formation,* ***c)*** *Peterson Creek Formation,* ***d)*** *Diverse Arc assemblage,* ***e)*** *Bernic Lake Formation.*

plots (Figure 9a) show negative-sloping profiles without conspicuous Eu anomalies, typical for F1-type felsic flows as defined by Lesher et al. (1986).

Diverse Arc assemblage

Massive and fragmental volcanic and epiclastic rocks of the Diverse Arc assemblage, up to 0.75 km thick, extend through the central and eastern part of the BRB north panel for approximately 24 km. This lithologically diverse assemblage is assumed to be in fault contact with the Northern MORB-type formation to the north, whereas its unexposed contact with the Peterson Creek Formation to the south is interpreted as either conformable or disconformable. The widest and most complete sequence of the Diverse Arc assemblage occurs in the central part of the greenstone belt, where it is structurally intercalated with the Peterson Creek Formation (Geoscientific

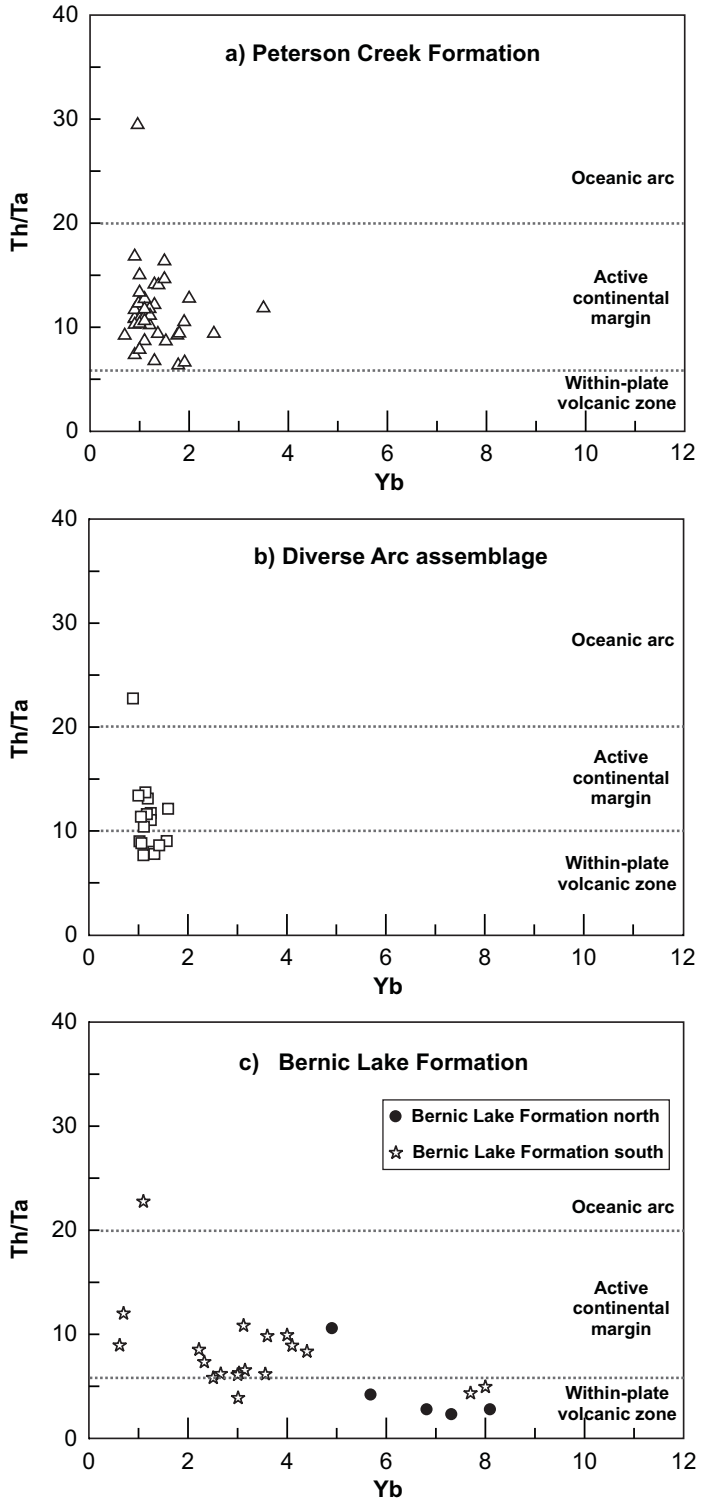

Figure 6: *Th/Ta versus Yb diagram of intermediate to felsic volcanic rocks from the Bird River Belt (Gorton and Schandl, 2000):* ***a)*** *Peterson Creek Formation,* ***b)*** *Diverse Arc assemblage,* ***c)*** *Bernic Lake Formation.*

Map MAP2008-1). Sporadic graded bedding in turbidite units suggests a repeated fold pattern in the northern part of the assemblage, and an anticlinal fold has been delineated farther to the south.

The lower, ~0.25 km wide part of the Diverse Arc assemblage consists of rock types that reflect phases of rapid sedimentation (turbidites and debris flows; Figure 7d–f) interspersed with relatively quiescent volcanic exhalative activity characterized by chert units (Figure 10a) and the accumulation of felsic and mafic tuffs, as well as extrusive felsic and mafic volcanic flows (Figure 10b). A polymictic conglomerate unit that overlies the lower part of the sequence consists mainly of unsorted basalt, gabbro and subordinate rhyolite, greywacke-siltstone and chert clasts (Figure 10c). Sporadic fragments of very coarse grained anorthositic gabbro are probably derived from the Bird River Sill. The source terrane for the conglomerate thus consists of volcanic and sedimentary rocks, in part derived from the lower part of the Diverse Arc assem-

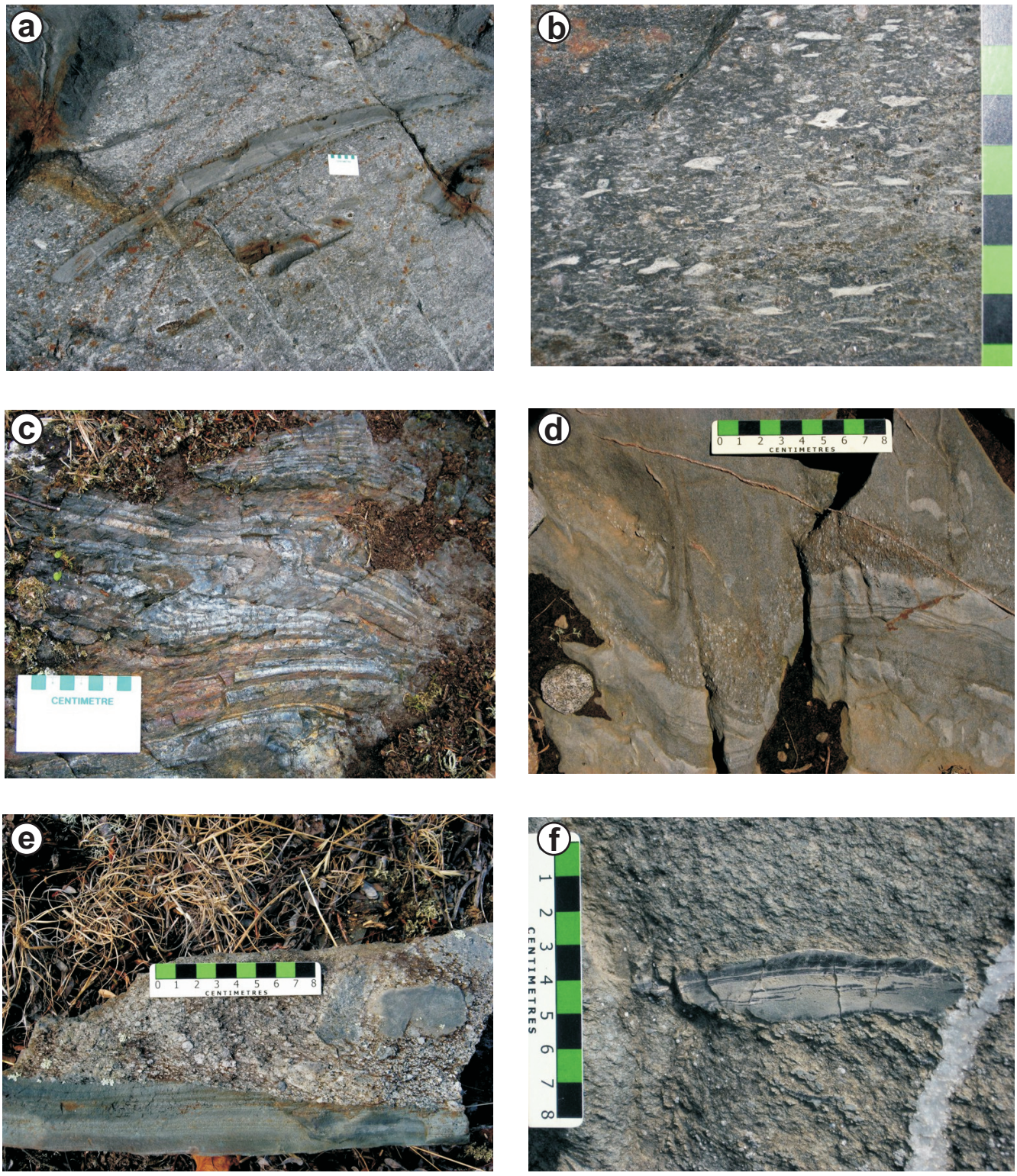

Figure 7: *Outcrop photographs of volcanic fragmental and sedimentary rocks in the north panel of the Bird River Belt:* ***a)*** *mass-flow deposit with pyroclastic and epiclastic detritus, Peterson Creek Formation (UTM 307375E, 5586964N);* ***b)*** *crystal-lithic tuff with raggedly shaped felsic clasts, possibly of ash-flow origin, Peterson Creek Formation (UTM 322542E, 5592810N);* ***c)*** *oxide-facies iron formation with thinly bedded chert and magnetiferous siltstone, Peterson Creek Formation (UTM 338163E, 5593140N);* ***d)*** *greywacke-siltstone turbidite showing graded bedding, scour and synsedimentary deformation, Diverse Arc assemblage (UTM 320596E, 559279N);* ***e)*** *laminated tuff scoured by mass flow that deposited the overlying lapilli-tuff bed, Diverse Arc assemblage (UTM 319917E, 5594973N);* ***f)*** *chert rip-up in lapilli tuff, interpreted as a reworked volcaniclastic deposit, Diverse Arc assemblage (UTM 318805E, 5592279N).*

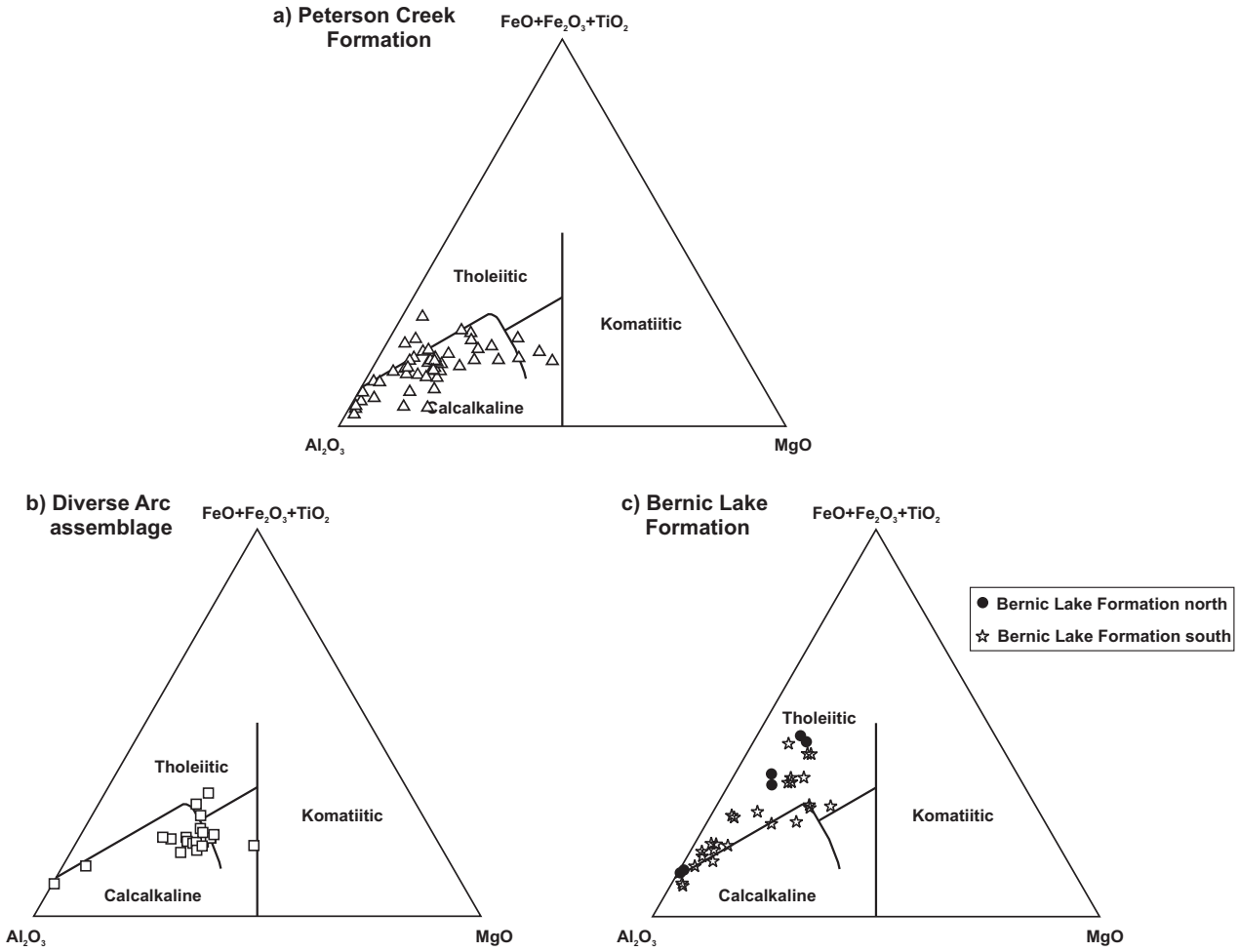

Figure 8: *Al_2O_3–[FeO^t+TiO_2]–MgO ternary diagram of mafic to felsic volcanic rocks (Jensen, 1976) from the Bird River Belt:* ***a)*** *Peterson Creek Formation,* ***b)*** *Diverse Arc assemblage,* ***c)*** *Bernic Lake Formation.*

blage and possibly the Northern MORB-type formation, as well as gabbroic to ultramafic rocks of the Bird River Sill. Relative uplift of this source terrane may have been due to extensional faulting, followed by erosion and the subsequent accumulation of coarse detritus as a littoral or fluvial-fan deposit. Andesitic flows, related fragmental rocks and greywacke in the upper part of the sequence overlying the polymictic conglomerate document a resumption of volcanism, together with emplacement of mass flows and turbidite sedimentation.

Extrusive volcanic rocks of the calcalkaline Diverse Arc assemblage (Figure 8b) range from basalt to dacite, with only subordinate rhyolite. The REE pattern and overall REE contents are similar to those of volcanic rocks in the Peterson Creek Formation, suggesting that the two may be magmatically related (Figure 4c, d; Figure 9b). As with the Peterson Creek Formation, the tectonic setting of the Diverse Arc assemblage is classified as ACM (Gorton and Schandl; Figure 6b) and felsic flows are of F1 type (Lesher et al., 1986).

South panel arc-type rocks

The BRB south panel arc-type sequence consists of abundant felsic and mafic volcanic rocks, unlike the mainly intermediate to felsic north panel. Geochemically, south panel rocks have a transitional, tholeiitic to calcalkaline affinity, in contrast to the calcalkaline affinity of the north panel sequence (Figure 8c). As in the north panel, geochemical indices of the volcanic rocks suggest a continental-arc affinity. The ε_{Nd} values of the south panel rocks (+0.7 to –2.4 at 2.7 Ga) indicate limited contamination by continental lithosphere during ascent of the source magma through the crust.

A sample of the supracrustal south panel arc-type rocks, which collectively constitute the Bernic Lake Formation, yielded a U-Pb zircon age of 2724.6 ±1 Ma (Table 1), suggesting that the BRB south panel may be slightly younger than the 2731.1 ±1 Ma north panel (age of the Peterson Creek Formation). This enigmatic relationship, whereby the north panel rocks are apparently older but geochemically more evolved (based on their calcalkaline character) than the transitional, tholeiitic to calcalkaline south panel sequence (Figure 8a–c), suggests that the two rock suites are not directly related components of an evolving geochemical system. Consequently the north and south panels are interpreted as separate arc-type remnants, juxtaposed along an inferred regional fault, roughly coincident with the site of the structurally emplaced Booster Lake Formation.

Bernic Lake Formation

The Bernic Lake Formation, approximately 2 km wide and 45 km along strike, consists of abundant felsic and mafic to intermediate volcanic rocks in the eastern part. Mafic volcanic rocks are predominant in the western part of the formation, as shown by recent (2008) field work in the area between Bernic

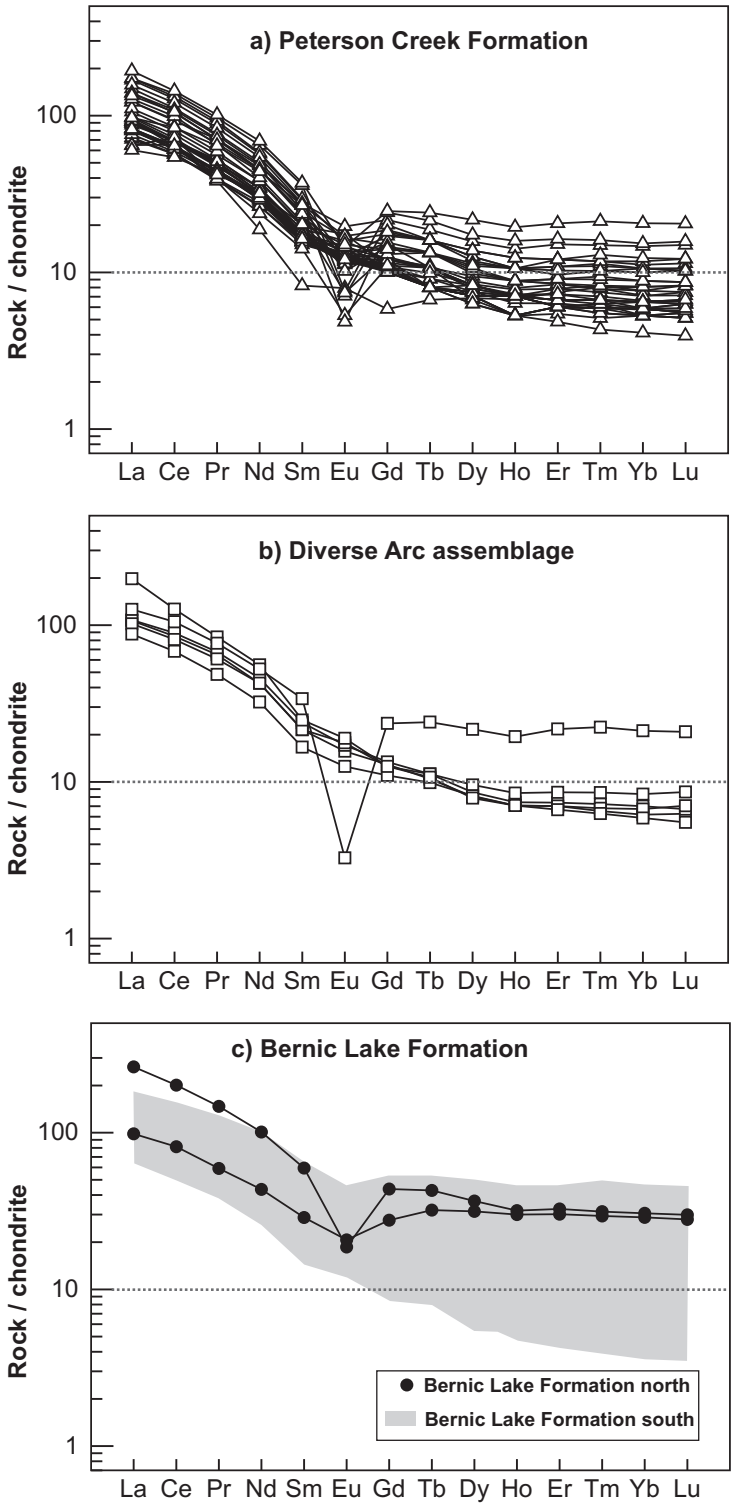

Figure 9: *Chondrite-normalized rare-earth–element plots of felsic volcanic rocks from the Bird River Belt (normalizing values from Sun and McDonough, 1989):* ***a)*** *Peterson Creek Formation,* ***b)*** *Diverse Arc assemblage,* ***c)*** *Bernic Lake Formation.*

Lake and the east shore of Lac du Bonnet (shown as unmapped in Figure 2 and on Geoscientific Map MAP2008-1). Rare structural indicators suggest a northward younging direction in the east-central part of the Bernic Lake Formation, consistent with the available geochemical data that indicate volcanic rocks in the northern part of the formation are geochemically more evolved than those in the sequence farther to the south.

Heterolithic volcanic breccia with mainly felsic fragments is a major component of the Bernic Lake Formation. The breccia is largely unsorted and primary clast shapes (where preserved) are angular to tabular (Figure 10d), precluding the conglomeratic origin suggested by Černý et al. (1981). Pervasive deformation and alteration render interpretation of this unit problematic; reworking and subsequent deposition of volcanic fragmental deposits by mass flows appears a likely mode of origin for the breccia. Massive, 10–30 m thick dacite and rhyolite flows, commonly associated with autoclastic fragmental deposits (Figure 10e) and related intrusive rocks, are

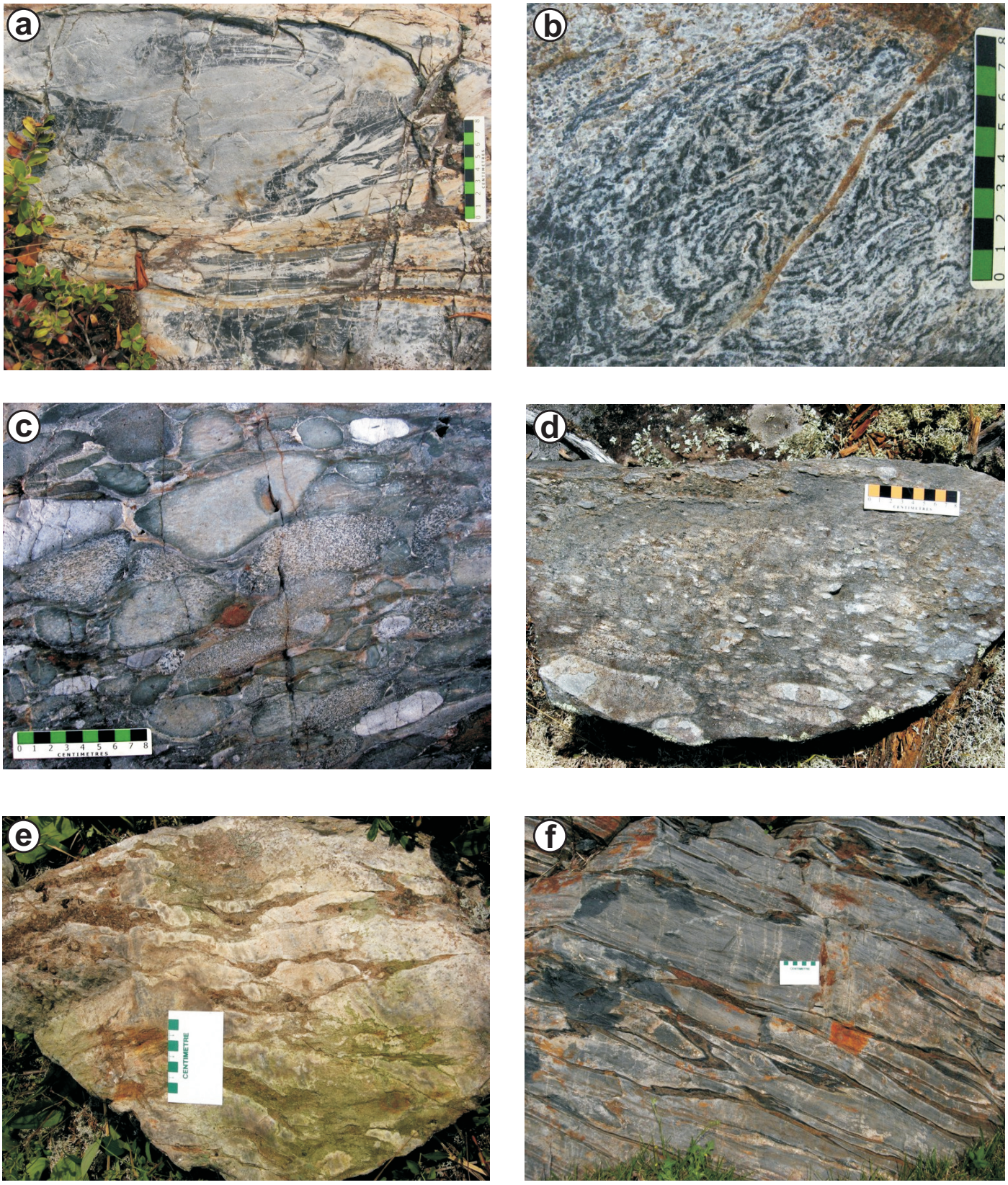

Figure 10: *Outcrop photographs of massive to fragmental volcanic and sedimentary rocks in the north and south panels of the Bird River Belt:* ***a)*** *laminated chert partly disrupted by synsedimentary deformation, Diverse Arc assemblage (UTM 319787E, 5594535N);* ***b)*** *spherulitic rhyolite flow with contorted flow lamination, Diverse Arc assemblage (UTM 319853E, 5594930N);* ***c)*** *polymictic conglomerate with volcanic, sedimentary, gabbroic and sporadic anorthositic fragments, Diverse Arc assemblage (UTM 320494E, 5592734N);* ***d)*** *reworked felsic volcanic breccia of the Bernic Lake Formation, unusual for its conspicuous sorting and normal size-grading (UTM 336150E, 5587872N);* ***e)*** *sparsely plagioclase-phyric rhyolite with* in situ *brecciation and alteration along fractures, Bernic Lake Formation (UTM 342018E, 5585254N);* ***f)*** *sparsely plagioclase-phyric pillowed basalt with disseminated pyrite in chloritic selvages, Bernic Lake Formation (UTM 303313E, 5585641N).*

widespread but subordinate to the heterolithic breccia facies. Felsic tuff and rare, fine-grained epiclastic interlayers also occur in the section. A 25 m thick, mineralized alteration zone in the (stratigraphically) central part of the Bernic Lake Formation may be derived from one such epiclastic unit (Gilbert, 2007a); the alteration zone is locally porphyroblastic and/or pyritic, and is associated with an aeromagnetic positive anomaly that extends along strike for approximately 10 km.

Mafic volcanic flows occur both as sporadic lenses within felsic volcanic rocks and in more extensive basaltic terranes within the Bernic Lake Formation (Figure 10f). The geochemically 'evolved', northern, 0.4 km wide part of the BRB south panel in the Rush Lake–Osis Lake area (Geoscientific Map MAP2008-1), interpreted as the upper part of the Bernic Lake Formation, consists of basalt and subordinate rhyolite. The mafic flows are aphyric and locally pillowed; one basalt-rhyolite contact is mineralized with traces of Cu, Ni, Zn (36–77 ppm), Au (18 ppb) and anomalous As (19 800 ppm). Zones of silicic and calcsilicate alteration are widespread in the Bernic Lake Formation. Pervasive, porphyroblastic amphibole-rich zones, possibly representing metamorphosed chloritic alteration zones, are especially common in the northern part of the formation.

Comparison between north and south panel arc-type rocks

The north and south panels are distinguished not only by their geochemical affinity (calcalkaline versus transitional tholeiitic-calcalkaline) but also by diagnostic element ratios indicating that Bernic Lake Formation rocks represent a transitional, convergent to extensional, arc-rift–type tectonic setting, in contrast to the predominantly convergent, subduction-type tectonic regime of the north panel rocks. Bird River Belt north panel volcanic rocks plot within the ACM field (convergent, subduction-type setting) on the Th/Ta versus Yb diagram (Figure 6a, b) of Gorton and Schandl (2000), whereas south panel rocks extend progressively from the ACM field into the 'within-plate volcanic zone' field (Figure 6c). This pattern within rocks of the BRB south panel is coincident with progression from lower to upper stratigraphic levels and suggests a transition from convergent to extensional crustal settings (Gorton and Schandl, 2000), consistent with a model of incipient arc-rifting. The transition is also shown in the Zr versus TiO_2 diagram, in which the northernmost (inferred youngest) part of the Bernic Lake Formation plots in the extension-related field (Figure 11c; Syme, 1998). This northern, 0.4 km wide section of the formation consists of a mafic to felsic 'enriched' volcanic suite with relatively higher REE contents compared to rocks in the same formation farther to the south (Figures 4e, 9c; Table 3). No such REE-enriched volcanic rocks have been mapped in the BRB north panel, although several felsic rocks in the Peterson Creek Formation plot in the extension-related field (Figure 11a) and may signify incipient arc-rifting.

Orogenic sedimentary formations

Booster Lake Formation

Turbiditic rocks of the Booster Lake Formation constitute a 1–2 km wide, fault-bounded structural enclave that extends through the centre of the BRB for approximately 44 km. This enclave is emplaced between the north and south panels of the greenstone belt except at the west end, where it extends into the BRB north panel. A second, smaller, turbiditic fault sliver occurs between the north and south panels in the western part of the belt (Figure 2).

The eastern part of the Booster Lake Formation displays a wide variety of turbidite features characteristic of classic Bouma-type sequences (Figure 12a, b; Gilbert, 2005, 2006b). Cyclic bedding is commonly accentuated by stratabound cordierite porphyroblasts that are widespread throughout the formation (Figure 12c). The depositional environment of the Booster Lake sedimentary basin is interpreted to have been at an intermediate distance from the detrital source but increasingly more proximal to the west, where the cyclic turbidite units give way to more thickly bedded (0.2–2 m scale) deposits. The turbiditic rocks are characterized by a structural pattern of repeated folds in which the axial traces are locally discordant to, and truncated by, the faults along the margins of the turbidite formation; the folds are thus interpreted as relatively older than the faults (Gilbert, 2007c).

Flanders Lake Formation

Arkosic sandstone and conglomerate of the Flanders Lake Formation truncate the main stratigraphic formations in the eastern part of the BRB (Geoscientific Map MAP2008-1). This formation is deformed by a major northwest-trending anticlinal fold and structurally overlies the BRB north panel due to northeast-directed thrusting. Arenaceous rocks of the Flanders Lake Formation are characterized by widespread crossbedding and pebbly horizons, locally associated with graded bedding and scour-and-fill structures. These rocks are intercalated with polymictic conglomerate that contains a wide variety of volcanic, sedimentary and granitoid cobbles and boulders, suggesting a fluvial-alluvial sedimentary environment (Figure 12d).

Detrital zircon data yield a maximum U-Pb age of 2697 ±18 Ma for the Flanders Lake Formation (Gilbert, 2006b) and indicate that the fluvial-alluvial deposits were derived mainly from two distinct sources defined by differences in age (ca. 2720 and 3020 Ma) — probably corresponding to BRB supracrustal rocks and older granitoid rocks of the contiguous cratonic blocks, respectively (North Caribou Superterrane and Winnipeg River Subprovince; Figure 1). Detrital zircon data also indicate a maximum depositional age of 2712 ±17 Ma for the Booster Lake Formation (Gilbert, 2006b), within error comparable to that of the Flanders Lake Formation and consistent with the interpretation that both formations are coeval with turbiditic and fluvial-alluvial rocks in the Neoarchean (ca. 2.7 Ga) English River Subprovince. The Flanders Lake Formation is also correlative with cover sequences elsewhere along the southern margin of the North Caribou Superterrane (e.g., the mainly fluvial-alluvial San Antonio assemblage in the Rice Lake belt, 70 km northwest of the BRB; Anderson, 2004).

Late diabase intrusions

Distinctive 'high-Th' porphyritic diabase dikes and sills occur sporadically in the central and western parts of the BRB.

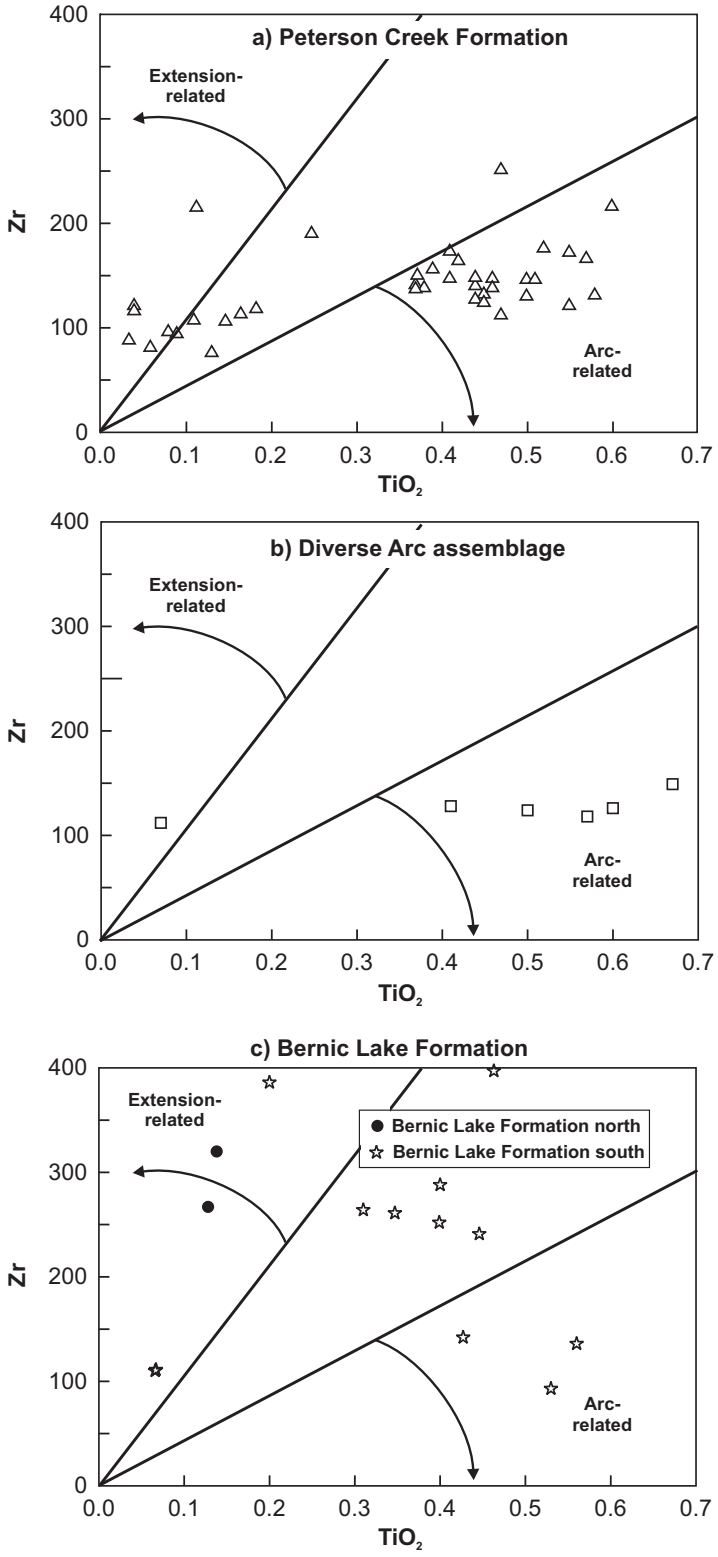

Figure 11: *Zr versus TiO_2 diagram of felsic volcanic rocks (Syme, 1998):* ***a)*** *Peterson Creek Formation,* ***b)*** *Diverse Arc assemblage,* ***c)*** *Bernic Lake Formation.*

These calcalkaline intrusions are hosted mainly by the Diverse Arc assemblage, but related dikes also occur sporadically in the Northern MORB-type, Peterson Creek and Booster Lake formations. The largest intrusion, up to 120 m thick and 2 km long, is emplaced at the contact between the Peterson Creek Formation and Diverse Arc assemblage in the central part of the BRB (Geoscientific Map MAP2008-1). The diabase is characterized by a distinctive porphyritic texture with 1–8 mm tabular plagioclases ± equant hornblende pseudomorphs (after pyroxene), and locally contains conspicuous, lensoid quartz amygdules up to 5 cm by 2 cm in size (Figure 12e). The basaltic to andesitic 'high-Th' diabase displays an arc-type REE pattern

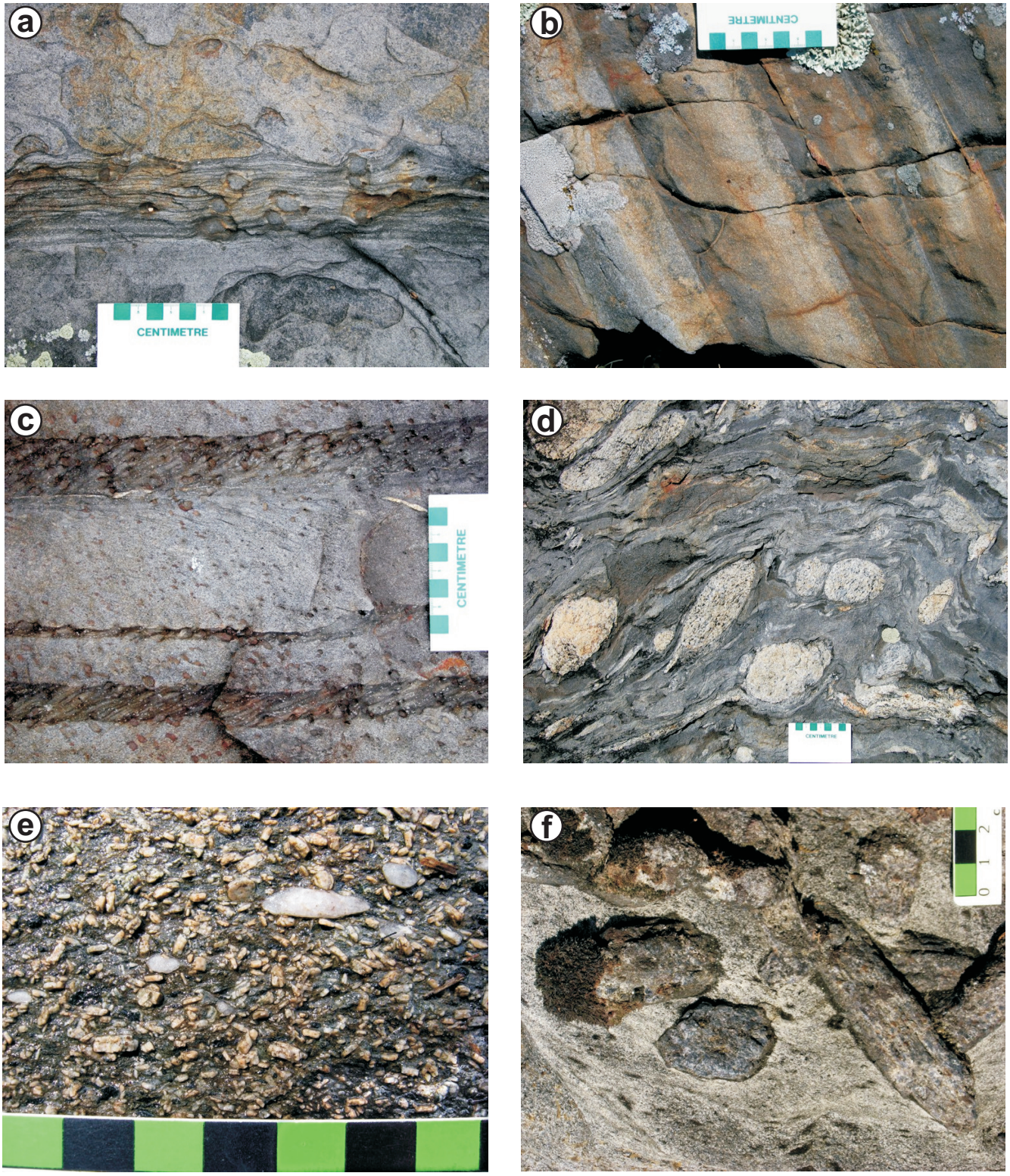

Figure 12: *Outcrop photographs of orogenic sedimentary rocks, late porphyritic diabase and porphyroblastic volcanic breccia in the north panel of the Bird River Belt:* ***a)*** *feldspathic greywacke with diffusely laminated siltstone unit, characterized by flame structures and cordierite porphyroblasts, Booster Lake Formation (UTM 337602E, 5590757N);* ***b)*** *cyclic layering with graded bedding in turbidite, Booster Lake Formation (UTM 337612E, 5591247N);* ***c)*** *cordierite-porphyroblastic siltstone beds within graded feldspathic greywacke of the Booster Lake Formation, displaying S_0/S_2 discordance as well as a discordant metamorphic fabric (S_1) confined to the feldspathic greywacke layer, apparently overprinted by S_2 only within the siltstone beds (UTM 337577E, 5590689N);* ***d)*** *polymictic conglomerate of the Flanders Lake Formation, with volcanic, sedimentary and plutonic fragments (foliation in granitoid clasts predates conglomerate deposition, but flattening and crenulation of mafic fragments are relatively later (UTM 339730E, 5590935N);* ***e)*** *plagioclase-hornblende–phyric diabase with quartz amygdules, late diabase intrusion (UTM 302808E, 5586144N);* ***f)*** *blue, euhedral to subhedral cordierite porphyroblasts, randomly oriented in the matrix of volcanic breccia, Diverse Arc assemblage (UTM 332078E, 5592946N).*

that is characterized by more pronounced light REE enrichment than any BRB arc-volcanic rocks (Figure 4f, c–e). Average La/Yb_{ch} values for the high-Th diabase (42.2) far exceed the averages for BRB volcanic rocks (10.6–12.6 for the north panel and 3–4.8 for the south panel; Table 3). Other late intrusions in the western BRB (aphyric diabase, coarse-grained gabbro and felsic porphyry) that are similarly enriched in Th and light REE may be related to the high-Th porphyritic diabase suite. This geochemically defined suite, which is largely undeformed and foliated only locally at the margins of some intrusive units, is interpreted as late or post-tectonic in age.

Structural geology

Microstructures and metamorphism

The Bird River Belt (BRB) underwent polyphase deformation that resulted in a composite regional foliation derived from at least three deformation events. This fabric is subvertical and approximately east striking in the central part of the belt, parallel to the axial planes of upright folds. The overprinting relationships between primary layering (S_0) and subsequent foliations (S_1 and S_2) are best preserved in the hinges of these folds. A later (S_3) foliation is conspicuous both in the Greer Lake pegmatitic granite on the south shore of the Winnipeg River (Geoscientific Map MAP2008-1) and within the Peterson Creek Shear Zone (PCSZ) in the Flanders Lake Formation, in the eastern part of the BRB. In the Booster and Flanders lakes areas, the regional foliation trends southeast, whereas it trends northeast farther west in the BRB, as well as farther southeast in the Eaglenest Lake area.

The regional foliation is characterized by synkinematic metamorphic minerals, such as green hornblende, biotite, cummingtonite and garnet in mafic rocks, and biotite, garnet and cordierite in felsic rocks. The regional foliation bears steep, down-dip stretching and mineral lineations, except in the northeastern part of the BRB (Davidson-Tulabi lakes area), where stretching lineations plunge shallowly to the southeast. The axes of sporadic intrafolial folds are parallel to this stretching lineation. Metamorphism in the central and northern parts of the BRB attained amphibolite-facies grade (approx. 550°C and 3–5 kb) and resulted in garnet, hornblende, biotite and cordierite porphyroblasts. The metamorphism outlasted the main deformation event, because these porphyroblasts overprint the main foliation (Figure 12f). Greenschist-facies retrogression is confined to narrow, late shear zones.

Macrostructures

Supracrustal rocks on the northern, weakly deformed flank of the BRB are in contact with the granitoid Maskwa Lake Batholith (Geoscientific Map MAP2008-1), in which a tonalitic phase dated at 2852.8 ±1.1 Ma (Table 1) predates the ca. 2730 Ma volcanic and sedimentary rocks of the BRB. Mafic dikes within the batholith are compositionally similar to basalts of the Northern MORB-type formation immediately to the south and may be synvolcanic feeder dikes. The Maskwa Lake Batholith thus apparently constitutes a basement for the Northern MORB-type formation and younger supracrustal rocks farther to the south (Peterson Creek Formation and Diverse Arc assemblage). The east-trending PCSZ represents an array of near-vertical anastomosing shears that display a north-side-up movement (Figure 2). These shears crosscut both the Maskwa Lake Batholith and Northern MORB-type and the Peterson Creek formations. The PCSZ extends east into the English River Subprovince, where the shear zone is characterized by a southeast trend and south-side-up, dextral strike-slip movement. The Eaglenest Lake Shear Zone (ELSZ) represents the southern boundary of the BRB, where it is in contact with the Winnipeg River Subprovince.

A conspicuous fault along the southern margin of the Booster Lake Formation may represent a deep crustal feature juxtaposing the BRB north panel (together with the younger, turbiditic Booster Lake Formation) against the BRB south panel (Bernic Lake Formation). Supracrustal rocks immediately south of this fault are highly strained. The fault contact between the Bernic Lake Formation to the south and the Booster Lake Formation to the north was tectonically reworked, resulting in a northeast-trending fault array that displays opposite vergences. Southwest of the inactive Maskwa-Dumbarton mine (Geoscientific Map MAP2008-1), the faults envelop northeast-trending upright folds, whereas, west of the junction between the TANCO mine road and Provincial Road 315, the faults envelop southeast-trending en échelon folds (Figure 13).

A major shear zone, up to 200 m wide, that separates the Bernic Lake and Southern MORB-type formations extends laterally for over 15 km, from Bernic Lake in the west to the area south of Booster Lake in the east (Figure 2). At Bernic Lake, the tectonic structures in the vicinity of this fault zone are subvertical and are interpreted as being the result of strongly coaxial deformation. Upright folding is indicated by sporadic top indicators within the Bernic Lake Formation immediately to the north (Kremer and Lin, 2006). The Birse Lake pluton (2723.2 ±0.7 Ma; Table 1), emplaced within the Southern MORB-type formation, displays highly strained margins with shear zones that are interpreted to envelop the lensoid pluton at depth (Figure 13).

The Booster Lake and Flanders Lake formations in the eastern BRB are separated by a south-dipping shear zone interpreted as a low-angle thrust, associated with northeast-directed tectonic movement. Both formations contain major folds assumed to be contemporaneous with the northeast-directed thrusting that resulted in the structural juxtaposition of the Booster Lake Formation onto the Flanders Lake Formation. The Booster Lake Formation is characterized by a synclinorial fold pattern defined by repeated folds with axial planes that dip moderately to steeply southwest (Gilbert, 2007a).

At the eastern margin of the BRB, the Marijane Lake pluton (Geoscientific Map MAP2008-1) is part of a plutonic complex that extends east for more than 40 km into Ontario. This pluton, which is interpreted to underlie the Flanders Lake Formation, represents the boundary between domains distinguished by contrasting styles of deformation, specifically, thrust tectonics in the southern domain and dextral strike-slip tectonism in the northern domain. The Marijane Lake pluton contains three granitoid phases, the younger two of which are synkinematic with respect to the main deformation events in the BRB. The youngest phase of this pluton has been dated at 2645.6 ±1.3 Ma (Table 1).

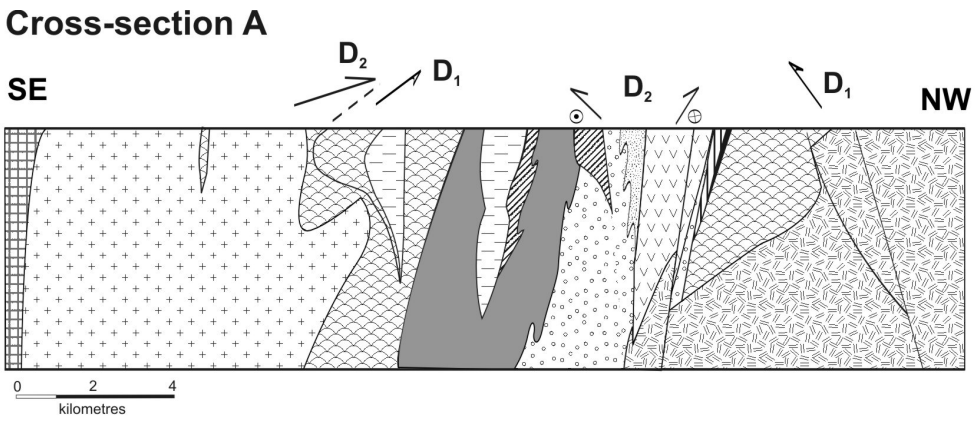

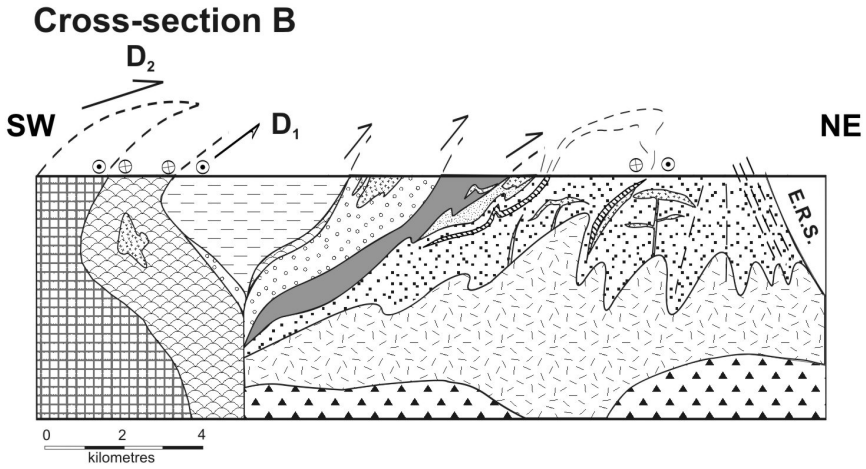

Flanders Lake Formation

Polymictic conglomerate

Arenite

Booster Lake Formation

Turbidite

Bernic Lake Formation

Pillow basalt, andesitic tuff, dacite

Felsic volcanic conglomerate and tuff, minor basalt (2724.6 ±1.1 Ma)

Gabbro

Peterson Creek Formation

Lapillistone, volcanic conglomerate, andesitic to dacitic tuff, rhyolite, minor massive basaltic flow (2731.1 ±1.0 Ma)

Bird River Sill

Peridotite, serpentinite

Gabbro (2744.7 ±5.2 Ma)

MORB-type basalt formations

Pillow basalt, massive to pillowed basalt, minor iron formation, gabbro

Plutonic rocks

Pegmatitic granite

Marijane Lake granite (2645.6 ±1.3 Ma)

Marijane Lake tonalite

Lac du Bonnet granite (2660.1 ±3.1 Ma)

Birse Lake diorite, quartz-feldspar porphry, granodiorite (2723.2 ±0.7 Ma)

Pointe du Bois tonalite (2729 ±8.7 Ma)

Maskwa Lake plutonic complex (2852.8 ±1.1 Ma)

D_1 Generation of deformation

Tectonic displacement (vertical down, up)

Geological contact

Shear zone

E.R.S. English River Subprovince

Figure 13: *Cross-sections of the Bird River greenstone belt. Section lines A and B are shown in Figure 2.*

Deformation history and kinematic interpretation of the Bird River greenstone belt

Three deformation events (D_1 to D_3) are recognized in the BRB. The D_1 deformation is characterized by north-side-up, non-coaxial deformation, and associated rock fabrics are well preserved, both to the south and to the northeast of the Maskwa Lake Batholith (Geoscientific Map MAP2008-1). The tonalite along the northeastern margin of the Maskwa Lake Batholith, contiguous with the English River Subprovince, is highly mylonitized and displays a conspicuous northeast-side-up shear sense. The same structural and kinematic features are found on the south side of the Maskwa Lake Batholith along the PCSZ, in which a north-side-up offset is clearly displayed. Immediately north and east of the Maskwa-Dumbarton mine, D_2 structures within the Maskwa Lake Batholith display folding and shearing textures that overprint the D_1 fabric. Similar features that demonstrate north-side-up shearing occur as relics within migmatitic tonalite located between the BRB and the English River Subprovince; these are also interpreted as D_1 in age. Although most structural features in supracrustal rocks within the BRB are of uncertain age, fabrics within the Peterson Creek Formation 2 km south of Bird Lake and at the sheared contact between the Bernic Lake and Southern MORB-type formations are probably D_1 in age. In the Peterson Creek Formation, synkinematic garnet porphyroblasts indicate early, north-side-up tectonic displacement. Within the Bernic Lake Formation, in the central part of the BRB south panel, D_1 features have been strongly transposed by subsequent deformation; late south-side-up shearing coeval with the intrusion of 2640 ±7 Ma pegmatitic granite (Baadsgaard and Černý, 1993) virtually obliterated early D_1 structures. A D_1 age of deformation is also inferred for tectonic fabrics showing north-side-up displacement at the North Winnipeg River Shear Zone (Geoscientific Map MAP2008-1), which displays evident reworking and overprinting by sinistral, south-side-up shearing.

The D_2 deformation is characterized by south-side-up, subvertical faulting and localized 'back-thrusting' that resulted in north-side-up displacement. Northeast-trending D_2 shear zones exhibit sinistral strike-slip movement, whereas southeast-trending shear zones are dextral. Within the BRB, sinistral south-side-up movement was predominant; the sigmoidal, S-shaped form of the Birse Lake pluton is attributed to this sinistral deformation. The south-side-up, sinistral ELSZ constitutes probably a first-order shear zone, responsible for the sigmoidal structural pattern of the BRB. A southeast-trending, dextral strike-slip fault zone at the boundary between the BRB and the English River Subprovince (Figure 2), also inferred to be D_2 in age, is associated with a low-angle stretching lineation.

Kinematic analysis based on D_2 structural features indicates a transpressive tectonic regime in which the BRB moved up relative to the adjacent terranes ('pop-up structure'; Figure 13). The D_2 deformation is associated with amphibolite-facies metamorphism that resulted in garnet and hornblende porphyroblastic overgrowth on the D_2 structural fabric, suggesting that peak metamorphism outlasted deformation. These relationships are especially well displayed by textures within supracrustal rocks in the Bernic Lake area. The M_2 metamorphism is probably directly related to rising geothermal gradients associated with granitoid intrusions.

The D_3 deformation resulted in 1) dextral shearing and folding along the PCSZ in the Starr Lake–Davidson Lake area (Geoscientific Map MAP2008-1), 2) faulting with south-side-up displacement in the Bernic Lake area, and 3) dextral shearing of the Greer Lake pegmatitic granite (2640 ±7 Ma; Baadsgaard and Černý, 1993) on the south shore of the Winnipeg River. The D_3 shearing is interpreted to be dominantly transpressive, similar to that in D_2 deformation zones. The D_3 fold structures and kinematics are not unlike those of D_2 and, in addition, D_3 fabrics locally appear to be coincident with pre-existing, composite D_1-D_2 textures; thus the D_2 and D_3 deformation events are commonly difficult to distinguish.

The D_3 deformation is interpreted as coeval with the emplacement of ca. 2640 Ma pegmatitic and leucogranitic intrusions (e.g., Marijane Lake pluton; 2645.6 ±1.3 Ma; Table 1). These granitic and pegmatitic intrusions are locally emplaced along D_3 structures. A possibly contemporaneous tectono-plutonic event has been documented in the Separation Lake greenstone belt in Ontario (2646 ±2 Ma for the Separation Rapids pegmatite; Larbi et al., 1999).

Economic geology

Mineral exploration and geological investigations in the Bird River area span the past century, dating from the pioneering work of Tyrrell (1900). Economic interest in the region has focused largely on two resource types: rare-element–bearing pegmatite bodies and mafic to ultramafic intrusive rocks containing base metals and PGE (Gilbert, 2006b). Investigation of a Cr showing on the Bird River in 1942 led to the discovery of a base-metal sulphide deposit at the north margin of the Bird River Sill, where Cu and Ni were produced for a decade until the mid-1970s at the Maskwa-Dumbarton mine (Geoscientific Map MAP2008-1). Plans are underway to open a new mine at Maskwa that will extract more than 9 million tonnes of ore over a period of 8 years (Mustang Minerals Corp., 2007b). In addition, Marathon PGM Corporation (2007) is prospecting for base metals and PGE in the vicinity of the Bird River Sill. Drilling is targeted on sulphide-facies iron formation and geophysical anomalies in basaltic/gabbroic hostrocks within the BRB north panel. Stratabound base-metal mineralization, locally associated with formational contacts, has also been documented within the volcanic Bernic Lake Formation of the BRB south panel.

Current exploration also includes ongoing investigations for new sources of rare elements in settings similar to that of the 'TANCO pegmatite' at Bernic Lake. Tantalum Mining Corporation of Canada Ltd. (TANCO), a wholly owned subsidiary of the United States–based Cabot Corporation, currently produces Ta, Li and Cs; the pegmatite at the TANCO mine contains approximately 80% of current global reserves of Cs.

References

Anderson, S.D. 2003: Geology and structure of the Garner Lake area, southeast Rice Lake greenstone belt, Manitoba (NTS 52L14); *in* Report of Activities 2003, Manitoba Industry, Economic Development and Mines, Manitoba Geological Survey, p. 178–195.

Anderson, S.D. 2004: Preliminary results and economic significance of geological mapping and structural analysis in the Rice Lake area, central Rice Lake greenstone belt, Manitoba (NTS 52M4 and 52L13); *in* Report of Activities 2004, Manitoba Industry, Economic Development and Mines, Manitoba Geological Survey, p. 216–231.

Anderson, S.D. 2005: Preliminary results and economic significance of geological mapping in the Gem Lake area, southeastern Rice Lake belt, Manitoba (NTS 52L11 and 14), with emphasis on the Neoarchean Gem assemblage; *in* Report of Activities 2005, Manitoba Industry, Economic Development and Mines, Manitoba Geological Survey, p. 104–116.

Baadsgaard, H. and Černý, P. 1993: Geochronological studies in the Winnipeg River pegmatite populations, southeastern Manitoba; Geological Association of Canada–Mineralogical Association of Canada, Joint Annual Meeting, Program with Abstracts, v. 18, p. A5.

Černý, P., Trueman, D.L., Ziehlke, D.V., Goad, B.E. and Paul, J. 1981: The Cat Lake–Winnipeg River and the Wekusko Lake pegmatite fields, Manitoba; Manitoba Energy and Mines, Mineral Resources Division, Economic Geology Report ER80-1, 215 p.

Cherniak, D.J., Lanford, W.A. and Ryerson, F.J. 1991: Lead diffusion in apatite and zircon using ion implantation and Rutherford backscattering techniques; Geochimica et Cosmochimica Acta, v. 55, p. 1663–1673.

Davis, D.W. 1994: Report on the geochronology of rocks from the Rice Lake Belt, Manitoba; Royal Ontario Museum, Toronto, Ontario Geology Department, unpublished report.

Davis, D.W. 2008: Sub-million year age resolution of Precambrian igneous events by thermal extraction (TE-TIMS) Pb dating of zircon: application to crystallization of the Sudbury impact melt sheet; Geology, v. 36, p. 383–386.

Duguet, M., Gilbert, H.P., Corkery, M.T. and Lin, S. 2006: Geology and structure of the Bird River Belt, southeastern Manitoba (NTS 52L5 and 6); *in* Report of Activities 2006, Manitoba Science, Technology, Energy and Mines, Manitoba Geological Survey, p. 170–183.

Duguet, M., Lin, S. Gilbert, H.P. and Corkery, M.T. 2007: Structural geology and kinematic evolution of the Bird River greenstone belt, English River Subprovince, Manitoba (NTS 52L5, 6); *in* Report of Activities 2007, Manitoba Science, Technology, Energy and Mines, Manitoba Geological Survey, p. 144–154.

Gilbert, H.P. 2005: Geological investigations in the Bird River area, southeastern Manitoba (parts of NTS 52L5N and 6N); *in* Report of Activities 2005, Manitoba Industry, Economic Development and Mines, Manitoba Geological Survey, p. 125–139.

Gilbert, H.P. 2006a: Geology of the east-central part of the Bird River area, Manitoba (NTS 52L6N); Manitoba Science, Technology, Energy and Mines, Manitoba Geological Survey, Preliminary Map PMAP2006-8, scale 1:20 000.

Gilbert, H.P. 2006b: Geological investigations in the Bird River area, southeastern Manitoba (NTS 52L5N and 6); *in* Report of Activities 2006, Manitoba Science, Technology, Energy and Mines, Manitoba Geological Survey, p. 184–205.

Gilbert, H.P. 2007a: Geology of the east part of the Bird River area, southeastern Manitoba (NTS 52L6); Manitoba Science, Technology, Energy and Mines, Manitoba Geological Survey, Preliminary Map PMAP2007-5, scale 1:20 000.

Gilbert, H.P. 2007b: Geology of the west part of the Bird River area, southeastern Manitoba (NTS 52L5); Manitoba Science, Technology, Energy and Mines, Manitoba Geological Survey, Preliminary Map PMAP2007-6, scale 1:20 000.

Gilbert, H.P. 2007c: Stratigraphic investigations in the Bird River greenstone belt, Manitoba (part of NTS 52L5, 6); *in* Report of Activities 2007, Manitoba Science, Technology, Energy and Mines, Manitoba Geological Survey, p. 129–143.

Gorton, M.P. and Schandl, E.S. 2000: From continents to island arcs: a geochemical index of tectonic setting for arc-related and within-plate felsic to intermediate volcanic rocks; Canadian Mineralogist, v. 38, p. 1065–1073.

Hawkesworth, C.J., Gallagher, K., Hergt, J.M. and McDermott, F. 1994: Destructive plate margin magmatism: geochemistry and melt generation; Lithos, v. 33, p. 169–188.

Hrabi, R.B. and Cruden, A.R. 2006: Structure of the Archean English River subprovince: implications for the tectonic evolution of the western Superior Province, Canada; Canadian Journal of Earth Sciences, v. 43 p. 947–966.

Jaffey, A.H., Flynn, K.F., Glendenin, L.E., Bentley, W.C. and Essling, A.M. 1971: Precision measurement of half-lives and specific activities of ^{235}U and ^{238}U; Physical Review, v. 4, p. 1889–1906.

Jensen, L.S. 1976: A new cation plot for classifying subalkaline volcanic rocks; Ontario Geological Survey, Miscellaneous Paper 66, 22 p.

Kremer, P.D. and Lin, S. 2006: Geology of the Bernic Lake area around the Tanco mine, Bird River greenstone belt, southeastern Manitoba (NTS 52L6); Manitoba Science, Technology, Energy and Mines, Manitoba Geological Survey, Preliminary Map PMAP2006-9, scale 1:10 000.

Krogh, T.E. 1973: A low contamination method for hydrothermal decomposition of zircon and extraction of U and Pb for isotopic age determinations; Geochimica et Cosmochimica Acta, v. 37, p. 485–494.

Krogh, T.E. 1982: Improved accuracy of U-Pb ages by the creation of more concordant systems using an air abrasion technique; Geochimica et Cosmochimica Acta, v. 46, p. 637–649.

Larbi, Y., Stevenson, R., Breaks, F., Machado, N. and Gariépy, C. 1999: Age and isotopic compositions of late Archean leucogranites: implications for continental collision in the western Superior Province; Canadian Journal of Earth Sciences, v. 36, p. 495–510.

Lemkow, D.R., Sanborn-Barrie, M., Bailes, A.H., Percival, J.A., Rogers, N., Skulski, T., Anderson, S.D., Tomlinson., K.Y., McNicoll, V., Parker, J.R., Whalen, J.B., Hollings, P. and Young, M. 2006: GIS compilation of geology and tectonostratigraphic assemblages, western Uchi Subprovince, western Superior Province, Ontario and Manitoba; Manitoba Science, Technology, Energy and Mines, Manitoba Geological Survey, Open File Report OF2006-30, 1 CD-ROM, scale 1:250 000.

Lesher, C.M., Goodwin, A.M., Campbell, I.H. and Gorton, M.P. 1986: Trace-element geochemistry of ore-associated and barren felsic metavolcanic rocks in the Superior Province, Canada; Canadian Journal of Earth Sciences, v. 23, p. 222–241.

Ludwig, K.R. 2003: User's manual for Isoplot 3.00 — a geochronological toolkit for Excel; Berkeley Geochronological Center, Special Publication 4, 71 p.

Marathon PGM Corporation 2007: Marathon extends mineralized zone to 800 m at the Coppermine zone, Bird River property, SE Manitoba; Marathon PGM Corporation, press release, August 29, 2007, URL http://tsedb.globeinvestor.com/servlet/WireFeedRedirect?cf=GlobeInvestor/tsx/config&date=20070829&archive=cnw&slug=C3402 [September 18, 2007].

Matthews, W. and Davis, W.J. 1999: A practical image analysis technique for estimating the weight of abraded mineral fractions used in U-Pb dating; *in* Radiogenic Age and Isotopic Studies: Report 12, Geological Survey of Canada, Current Research 1999-F, p. 1–7.

Mattinson, J.M. 2005: Zircon U–Pb chemical abrasion ('CA-TIMS') method: combined annealing and multi-step partial dissolution analysis for improved precision and accuracy of zircon ages; Chemical Geology, v. 220, p. 47–66.

Mealin, C.A. 2006: Geology of the Bird River Sill, southeastern Manitoba (part of NTS 52L5); Manitoba Science, Technology, Energy and Mines, Manitoba Geological Survey, Preliminary Map PMAP2006-10, scale 1:10 000.

Mustang Minerals Corp. 2007a: Mustang appoints new VP Exploration, drilling underway at Owyhee property; Mustang Minerals Corp., press release, May 30, 2007, URL http://www.integratir.com/newsrelease.asp?news=2130983002&ticker=V.MUM&lang=EN [July 13, 2008].

Mustang Minerals Corp. 2007b: Mustang Minerals prefeasibility study update $2 million financing announcement; Mustang Minerals Corporation, press release, September 6, 2007, URL http://www.integratir.com/newsrelease.asp?news=2130983820&ticker=V.MUM&lang=EN [September 18 2007].

Nitescu. B., Cruden, A.R. and Bailey, R.C. 2006: Integrated potential-field and seismic constraints on the structure of the Archean metasedimentary English River Belt, western Superior craton, Canada; Precambrian Research, v. 144, p. 261–277.

Pearce, J.A. 1983: Role of the sub-continental lithosphere in magma genesis at active continental margins; *in* Continental Basalts and Mantle Xenoliths, C.J. Hawkesworth and M.J. Norry (ed.), Nantwich, United Kingdom, p. 230–249.

Percival, J.A., McNicoll V. and Bailes, A.H. 2006a: Strike-slip juxtaposition of ca. 2.72 Ga juvenile arc and >2.98 Ga continent margin sequences and its implications for Archean terrane accretion, western Superior Province, Canada; Canadian Journal of Earth Sciences, v. 43, p. 895–927.

Percival, J.A., Sanborn-Barrie, M., Skulski, T., Stott, G.M., Helmstaedt, H. and White, D.J. 2006b: Tectonic evolution of the western Superior Province from NATMAP and LITHOPROBE studies; Canadian Journal of Earth Sciences, v. 43, p. 1085–1117.

Romer, R.L. and Smeds, S-A. 1994: Implications of U-Pb ages of columbite-tantalites from granitic pegmatites for the Paleoproterozoic accretion of 1.90–1.85 Ga magmatic arcs to the Baltic Shield; Precambrian Research, v. 67, p. 141–158.

Romer, R.L. and Wright, J. E. 1992: U-Pb dating of columbites: a geochronologic tool to date magmatism and ore deposits; Geochimica et Cosmochimica Acta, v. 56, p. 2137–2142.

Saunders, A.D. and Tarney, J. 1991: Back-arc basins; *in* Oceanic Basalts, P.A. Floyd (ed.), Blackie and Son, Glasgow, United Kingdom, p. 219–263.

Sinton, J.M. and Fryer, P. 1987: Mariana Trough lavas from 18°N: implications for the origin of back-arc basin basalts; Journal of Geophysical Research, v. 92, no. B12, p. 12 782–12 802.

Stacey, J.S. and Kramers, J.D. 1975: Approximation of terrestrial lead isotope evolution by a two-stage model; Earth and Planetary Science Letters, v. 26, p. 207–221.

Stern, R.A., Syme, E.C., Bailes, A.H. and Lucas, S.B. 1995a: Paleoproterozoic (1.90–1.86 Ga) arc volcanism in the Flin Flon Belt, Trans-Hudson Orogen, Canada; Contributions to Mineralogy and Petrology, v. 119, p. 117–141.

Stern, R.A., Syme, E.C. and Lucas, S.B. 1995b: Geochemistry of 1.9 Ga MORB- and OIB-like basalts from the Amisk collage, Flin Flon belt, Canada: evidence for an intra-oceanic origin; Geochimica et Cosmochimica Acta, v. 59, p. 3131–3154.

Sun, S.S and McDonough, W.F. 1989: Chemical and isotopic systematics of oceanic basalts: implications for mantle composition and processes; Geological Society, Special Publication 42, p. 313–345.

Syme, E.C. 1998: Ore-associated and barren rhyolites in the central Flin Flon belt: case study of the Flin Flon mine sequence; Manitoba Energy and Mines, Geological Services, Open File Report OF98-9, 26 p.

Tyrrell, J.B. 1900: East shore, Lake Winnipeg; Geological Survey of Canada, Annual Report, 1898, v. 11, pt. G.

Wang, X. 1993: U-Pb zircon geochronology study of the Bird River greenstone belt, southeastern Manitoba; M.Sc. thesis, University of Windsor, Windsor, Ontario, 96 p.

White, W.M. and Dupré, B. 1986: Sediment subduction and magma genesis in the Lesser Antilles: isotopic and trace element constraints; Journal of Geophysical Research, v. 91, p. 5927–5941.

Appendix — Uranium-lead geochronology on minerals from the Bird River Belt, using isotope dilution–thermal ionization mass spectrometry (ID-TIMS) and thermal extraction–thermal ionization mass spectrometry (TE-TIMS)

Introduction

This appendix presents analytical details of U-Pb age data on zircon, monazite, apatite, plagioclase, columbite and cassiterite from intrusive units in and around the Bird River Belt. The U-Pb age data were acquired at the Department of Geology, University of Toronto.

Analytical methods include isotope dilution (ID-TIMS) following both air abrasion (Krogh 1982) and chemical abrasion (CA; Mattinson, 2005), as well as thermal extraction thermal ionization mass spectrometry (TE-TIMS; Davis 2008). Both CA and TE-TIMS are relatively new techniques, which are still in the process of being developed.

Methods

Rocks were crushed using a jaw crusher followed by a disk mill. Initial separation of heavy minerals was carried out with a Wilfley® table. This was followed by paramagnetic separations with the Frantz® isodynamic separator and density separations using bromoform and methylene iodide. Final sample selection was by hand-picking under a microscope, choosing the freshest, least cracked zircon grains.

Polished crystals were imaged using a JEOL JSM-840 scanning electron microscope equipped with detectors for scanning electron imaging (SEI), electron-backscatter (BSE) imaging and energy-dispersive X-ray (EDS) analysis.

Sample pre-treatment

Exterior surfaces of some zircon and monazite grains were removed by air abrasion (Krogh, 1982) and the rounded grains carefully picked to avoid cracks and evidence of alteration. Zircon grains that underwent CA treatment were annealed in quartz or platinum crucibles at 1000°C for 3–5 days. This removes much, although not all, of the radiation damage induced by decay of U and Th contained in the mineral, rendering the zircon more inert to chemical attack. The annealed grains were subsequently leached in concentrated hydrofluoric acid (HF) in a Teflon® bomb at 200°C for periods of 3–6 hours. These are the same conditions used to dissolve zircon but for a shorter period of time. The altered parts of the crystals, which contain isotopically disturbed Pb, dissolve more rapidly than annealed, unaltered crystal domains. For normal Archean zircon, which is often cracked and partially altered along high-U zones, the residue consists of whitish grains and fragments with a fragile, hollowed-out structure because of extensive dissolution along cracks and zones.

Columbite grains typically contain quantities of U similar to zircon, but can vary greatly in radiogenicity due to variable concentrations of common Pb. Reconnaissance U-Pb isotopic analyses were carried out on columbite fragments using a VG ExCell quadrupole inductively coupled plasma–mass spectrometer equipped with a Nu-Wave 213 nm laser-ablation system (LA-ICP-MS). Fragments were arrayed on double-sided tape and generally sampled using 50–100 μm diameter spots with a pit depth of about 30 μm. No attempt was made to calibrate U/Pb ratios, as the data were much less precise than could be achieved using isotope dilution–thermal ionization mass spectrometry (ID-TIMS). Fragments showing the most radiogenic and relatively concordant U-Pb data were then selected for ID-TIMS analysis. In some cases, partially altered columbite crystals were leached and partially dissolved in dilute HF following a procedure recommended by Romer and Wright (1992). Leaching was carried out on small fractions in 3 ml Savillex® capsules heated to about 100°C for 30 minutes, followed by ultrasonic agitation for 10 minutes. The freshest-looking fragments were then chosen for analysis. Acid attack varied from sample to sample and was tried with a variety of HF concentrations. It was generally found that 20% HF resulted in severe attack, leaving almost no shiny fragments, whereas there was little visible attack with 5% HF.

Weights of mineral fractions chosen for analysis were estimated from photomicrographs (Matthews and Davis, 1999). Estimated weights should be accurate to about ±20%. This affects only U and Pb concentrations, not age information, which depends only on isotope ratio measurements (Table 1). Samples were washed briefly in HNO_3 prior to dissolution. A ^{205}Pb-^{235}U spike was added to the dissolution capsules during sample loading.

Mineral dissolution and separation of Pb and U

Zircon grains were dissolved using concentrated HF in Teflon® bombs at 200°C and redissolved in 3N HCl to ensure equilibration with the spike (Krogh, 1973). Uranium and lead were separated using 50 μL anion exchange columns. Monazite and apatite were dissolved in 6N HCl in Savillex vials at 100°C. Chemical separation of Pb and U from monazite was the same as for zircon. For apatite solutions, Pb was purified in HBr and U in 7N HNO_3. Plagioclase was dissolved in HF at 100°C using Savillex vials, and Pb and U were separated using the same procedure as for apatite. Cassiterite is extremely difficult to dissolve and was therefore analyzed by thermal extraction–thermal ionization mass spectrometry (TE-TIMS).

The procedure for columbite is more elaborate and will be described in detail. Columbite was dissolved using concentrated HF at 100°C for at least 1 day. Tantalum and niobium strongly suppress lead emission in the mass spectrometer and must therefore be completely removed from the samples. The chemical procedures were adapted from those of Romer and Smeds (1994) and Romer and Wright (1992). Sample HF solutions were taken to dryness. The dry sample was wetted with one or two drops of concentrated HF, which resulted in immediate dissolution in most but not all cases. Dissolution was complete in all cases following addition of 10 drops 1N HBr. The vials were then capped and warmed on the hot plate for several minutes, taking care that condensation on the walls did not reduce the samples to dryness. Two sets of 50 μL anion exchange columns (Bio-Rad AG-1 resin) were prepared and cleaned by alternate washes with 6N HCl, 7N HNO_3 and H_2O. The HBr solutions were loaded into one set of cleaned columns, which strongly and preferentially adsorb Pb. The vials were then placed beneath their respective columns to collect all of

the solutions, which contain the U as well as Ta and Nb. These solutions were dried and redissolved in 10 drops 7N HNO_3. The Pb fractions were washed from the columns with 1N HBr followed by 3N HCl. They were then eluted into clean PMP beakers in 6N HCl, dried and redissolved in 10 drops 1N HBr. The U solutions were re-loaded into the columns and washed using 7N HNO_3, which removes Ta and Nb, followed by 6N HCl. The U was then eluted back into the Savillex vials in H_2O, dried and redissolved in 7N HNO_3. The Pb HBr solutions were reloaded into the second set of columns, washed with 1N HBr followed by 3N HCl and eluted back into the PMP beakers in 6N HCl. Two drops of 0.05N H_3PO_4 were added before drying the solution, which was held for analysis. The H_3PO_4 is hygroscopic and allows the sample to be identified by a small drop in the beaker. The U solutions were reloaded into this second set of columns, washed with 7N HNO_3 and eluted into the rinsed Savillex vials with H_2O. Two drops of 0.05N H_3PO_4 were added, but the solutions were not dried down at this stage.

Lead and uranium were analyzed on a VG354 mass spectrometer using a Daly collector in pulse counting mode for small samples. The mass discrimination correction for this detector is constant at 0.07%/AMU. Larger samples were analyzed in multidynamic mode using three high-mass Faraday collectors and the axial Daly detector. The Daly gain was continually monitored by measuring the ^{205}Pb signal in the Daly and adjacent Faraday collectors. Thermal mass-discrimination corrections are 0.10%/AMU. Dead time of the Daly system (about 20 ns) and multicollector Faraday cup efficiencies were monitored using the SRM982 Pb standard. Faraday amplifier gains were monitored daily using a constant current source.

Thermal extraction–thermal ionization mass spectrometry (TE-TIMS) methodology

Grains selected for analysis by TE-TIMS were not abraded. They were all cracked and/or partly altered. Grains were crimped within a fold in a Re filament and heated in vacuum to about 1450°C for at least 30 minutes to evaporate Pb with disturbed isotopic compositions from altered domains within the crystal. The zircon was then embedded in silica glass on a Re filament by fusing a large quantity of silica gel around it. This load was mounted into the mass spectrometer and reheated. The $ZrSiO_4$ breaks down at about 1500°C to ZrO_2, releasing its radiogenic Pb into the silica melt. The melt acts as a chemical ionization activator, greatly boosting the proportion of Pb that evaporates as Pb^+ ions. The Pb masses are measured using a multidynamic program similar to the one for TE-TIMS analyses, except that there is no ^{205}Pb present. Uranium is decoupled from Pb by the evaporation process, so only $^{207}Pb/^{206}Pb$ age information can be obtained. All Pb isotopic ratios are measured using simultaneous peak measurements in adjacent collectors. Data are collected in blocks of nine cycles, each cycle containing two simultaneous $^{207}Pb/^{206}Pb$ measurements. The $^{207}Pb/^{206}Pb$ ratios are corrected for common Pb using $^{207}Pb/^{204}Pb$ on a cycle-by-cycle basis and converted into $^{207}Pb/^{206}Pb$ ages. Measurement of ^{204}Pb relies on the Daly collector, which has a gain drift of about +/–1%, but this error has a negligible effect on the corrected $^{207}Pb/^{206}Pb$ age because the common Pb contribution is normally so small. A detailed description of the analytical method is given in Davis (2008).

Results and interpretations

Results are given in Tables 1, 4 and 5 and Figures 14–22, which include selected images. Average age errors are given at 95% confidence levels. Data reduction, regressions and plotting were carried out using the program of Ludwig (2003). Probabilities of fit would be expected to average 50% for random data with correctly chosen analytical errors. All age errors in this report are given at the 2σ or 95% confidence level.

MD05-222B: rhyolite, Peterson Creek Formation

The rhyolite yielded a small amount of zircon in the form of stubby, brown, euhedral to subrounded crystals (Figure 14a). Brown colouration is normally an indication of high uranium content and extensive radiation damage; however, many uncracked grains appeared to be fairly fresh. Electron-backscattered (BSE) images of cracked grains show well-developed zoning (Figure 14b) and darker areas that probably correspond to altered domains. The freshest looking crack-free grains were selected for abrasion. Analysis of three of these grains (Figure 14a) gave one slightly discordant and two concordant data with overlapping $^{207}Pb/^{206}Pb$ ages that average to 2731.1 ±1.0 Ma (Figure 14a). Since there is no evidence for cores in the images or inheritance in the data, this is likely to be the age of emplacement of the rhyolite.

MD05-1081: dacite, Bernic Lake Formation

The dacite yielded more abundant zircon, generally in the form of stubby, pale brown, euhedral crystals (Figure 15a). In many cases, crystals show a sector zonation from colourless to brownish, which is also evident in BSE images (Figure 15b). The population is fairly fresh and analysis of three uncracked abraded crystals (Figure 15a) gave near-concordant to concordant data with overlapping $^{207}Pb/^{206}Pb$ ages that average to 2724.6 ±1.1 Ma (Figure 15a). Again, there is no evidence for cores or inheritance, so this most likely represents the age of eruption of the dacite.

Two TE-TIMS analyses on multiple unabraded cracked grains, MD05-1081A and B, gave stable plateaus with average ages of 2724.9 ±0.4 and 2724.6 ±0.6 Ma when corrected for a Pb mass discrimination of 0.18%/AMU in the mass spectrometer (Figure 15c). This correction has also been found for a number of other samples where ID-TIMS and TE-TIMS data from simple Precambrian zircon populations have been compared, and is discussed in Davis (2008). It is used to correct all TE-TIMS data.

LIN06-2356: Marijane Lake pluton (granodiorite)

This sample yielded only a tiny amount of altered zircon grains, many of which show visible cores. Therefore, the sample cannot be easily dated using zircon. However, abundant monazite is present in the 1 Amp magnetic fraction at 10° of tilt on the Frantz® isodynamic separator. The monazite grains are generally cloudy and altered, but a fraction of relatively clear grains and fragments was picked (Figure 16). Analyses of three unabraded grains (Figure 16) produced data lying above concordia and with slightly dissimilar $^{207}Pb/^{206}Pb$ ages (Figure 16). Four more grains were abraded and dissolved (Figure 16). Only two of these analyses succeeded, and these data were also above concordia, although analysis DWD5063 is nearly

concordant, giving the oldest $^{207}Pb/^{206}Pb$ age at 2645.6 ±1.3 Ma. Three other data fit a regression line with this analysis (Figure 16, filled ellipses), also giving 2645.6 ±1.3 Ma for the upper concordia intercept age. Its lower age intercept is slightly to the right of zero. The fifth reversely discordant data cluster gives a distinctly younger $^{207}Pb/^{206}Pb$ age of 2634 ±2 Ma. The reverse discordance is probably due to a greater proportion of U loss compared to Pb loss from the high-U monazite crystals. The youngest datum may have been affected by decoupled Pb and U loss at different times. Monazite probably has a higher thermal-blocking temperature than zircon and is generally much more resistant to alteration. However, its exceptionally high U and Th concentrations likely result in extensive radiation damage, so it is often difficult, as in the present case, to recover completely pristine material. It is clear from these data that crystallization of the granite was very late in the orogenic development of the region and the best estimate for this age is given by the intercept of the four collinear data clusters at 2645.6 ±1.3 Ma.

MD07-2622: Maskwa Lake Batholith (tonalite)

This rock yielded a moderately large amount of zircon as long and short, generally highly cracked prisms (Figure 17a). Chemical abrasion analyses on six grains produced data on or near concordia, indicating two possible ages. The two youngest data define an age of 2853 ±1 Ma, while the other data average to 2857.7 ±1.9 Ma, although the agreement is marginal (6% probability of fit, Figure 17b). One datum is reversely discordant. This was from a highly etched grain (DWD5315, Figure 17b) and the reverse discordance may be due to alpha recoil implantation of Pb from high-U into adjacent low-U zones. The high-U zones are removed during leaching of the annealed grains, leaving excess radiogenic Pb in the low-U residue. This should not affect the $^{207}Pb/^{206}Pb$ age for small levels of discordance (~1%). There are small cores visible in BSE images of polished grains (Figure 17a), which may account for the slightly older ages. However, it is also possible that the younger data have been slightly updated by overgrowth from 2.7 Ga metamorphism that was incompletely removed by abrasion. In any case, the restricted scatter of the data suggests that the magmatic age is around 2855 ±4 Ma.

One apatite fraction was analyzed, as well as a fraction of feldspar (probably plagioclase), to determine the isotopic composition of the initial Pb in the apatite. The feldspar fraction decomposed in HF, leaving an insoluble residue, probably because of a high concentration of Ca. The spiked solution was drawn off and the residue re-spiked and dissolved in 6N HCl. The two feldspar data are slightly different on a Pb-Pb diagram (Figure 17c) but appear to be on a Pb-Pb isochron that intersects the Stacey and Kramers (1975) growth curve at about 2650 Ma. The dotted ellipses on Figure 17c are the Pb isotopic values corrected for decay of U over 2650 Ma, using the measured $^{238}U/^{204}Pb$ ratio. This ratio is likely to have been fractionated by leaching, so the uncorrected value of the residue was used as the initial Pb composition in the apatite. The differences in the apatite datum (Figure 17d), based on correction with any of these values, are much less than the size of the error ellipse because the apatite analysis is highly radiogenic. The apatite datum shown in Figure 17d has been corrected for the Stacey and Kramers (1975) initial Pb composition with errors of ±2%, and also corrected for the plagioclase residue Pb composition with errors of ±0.1%, which is larger than the measurement error. The resulting radiogenic $^{207}Pb/^{206}Pb$ age of 2652.1 ±1.7 Ma is much younger than the zircon age and probably dates the time at which the apatite became closed to diffusion of Pb. This should be when the temperature last cooled below about 500°C, based on diffusion measurements of Cherniak et al. (1991).

MD06-2598: Maskwa Lake Batholith (granodiorite)

This rock contained only a small amount of zircon as long and short prisms. Most are highly cracked and some have visible cores. Analysis by ID-TIMS of six abraded zircon grains gave concordant or near-concordant data, but $^{207}Pb/^{206}Pb$ ages scatter slightly outside of error (Figure 18a). Omitting the youngest datum (2829.7 ±1.6 Ma) produces an overlapping data set with an average $^{207}Pb/^{206}Pb$ age of 2832.3 ±0.9 Ma (44% probability of fit). This is the best estimate for crystallization of the pluton. As with the above sample (MD07-2622), the omitted datum might have contained metamorphic overgrowth, or the slightly older cluster might be biased by very small amounts of inheritance. Again, the general clustering of data indicate that the age is likely to be close to 2830 ±3 Ma.

Analysis by TE-TIMS of one zircon from this sample, MD06-2598E, gave a continually increasing age profile over the range 2792–2830 Ma (Figure 18b), while a second grain, MD06-2598F, gave a plateau with an age of 2840 ±0.3 Ma for the first nine cycles, but subsequent data gave ages increasing up to 2846 Ma. The reason for the inconsistencies may be a combination of older cores and disturbed Pb that was incompletely removed from altered domains.

PK06-1250: Birse Lake pluton (granodiorite)

Zircon is moderately abundant in this rock. The grains are brownish and have a euhedral short-prismatic or stubby morphology (Figure 19a). Four ID-TIMS data are concordant or near concordant and have overlapping $^{207}Pb/^{206}Pb$ ages with an average of 2723.2 ±0.7 Ma (48% probability of fit, Figure 19a). This is the best estimate for crystallization of the pluton. One TE-TIMS analysis, PK06-1250C, gives a stable plateau age of 2723.0 ±0.2 Ma, while ages from a second analysis, PK06-1250D, show a slight but persistent increase with an average of 2722.5 ±0.4 Ma (Figure 19b). Taking the last five data, which fit within error, gives a slightly higher average of 2722.8 ±0.3 Ma. All of these results are within error of the ID-TIMS age.

PK06-1197: gabbro pegmatite

This sample yielded abundant zircon, generally as large, highly cracked fragments and rounded grains, although there was also abundant fresh material (Figure 20). One abraded fragment and two rounded grains produced near-concordant overlapping ID-TIMS data with an average $^{207}Pb/^{206}Pb$ age of 2723.1 ±0.8 Ma (81% probability of fit, Figure 20). This age agrees with that of the Birse Lake granodiorite.

MD07-2679: syn-shear granite

Sample MD07-2679 yielded little zircon, no titanite but abundant monazite, which is characteristic of an S-type granite.

The small zircon yield consists of tiny, highly cracked needles that are probably primary but are too small and damaged to analyze, and larger equant grains have fine-scale zoning (see BSE images in Figure 21a). All the primary zircon is highly cracked and altered. There are some clear rounded grains, but these are almost certainly detrital cores. After annealing and leaching, the equant grains tend to fall apart into onion skin–like zones, surrounding clear detrital cores (see microphotograph in Figure 21a). To avoid cores, two thin zonal fragments were analyzed (Figure 21b). The results are quite reversely discordant, as expected, and disagree in $^{207}Pb/^{206}Pb$ age (2690 and 2682 Ma). It is notable that the calculated Th/U values of the zircon are quite low (<0.05, Table 2). This presumably indicates that zircon crystallized from the magma after it had been depleted in Th relative to U, possibly by prior crystallization of monazite.

Both strongly abraded and unabraded monazite were also analyzed (Figure 21b, c), but the data show a range of ages (2690–2670 Ma) that do not seem to correlate with the degree of abrasion. Three analyses are tightly clustered, with an average age of 2684 ±1 Ma, but this agreement might be fortuitous. There could be older detrital monazite cores, but more likely there is a later generation of metamorphic monazite. If so, the 2690 ±2 Ma age of the oldest monazite should be a minimum age estimate for crystallization of the magma. Assuming that the leached zircon zones contain no inheritance and that the spread in both Pb/U and $^{207}Pb/^{206}Pb$ ages is due to differential alpha recoil, the magmatic age can be estimated by extrapolating these two data to concordia. This gives a rather imprecise age of 2714 ±13 Ma because of the limited spread of the two data. Alpha recoil is likely to bias $^{207}Pb/^{206}Pb$ ages of reversely discordant data toward younger values because the ^{238}U decay chain emits one more alpha particle than the ^{235}U chain, resulting in a slightly greater excess of ^{206}Pb relative to ^{207}Pb (the discordia line is rotated counterclockwise). Therefore, the 2690 ±2 Ma age of the least discordant zircon fragment should represent a minimum age estimate, which is similar to that of the monazite.

PK05-1050: granitoid pegmatite, shear-zone hosted

This sample yielded only a small amount of zircon, mostly as altered, cracked euhedral grains (Figure 22a). The sample also contains columbite and cassiterite. Several zircon grains were annealed for 5 days, but they all dissolved after a 3 hour leach. The TE-TIMS analysis was more successful at retrieving age information (Figure 22b). The first grain, PK05-1050A, did not emit well and gave only a small amount of data. The last three data may form a plateau at 2651 ±4 Ma, but the fit is poor. The most precise datum is also the oldest, with an age of 2651.4 ±1.0 Ma. A second grain, PK05-1050B, gave much more data with a well-defined plateau age of 2650.7 ±0.2 Ma. A third grain, PK05-1050C, also gave abundant data but the age increases from about 2652 to 2658 Ma and then decreases to about 2644 Ma, at which point the signal becomes too low to measure precisely. This suggests that there is more than one age component in the zircon population.

The zircon grains are unusually low in Th/U, as measured from radiogenic $^{208}Pb/^{206}Pb$, and there is no apparent trend in this ratio as any of the grains break down. Low Th/U is normal for pegmatitic zircon because Th is highly insoluble in water-rich fluids. The fact that Th/U is fairly constant through the grains suggests that there is no inherited magmatic component, which would have had a Th/U ratio an order of magnitude larger. Electron-backscattered (BSE) images of polished zircon grains (Figure 22a) show that they are zoned with thin, very high U (bright) overgrowths in some cases. In other cases, zones are irregular, suggesting recrystallization. The small, dark amoeboid areas consist of alteration.

Laser-ablation ICP mass spectrometry on the columbite and cassiterite shows that both minerals contain radiogenic Pb. The columbite generally takes the form of flat black crystals (Figure 22c). The surfaces are generally dull grey, rather than shiny, indicating that the crystals are somewhat altered. Two ID-TIMS analyses on unleached grains show that the mineral is high in U (600–1100 ppm) and contains highly radiogenic Pb. The data are similarly discordant but have dissimilar $^{207}Pb/^{206}Pb$ ages (2638 ±1 and 2649 ±1 Ma). Analysis of a fraction of columbite that was leached in 10% HF produced a concordant datum with a much lower U concentration and an age of 2647 ±2 Ma, overlapping with one of the discordant data and slightly younger than the best TE-TIMS zircon age (Figure 22c).

Analysis by TE-TIMS of one cassiterite crystal produced relatively nonradiogenic Pb with an imprecise late Archean age for the lower temperature steps. As the temperature was increased, the emitted Pb became much more radiogenic and the corrected age increased to about 3.0 Ga (Figure 22b). This most likely reflects diffusion of Pb out of a xenocrystic zircon inclusion in the cassiterite crystal. The inclusion therefore gives the age of one component of crust through which the pegmatite passed. It might also represent a detrital zircon grain if the host rocks are metasedimentary.

PK06-1251: granitoid pegmatite, post-shear

A sample of a postdeformational, fracture-hosted pegmatite (PK06-1251) did not yield zircon. However, it does contain columbite in the form of somewhat altered prismatic crystals and fragments. Four single crystals were selected for ID-TIMS analysis following reconnaissance analysis by LA-ICP-MS to select for the most radiogenic Pb. Uranium concentrations are about an order of magnitude less than in the unleached grains from the previous sample, but Pb is still quite radiogenic. The U-Pb data on leached and unleached grains are mostly variably discordant but do not define a consistent Pb loss line (screened text in Figure 22c). Two data overlap with concordia but have very dissimilar $^{207}Pb/^{206}Pb$ ages of 2623 ±1 and 2647 ±1 Ma. The latter overlaps with the analysis of the leached fraction from PK05-1050. Another leached fraction produced a discordant datum with an age of 2659 ±1 Ma, which is older than any of the previous columbite analyses but similar to the oldest ages obtained from TE-TIMS analyses on zircon. Five of the columbite data (two from PK05-1050 and three from PK06-1251) define a consistent Pb loss line with an upper concordia intercept of 2647.4 ±1.0 Ma and a lower intercept of 517 ±20 Ma (34% probability of fit). It is unclear whether this fit is fortuitous. In any case, agreement between two concordant data, one from each pegmatite, and near-agreement with the TE-TIMS zircon plateau ages suggest that 2650 Ma, approximately, represents a significant age of mineral growth. However, there appears to

be more than one age component. This might reflect a multi-stage process of growth from different fluids that may have penetrated the two pegmatites at different times, as suggested by the concordant 2623 ±1 Ma datum. Some of the scatter, and the pre-2650 Ma ages from zircon and columbite, might be due to xenocrystic inclusions, as suggested by the cassiterite data.

Discussion

The chemical abrasion method is highly effective for eliminating secondary Pb loss, even from highly cracked grains. This enables larger samples to be analyzed than is usually the case with air abrasion alone, leading to sub–million-year age precision that is mostly limited by the uncertainty in Pb fractionation (about ±0.6 Ma for Neoarchean zircon). It also enables analysis of grains that are much more representative of the main population (highly cracked and damaged) than would be possible with air abrasion alone, where analysis is limited to very small crack-free grains and fragments, which might represent xenocrysts or separated cores. Leaching of annealed grains often makes low-U cores more visible, as in the case of sample MD07-2679. Separation of individual growth zones from leached crystals also provides a strategy for avoiding inherited cores. However, strongly zoned zircon can show reverse discordance following CA treatment, possibly due to alpha recoil effects. To what extent this can bias Pb ages remains to be tested. Chemical abrasion is less effective with Precambrian zircon uniformly high in U because 1) the 1000°C annealing only partially removes radiation damage, and 2) the difference between the dissolution rate of partly annealed unaltered zircon and altered domains is reduced. The annealing temperature is limited to 1000°C to avoid the possibility of fractionating Pb by evaporation from the zircon, the process that occurs during TE-TIMS.

Thermal extraction–thermal ionization mass spectrometry (TE-TIMS) relies only on Pb isotopic information for age determination. This is an effective strategy for simple zircon populations, where it can generate reproducible ages of higher precision than normal isotope dilution–thermal ionization mass spectrometry (ID-TIMS) because of more constant fractionation (Davis, 2008). However, constant age plateaus cannot be achieved in some cases, either because of inheritance in the sample or because of failure to remove all disturbed Pb from altered domains during thermal pretreatment. A suggested solution would be to leach thermally pretreated zircon following the CA procedure and then analyze it by TE-TIMS. The approximate 1400°C temperature of pretreatment might remove all radiation damage, even from highly damaged zircon, while the leach would assure removal of altered domains. The combined procedure would still not require clean chemistry, which is the most difficult and expensive part of ID-TIMS.

Age results show that phases of the Maskwa Lake Batholith have different magmatic ages (ca. 2832 Ma and ca. 2855 Ma) and intruded prior to the 2.7 Ga final accretion of the Superior Province, which is dated at about 2690 Ma by the syn-shear granite. Cooling of the region below about 500°C occurred at 2652 ±2 Ma, based on the age of apatite in the oldest phase. The early phases may correlate with other 2.85–2.8 Ga units in the Sachigo and Uchi subprovinces.

The host rocks to the TANCO pegmatite are, in large part, 2723 Ma in age, as given by both the Birse Lake granodiorite and gabbro. The pegmatite shows a complex age pattern from zircon and columbite. The best estimate for primary emplacement is 2650 ±2 Ma, but there may have been growth or disturbance of columbite as young as 2623 Ma. Cassiterite contains inheritance from a 3.0 Ga source.

Table 4: Results of isotope dilution–thermal ionization mass spectrometry (ID-TIMS) analysis of rocks from the Bird River Belt.

No.	Analysis	Fraction	Wt. (µg)	U (ppm)	Th/U	Pb_{com} (pg)	$^{207}Pb/^{204}Pb$ meas.	$^{206}Pb/^{238}U$ age (Ma)	2σ	$^{207}Pb/^{235}U$ age (Ma)	2σ	$^{207}Pb/^{206}Pb$ Age (Ma)	2σ	Disc. (%)	ρ
1	**MD05-222B**	**Rhyolite, Peterson Creek Formation**													
1	dwd5093	1 Ab zr, eq, brn	0.000	533	0.51	1.6	661	2725.6	6.4	2728.9	3.1	2731.4	2.1	0.3	0.91979
2	dwd5092	1 Ab zr, eq, brn	0.000	414	0.58	0.7	2236	2705.0	5.5	2720.1	2.6	2731.4	1.8	1.2	0.91484
3	dwd5091	1 Ab zr, eq, brn	0.000	406	0.55	0.4	3536	2723.8	5.4	2727.8	2.6	2730.8	1.5	0.3	0.94753
2	**MD05-1081**	**Dacite, Bernic Lake Formation**													
1	dwd5095	1 Ab zr, pale brn, rod incl	0.001	208	0.56	1.3	1146	2716.1	6.4	2721.4	3.1	2725.3	1.6	0.4	0.95788
2	dwd5094	1 Ab zr, pale brn, melt incl	0.001	208	0.57	2.4	820	2701.9	7.7	2715.1	3.5	2724.9	2.3	1.0	0.92926
3	dwd5096	1 Ab zr, pale brn, rod incl	0.001	206	0.59	1.2	1084	2722.8	7.9	2723.2	3.6	2723.4	2.0	0.0	0.94494
3	**Lin06-2356**	**Marijane Lake pluton (granodiorite)**													
1	dwd5063	1 Ab monazite frag	0.002	4624	16.6	6.0	10520	2651.2	4.3	2648.0	2.2	2645.6	1.3	-0.3	0.95323
2	dwd5065	1 Ab monazite frag, incl	0.000	5499	14.3	19.6	732	2690.3	7.2	2663.4	3.4	2643.0	2.0	-2.2	0.94411
3	dwd5016	1 monazite rnd, incl	0.003	3062	14.0	89.7	590	2747.2	11	2686.7	5.1	2641.5	2.1	-4.9	0.97177
4	dwd5017	1 monazite, euh	0.003	2886	13.4	161.8	371	2706.5	35	2668.7	15	2640.1	3.2	-3.1	0.99274
5	dwd5018	1 monazite frag, incl	0.023	3464	10.7	113.6	3573	2665.7	23	2647.8	9.9	2634.2	1.5	-1.5	0.99642
4	**MD07-2622**	**Maskwa Lake Batholith (tonalite)**													
1	dwd5312	1 CA zr, no etching	7.3	82	0.44	31.3	156	2858.2	6.0	2860.4	5.0	2861.9	5.8	0.2	0.79924
2	dwd5313	1 CA zr, crk, etched	6.2	136	0.55	0.7	9128	2855.8	5.2	2857.6	2.5	2858.8	1.3	0.1	0.95105
3	dwd5314	1 CA zr, crk, etched	3.2	186	0.57	1.1	4103	2858.2	5.0	2857.7	2.4	2857.4	1.4	-0.0	0.94486
4	dwd5354	1 CA zr, lpr frag, clr, crk	3.4	135	0.67	0.6	5833	2860.2	5.3	2858.1	2.5	2856.7	1.3	-0.2	0.95740
5	dwd5315	1 CA zr, str etch , crk	8.5	150	0.47	17.5	550	2877.9	7.9	2863.5	3.6	2853.4	2.1	-1.1	0.94065
6	dwd5353	1 CA zr, lpr frag, clr, crk	4.5	119	0.68	0.4	11049	2849.3	5.1	2851.2	2.5	2852.5	1.3	0.1	0.95599
7a	dwd5316sk	Apatite, clr rods, subhedral	300	34	0.66	260	207	2643.9	5.6	2649.3	4.0	2653.5	5.3	0.4	0.64852
7b	dwd5316f	Apatite, clr rods, subhedral	300	34	0.65	267	207	2642.7	5.5	2648.2	2.8	2652.3	1.7	0.4	0.94472
5	**MD06-2598**	**Maskwa Lake Batholith (granodiorite)**													
1	dwd5196	1 Ab zr, stubby, clr, incl	1.2	36	0.34	0.6	561	2827.7	7.7	2831.2	3.6	2833.7	2.4	0.3	0.91891
2	dwd5198	1 Ab zr, stubby, clr	0.6	42	0.37	0.3	676	2835	12	2834.2	5.2	2833.3	1.9	-0.1	0.97632
3	dwd5257	1 Ab zr, stubby clr-brn	0.9	169	0.34	0.4	2755	2812.6	6.4	2823.8	2.9	2831.8	1.5	0.8	0.95837
4	dwd5213	1 Ab zr, stubby, no incl	0.3	68	0.35	0.2	917	2831	15	2831.2	6.2	2831.6	2.4	0.0	0.97343
5	dwd5258	1 Ab zr, clr	0.4	65	0.34	0.5	361	2826	12	2829.1	5.5	2831.2	3.0	0.2	0.94971
6	dwd5197	1 Ab zr, stubby, clr	1.1	61	0.24	0.2	1950	2823.6	9.9	2827.1	4.3	2829.7	1.6	0.3	0.97582
6	**PK06-1250**	**Birse Lake pluton (granodiorite)**													
1	dwd5209	1 Ab zr, brn prism	2.0	181	0.49	0.4	6541	2718.2	5.4	2720.8	2.5	2722.8	1.7	0.2	0.92818
2	dwd5210	1 Ab zr, brn, eq, incl	2.6	122	0.55	0.5	4226	2711.5	5.5	2718.6	2.6	2723.8	1.4	0.6	0.95527
3	dwd5211	1 Ab zr, brn, eq, incl	2.5	109	0.53	0.5	3268	2722.4	4.4	2723.1	2.2	2723.7	1.4	0.1	0.93224
4	dwd5212	1 Ab zr, brn, eq, incl	2.0	145	0.56	0.2	8474	2729.3	4.9	2725.4	2.4	2722.5	1.3	-0.3	0.95575

Table 4: Results of isotope dilution–thermal ionization mass spectrometry (ID-TIMS) analysis of rocks from the Bird River Belt. *(continued)*

No.	Analysis	Fraction	Wt. (µg)	U (ppm)	Th/U	Pb_{com} (pg)	$^{207}Pb/^{204}Pb$ meas.	$^{206}Pb/^{238}U$ age (Ma)	2σ	$^{207}Pb/^{235}U$ age (Ma)	2σ	$^{207}Pb/^{206}Pb$ Age (Ma)	2σ	Disc. (%)	ρ
7	**PK06-1197**	**Gabbro pegmatite**													
1	dwd5241	1 Ab zr frag, eq, brn-clr, incl	5.8	158	0.54	2.6	2218	2716.6	5.2	2720.3	2.6	2723.1	1.4	0.3	0.95558
2	dwd5242	1 Ab rnd zr, eq, clr	3.6	339	0.47	1.7	4583	2717.5	5.5	2720.8	2.6	2723.3	1.3	0.3	0.96007
3	dwd5243	1 Ab rnd zr, stubby, brn, crk	4.5	268	0.45	1.3	6087	2718.5	5.1	2720.9	2.5	2722.7	1.3	0.2	0.95484
8	**MD07-2679**	**Syn-shear granite**													
1	dwd5355	1 CA zr, etched out zone	1	92	0.03	0.4	1497	2753.0	5.6	2716.6	2.6	2689.6	2.1	-2.9	0.87992
2	dwd5356	2 CA zr etched out zone	1	551	0.02	0.6	5965	2764.9	6.4	2717.4	2.9	2682.3	1.8	-3.8	0.93039
3	dwd5359	1 Ab monazite gr, incls	1.2	2658	15.47	21.4	824	2631.5	4.6	2664.7	2.4	2689.9	1.7	2.6	0.91432
4	dwd5318	1 monazite, euh, clr	2.2	6618	10.14	8.6	8876	2675.3	4.6	2681.6	2.3	2686.4	1.3	0.5	0.95262
5	dwd5358	1 monazite gr, clr, crk	1.4	2345	17.01	1.0	20495	2679.4	4.6	2682.3	2.3	2684.4	1.3	0.2	0.95151
6	dwd5360	1 Ab monazite gr, clr	1.8	2728	10.73	6.9	4357	2681.5	4.6	2683.1	2.3	2684.4	1.4	0.1	0.94404
7	dwd5319	1 monazite, euh, clr, incl	2.0	7053	16.16	44.6	1639	2676.3	5.2	2680.6	2.6	2683.8	1.5	0.3	0.94986
8	dwd5357	1 monazite gr, clr, euh	1.4	2913	16.88	3.2	7807	2675.6	5.4	2678.8	2.6	2681.3	1.3	0.3	0.96509
9	dwd5320	1 Ab monazite, incl, cloudy	10.1	6132	11.50	134.2	2340	2655	35	2665	15	2671.6	1.4	0.7	0.99864
9	**PK05-1050**	**Granitoid pegmatite, shear-zone hosted, columbite**													
1	dwd5275	1 flat crystal	24	1095	0.01	24.9	5160	2581.9	4.7	2619.8	2.4	2649.2	1.4	3.1	0.95223
2	dwd5286	1 frag, leached	15	79	0.01	2.9	2243	2642.7	5.9	2645.3	2.8	2647.4	1.6	0.2	0.94480
3	dwd5274	1 flat crystal	36	619	0.01	11.4	9469	2554.3	6.8	2601.3	3.3	2638.2	1.3	3.8	0.97694
10	**PK06-1251**	**Granitoid pegmatite, post-shear, columbite**													
1	dwd5285	1 fresh frag, leached	58	62	-0.00	3.8	5156	2603.8	5.0	2634.8	2.5	2658.8	1.4	2.5	0.95230
2	dwd5284	1 fresh frag, leached	85	38	0.00	10.9	1527	2646.4	7.0	2646.5	3.3	2646.7	1.4	0.0	0.97041
3	dwd5279	1 frag	11	155	0.00	9.0	898	2475.5	5.1	2559.9	2.6	2627.5	1.8	7.0	0.92701
4	dwd5276	1 frag	148	59	0.00	8.3	5335	2614.6	5.3	2619.4	2.6	2623.1	1.4	0.4	0.95289
5	dwd5277	1 frag	143	71	0.00	60.7	590	1963.1	3.5	2301.9	2.4	2618.0	2.2	28.9	0.86301
6	dwd5278	1 frag	57	138	0.01	114.9	246	2002.4	3.5	2290.0	3.2	2557.6	4.6	25.2	0.62744

Fractions are ordered from highest to lowest $^{207}Pb/^{206}Pb$ age
Abbreviations in 'Fraction' column: zr, zircon grain; CA, chemical abrasion; Ab, air abrasion; lpr, long prism; spr, short prism; equ, equant; frag, fragment; clr, clear, colourless; rnd, rounded; brn, brownish; str etch, strongly etched after CA; pop, zircon population; crk, cracked
Pb_{com} - common Pb assuming the isotopic composition of laboratory blank
206/204 - 18.221; 207/204 - 15.612; 208/204 - 39.360 (errors of 2%)
Th/U calculated from radiogenic $^{208}Pb/^{206}Pb$ ratio and $^{207}Pb/^{206}Pb$ age assuming concordance
Disc. - percent discordance for the given $^{207}Pb/^{206}Pb$ age
ρ - error correlation coefficient
Uranium decay constants from Jaffey et al. (1971)

Table 5: Results of Pb-Pb isotope analysis of rocks from the Bird River Belt.

No.	Analysis	Fraction	Wt. (µg)	U (ppm)	Th/ U	Pb_{tot} (pg)	$^{208}Pb/^{204}Pb$	2σ	$^{206}Pb/^{204}Pb$	2σ	$^{207}Pb/^{204}Pb$	2σ	ρ
5	**MD07-2622**	**MD07-2622 Maskwa Lake Batholith tonalite:**											
7	dwd5316	Apatite, clear rods, subhedral	0.3	34	0.66	6359	227.06	1.18	1085.83	5.11	207.66	1.01	0.98524
8	dwd5317s	Plagioclase, HF leach solution	0.5	0.16	0.00	3639	34.041	0.165	14.541	0.058	14.902	0.045	0.60447
				Corrected for U decay since 2650 Ma:					13.911		14.789		
9	dwd5317p	Plagioclase, residue	0.5	0.01	0.00	1548	33.759	0.110	14.293	0.025	14.858	0.036	0.97437
				Corrected for U decay since 2650 Ma:					14.163		14.835		

ρ - error correlation coefficient

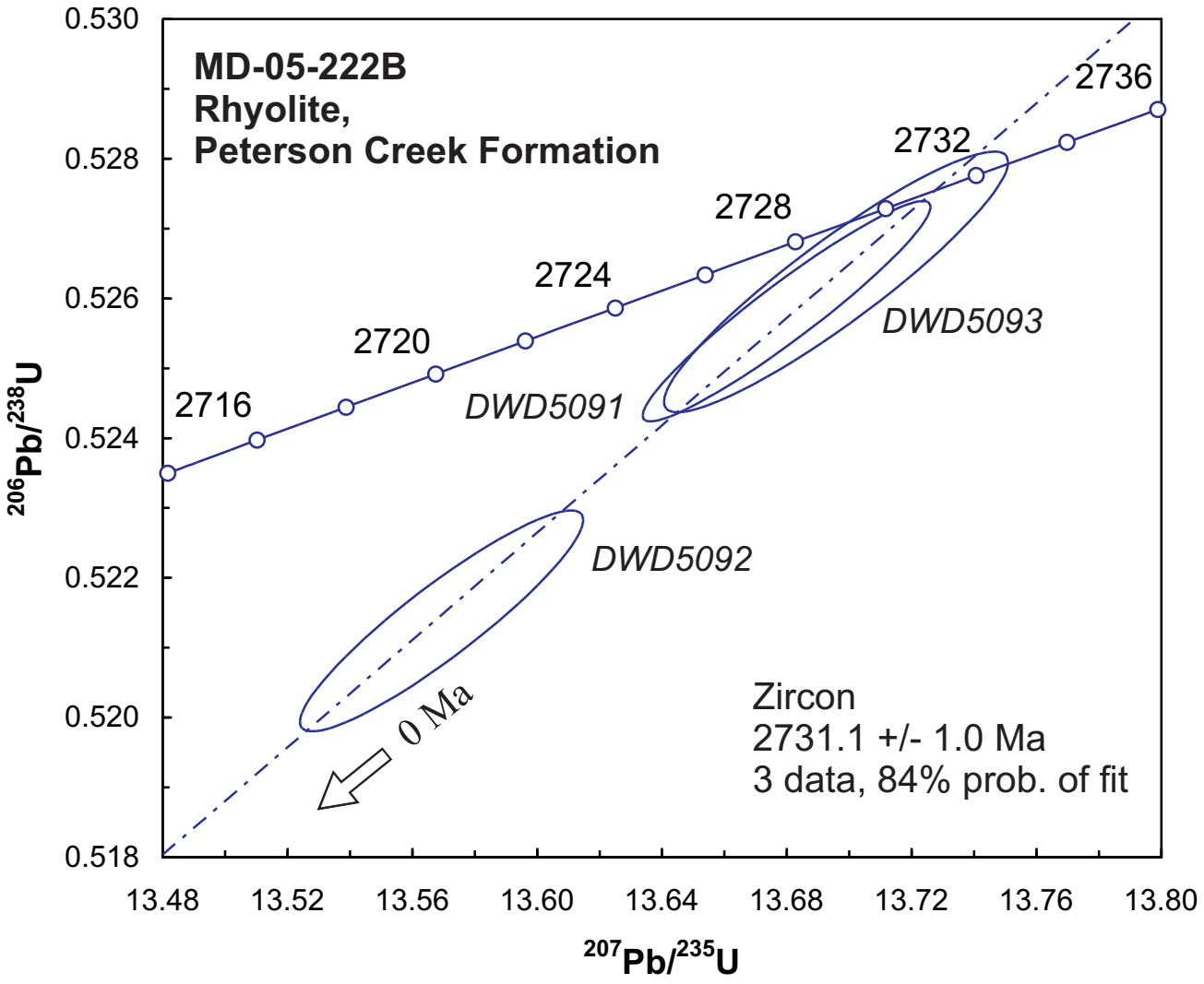

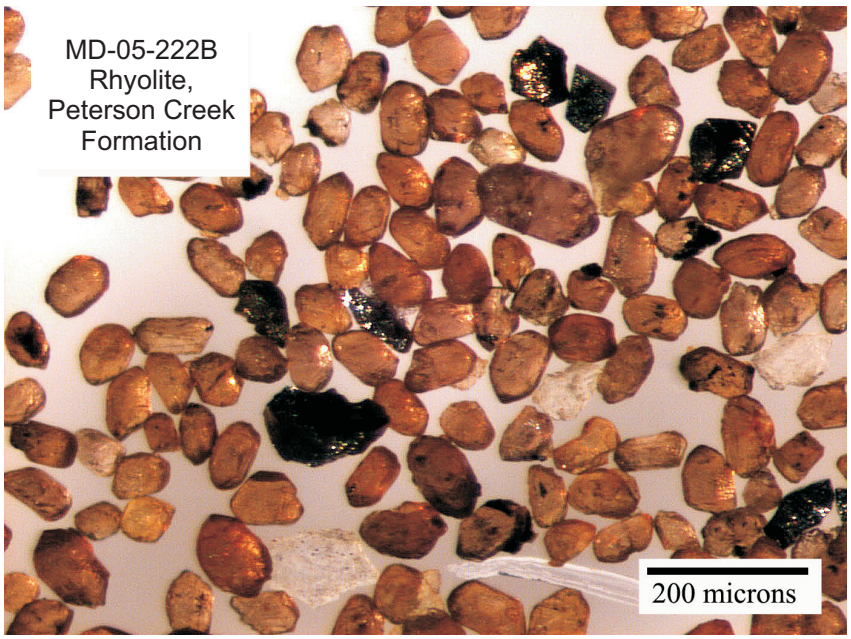

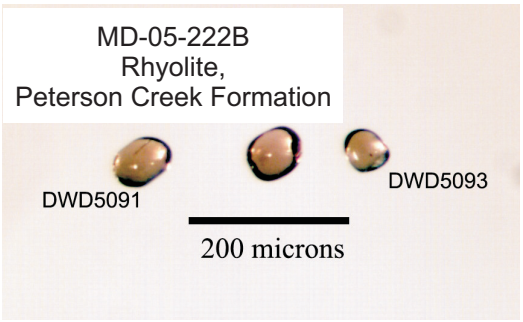

Figure 14: a) *U-Pb concordia diagram of isotope dilution–thermal ionization mass spectrometry (ID-TIMS) age data on zircon in rhyolite from the Peterson Creek Formation (sample MD-05-222B). Photomicrograph in lower left part of figure shows least magnetic, zircon-rich heavy mineral population, from which three zircon crystals (photomicrograph in lower right part of figure) were hand-picked for U-Pb dating.*

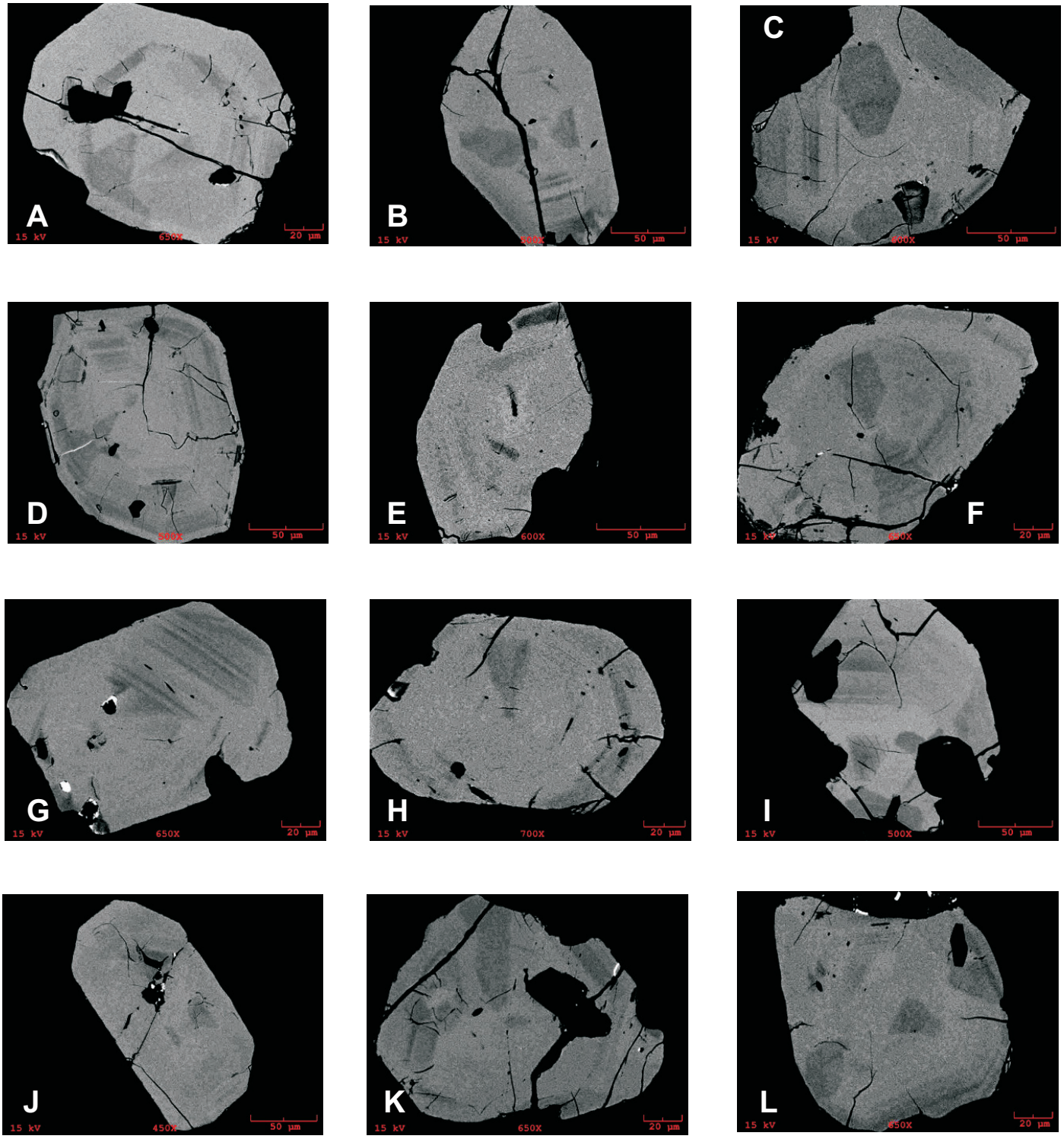

Figure 14: b) *Scanning electron microscope backscatter images of zircon from the Peterson Creek Formation rhyolite (sample MD-05-222B).*

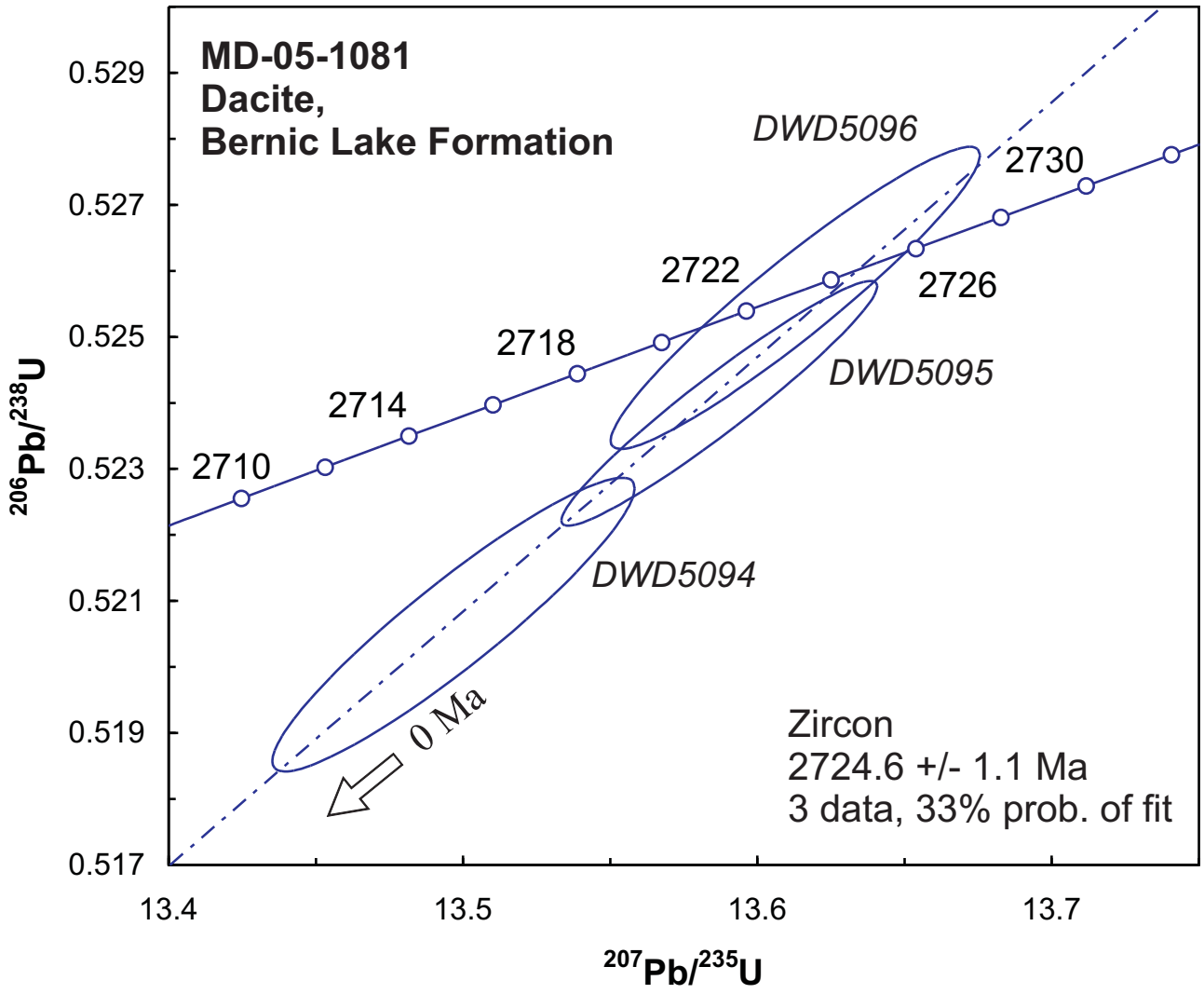

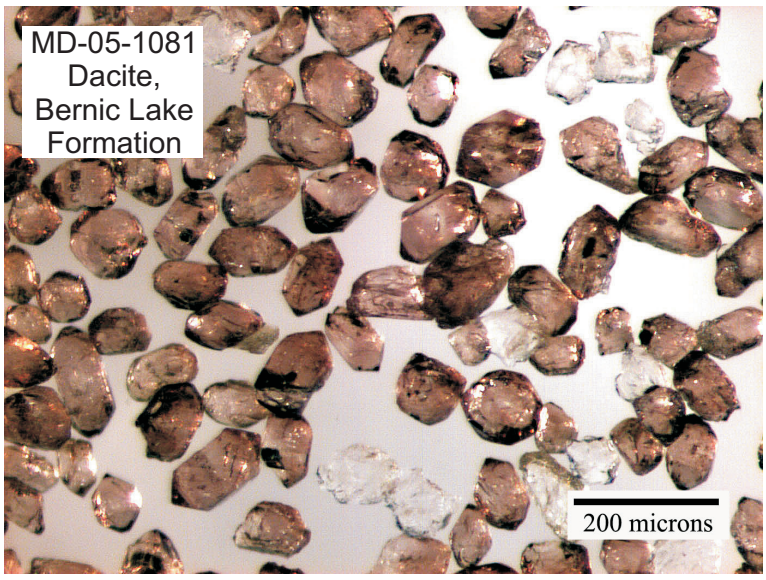

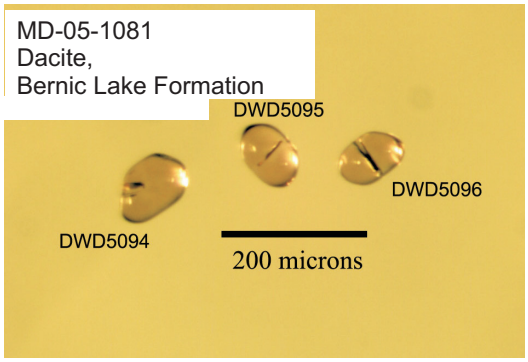

Figure 15: a) *U-Pb concordia diagram of isotope dilution–thermal ionization mass spectrometry (ID-TIMS) age data on zircon in dacite from the Bernic Lake Formation (sample MD-05-1081). Photomicrograph in lower left part of figure shows least magnetic, zircon-rich heavy mineral population, from which three zircon crystals (photomicrograph in lower right part of figure) were hand-picked for U-Pb dating.*

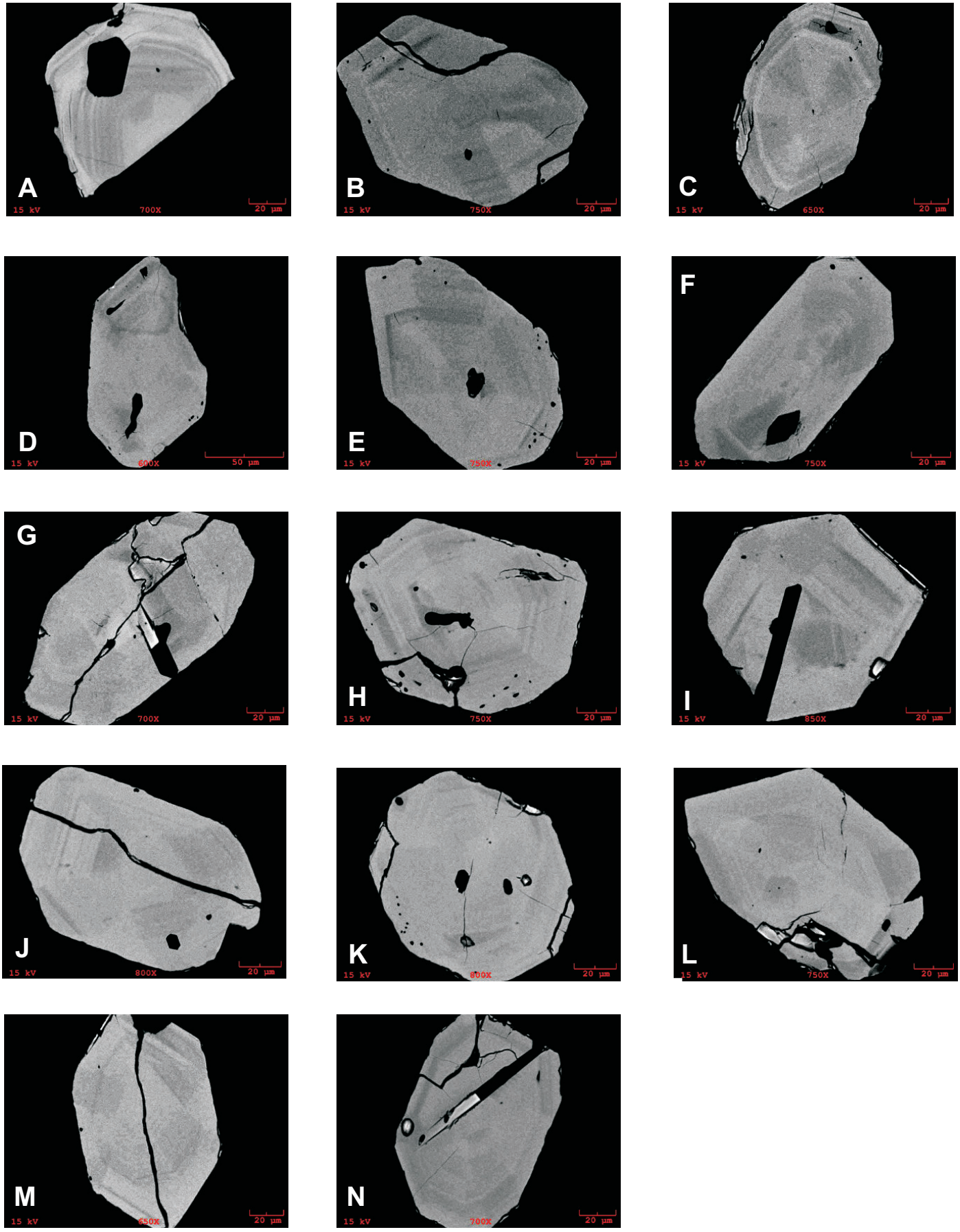

Figure 15: b) *Electron-microprobe backscatter images of zircons from the Bernic Lake Formation dacite (sample MD-05-1081).*

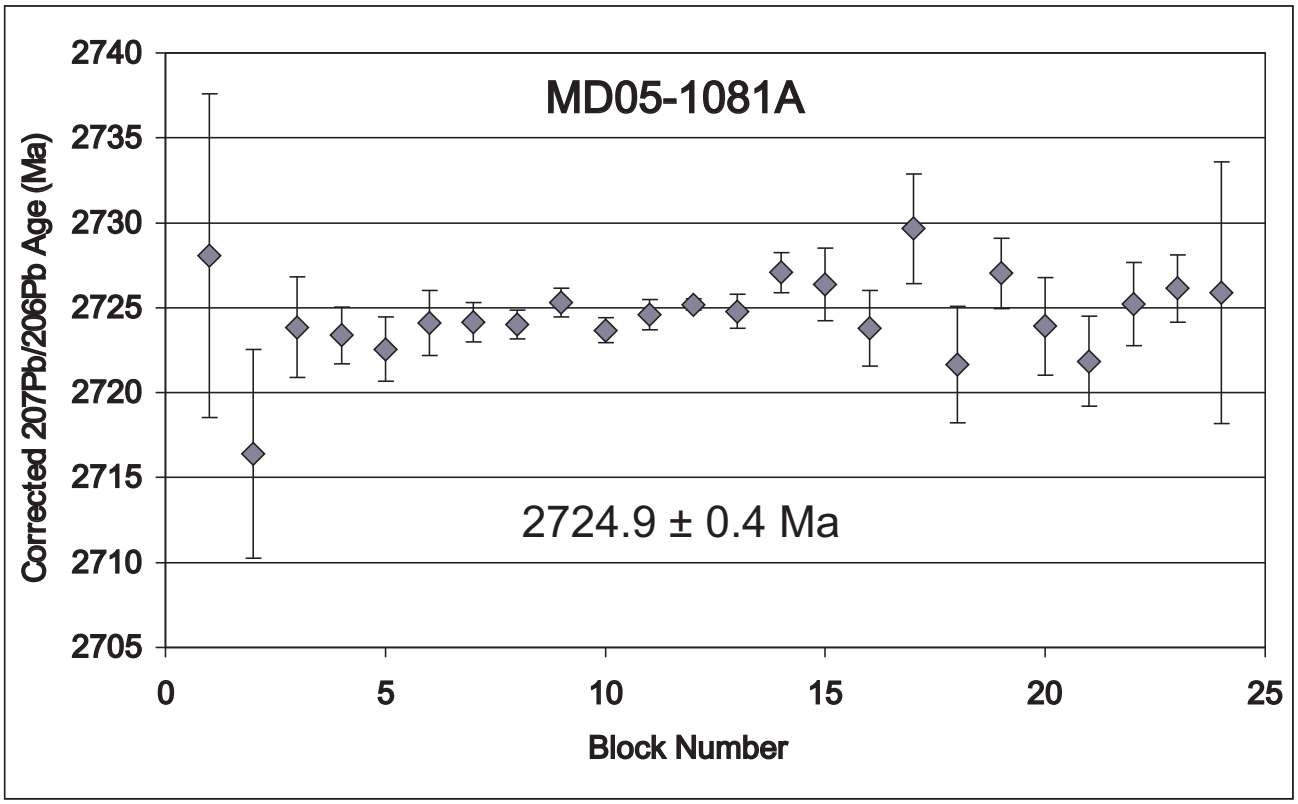

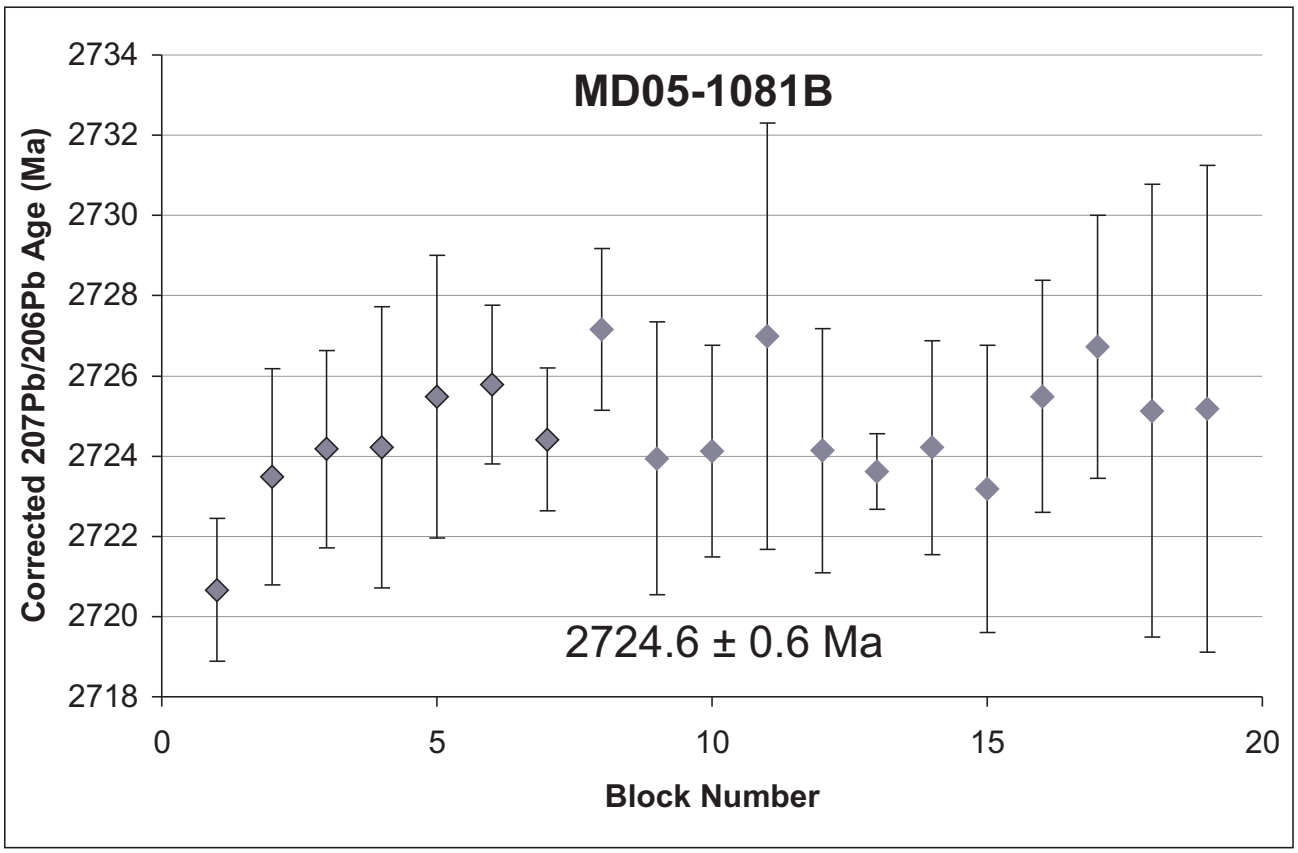

Figure 15: c) *Progression of corrected $^{207}Pb/^{206}Pb$ ages during TE-TIMS data collection on two zircon grains from the Bernic Lake Formation dacite (sample MD-05-1081).*

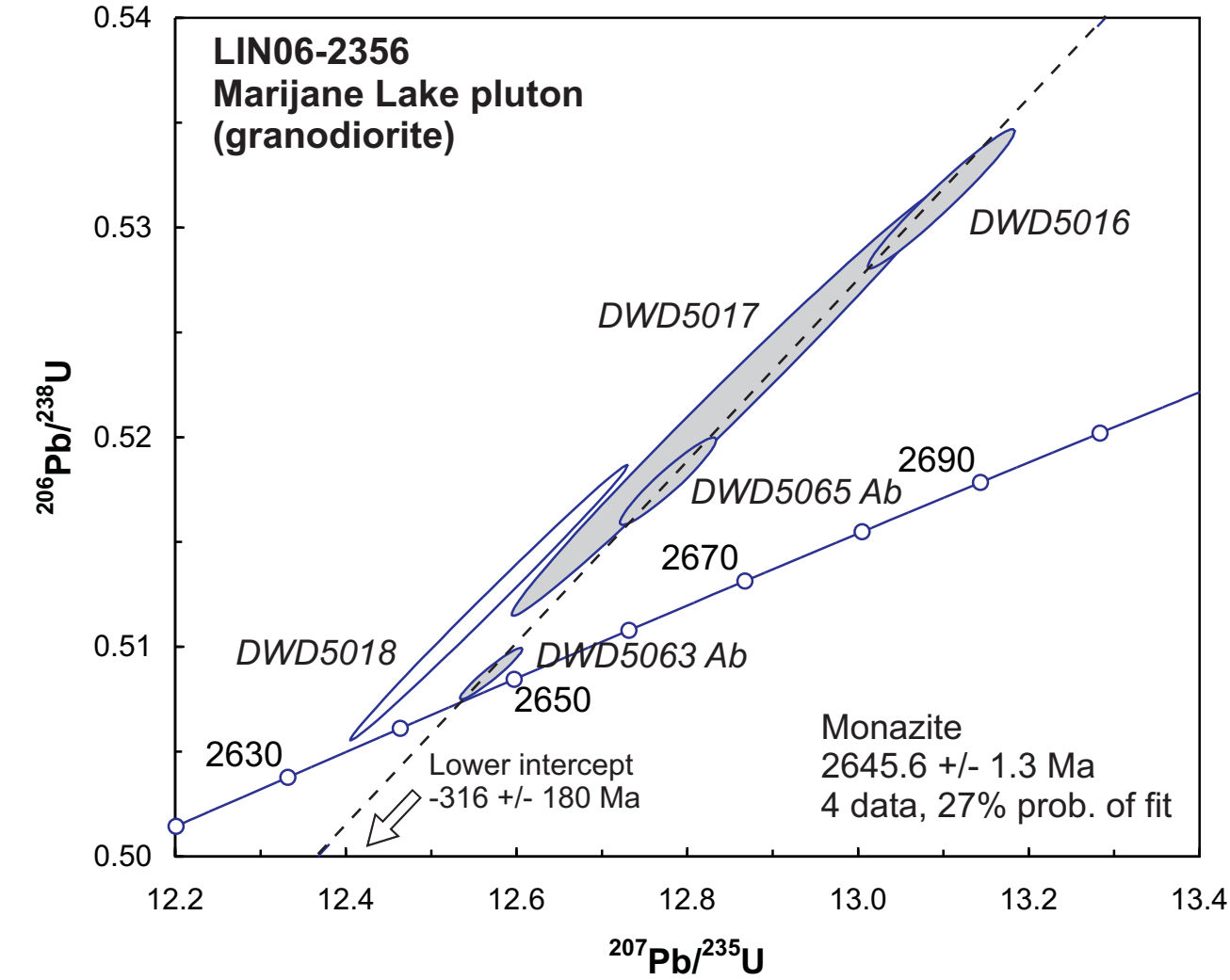

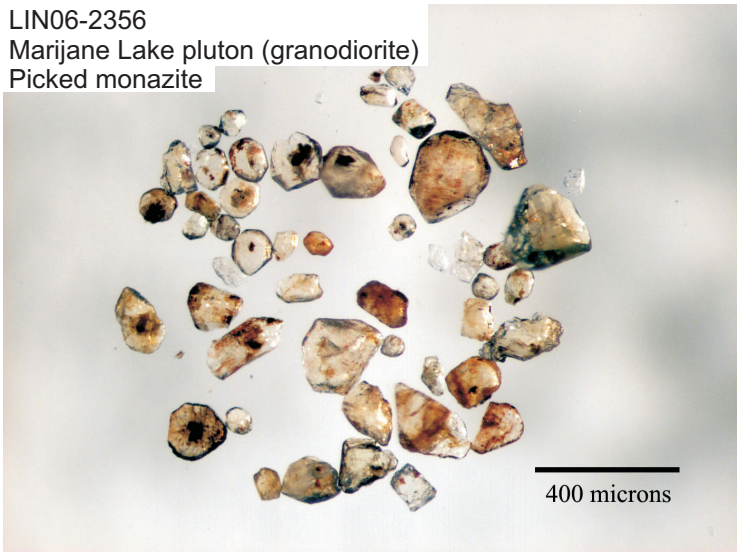

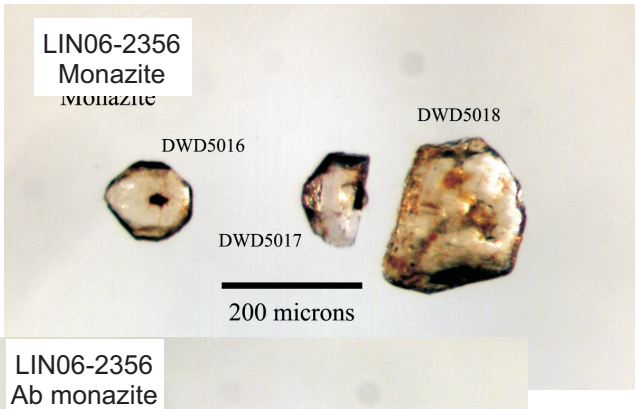

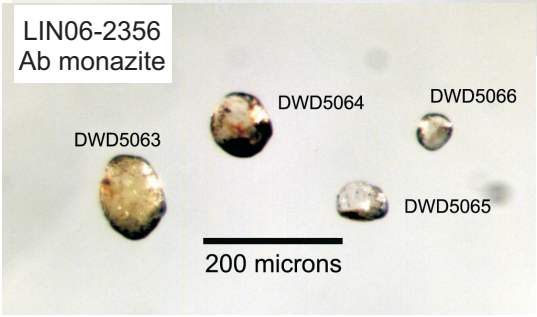

Figure 16: *U-Pb concordia diagram of isotope dilution–thermal ionization mass spectrometry (ID-TIMS) age data on monazite in granodiorite from the Marijane Lake pluton (sample LIN06-2356). Photomicrograph in lower left part of figure shows hand-picked monazite, of which seven single crystals (photomicrograph in lower right part of figure) were selected for U-Pb dating.*

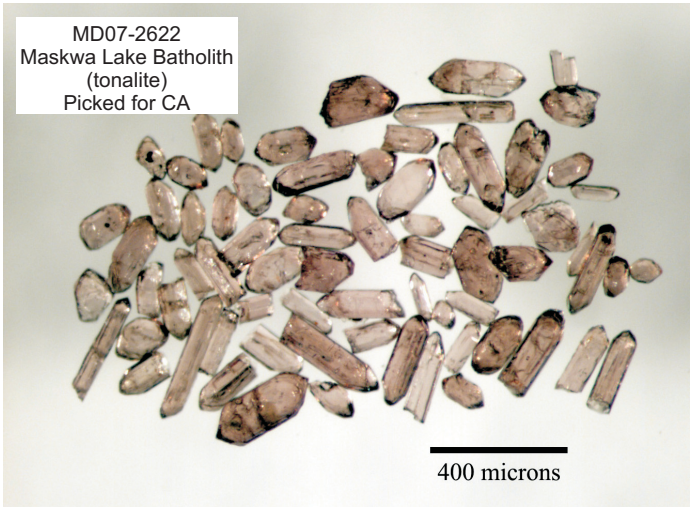

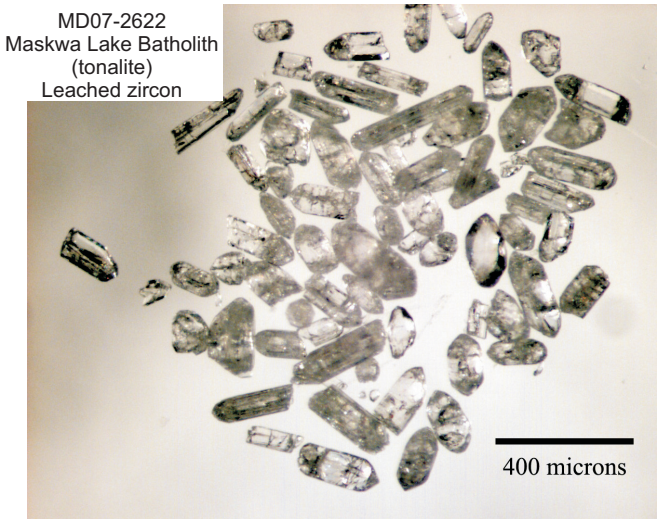

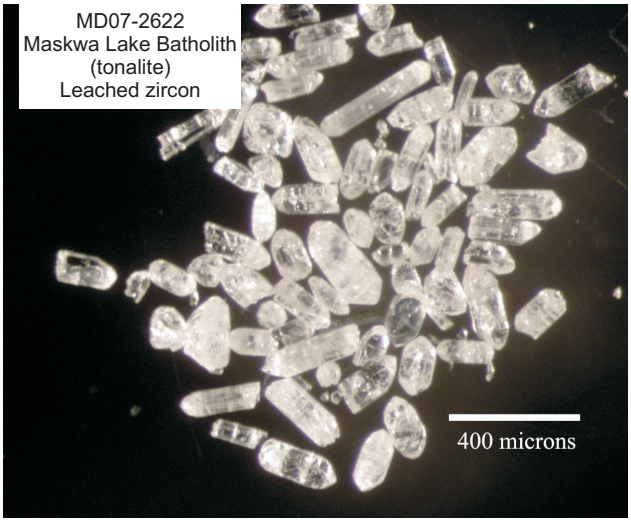

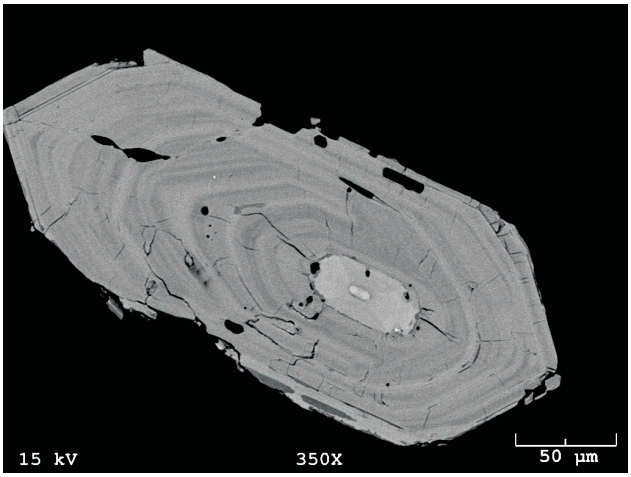

Figure 17: a) *Photomicrographs of picked zircon before and after annealing followed by HF leaching along with electron-microprobe backscatter images of unannealed zircon in tonalite from the Maskwa Lake Batholith (sample MD07-2622).*

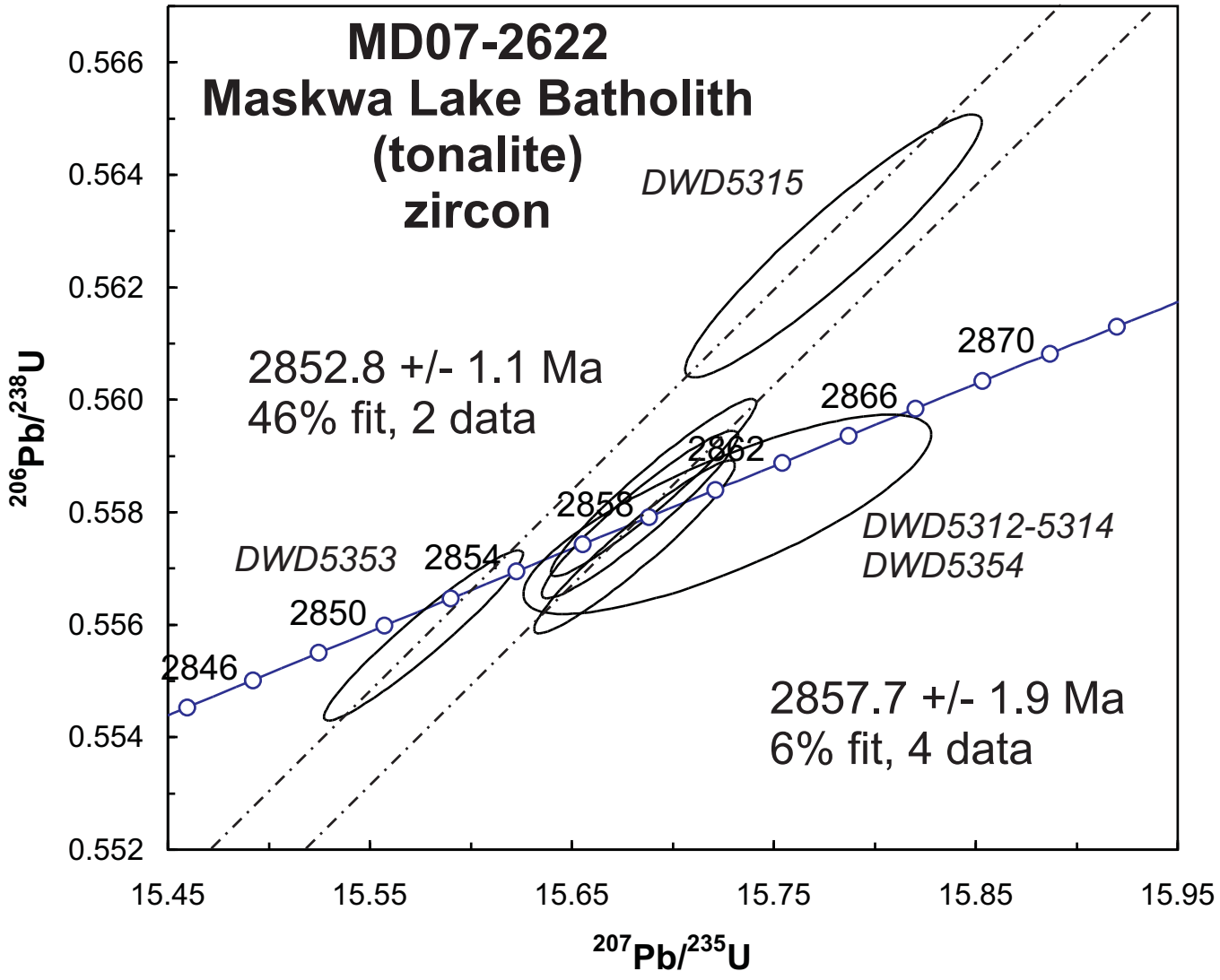

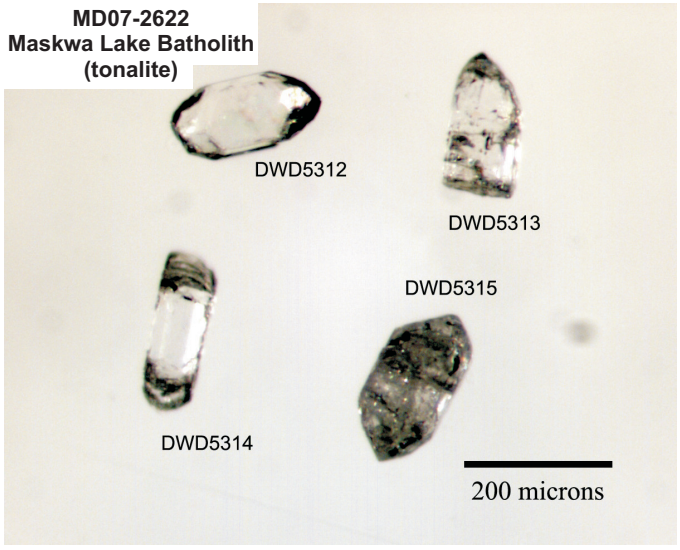

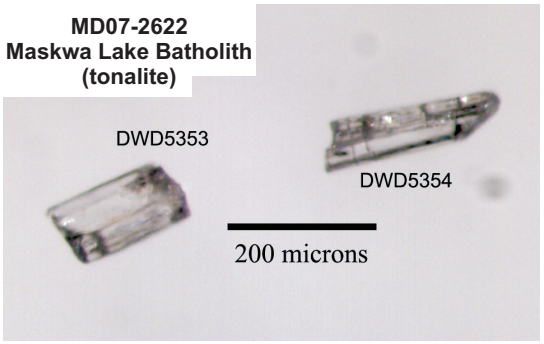

Figure 17: b) *U-Pb concordia diagram showing isotope dilution–thermal ionization mass spectrometry (ID-TIMS) age data on zircon in tonalite from the Maskwa Lake Batholith (sample MD07-2622). Photomicrographs in lower part of figure show six single zircon grains selected for U-Pb dating.*

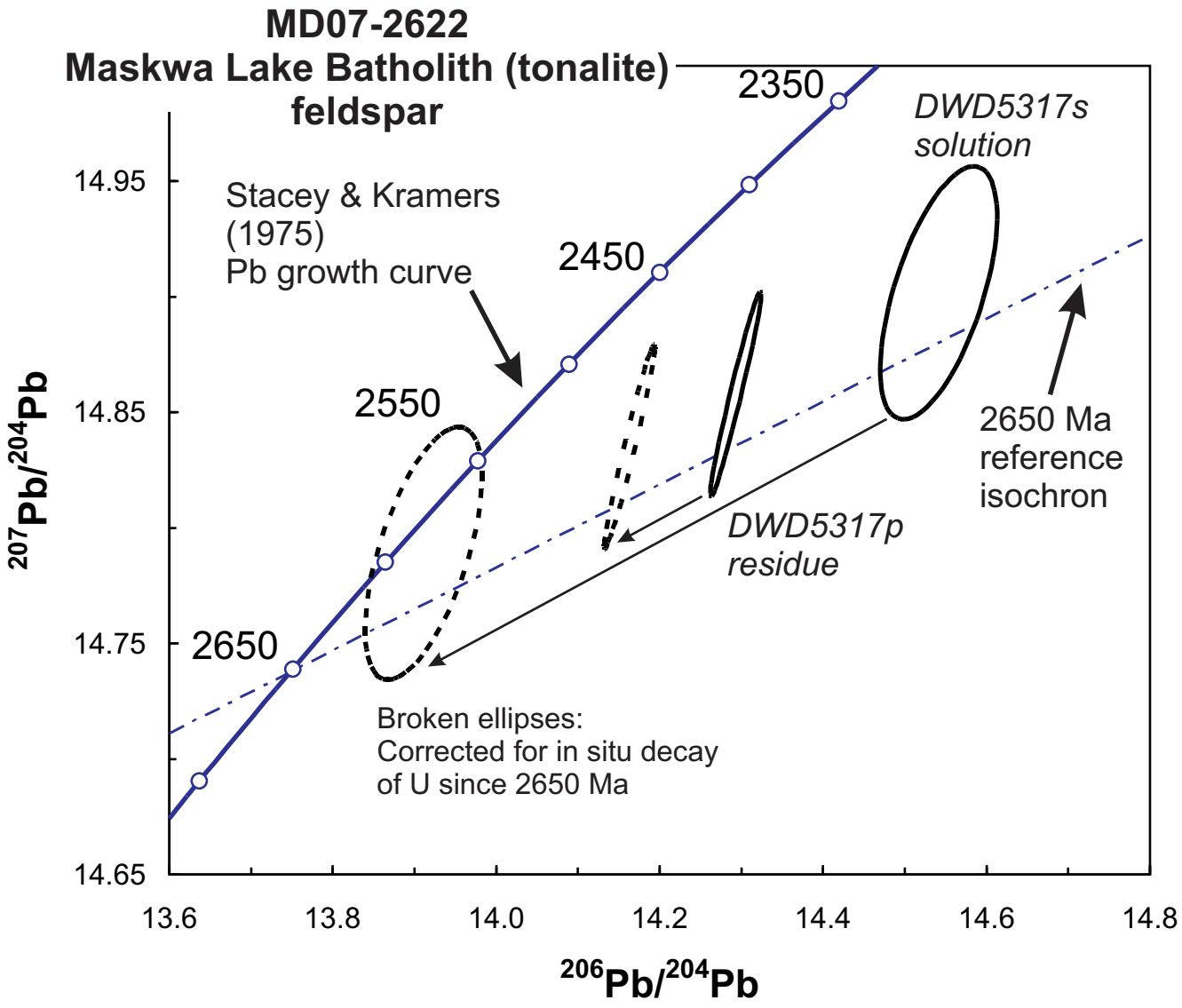

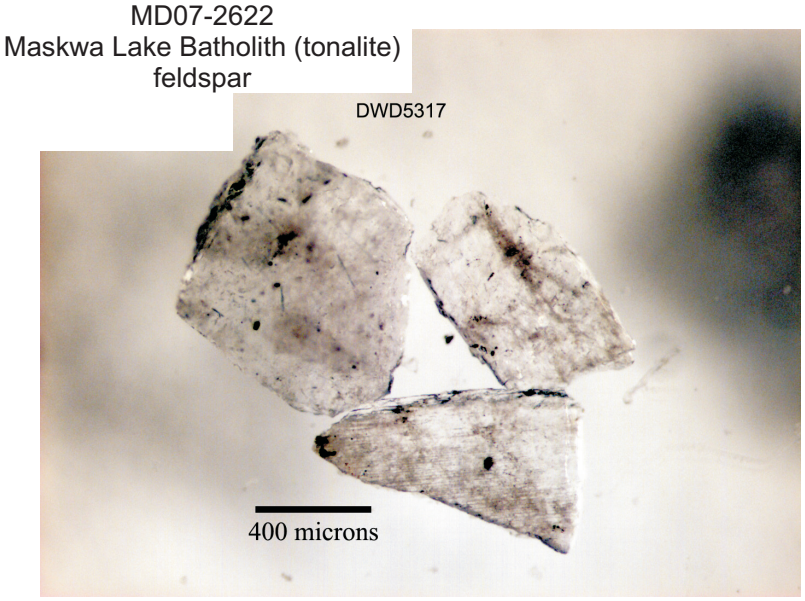

Figure 17: c) *Pb-Pb diagram showing isotope dilution–thermal ionization mass spectrometry (ID-TIMS) data on feldspar in tonalite from the Maskwa Lake Batholith (sample MD07-2622). Photomicrograph in lower part of figure shows feldspar fragments selected for U-Pb isotopic analysis.*

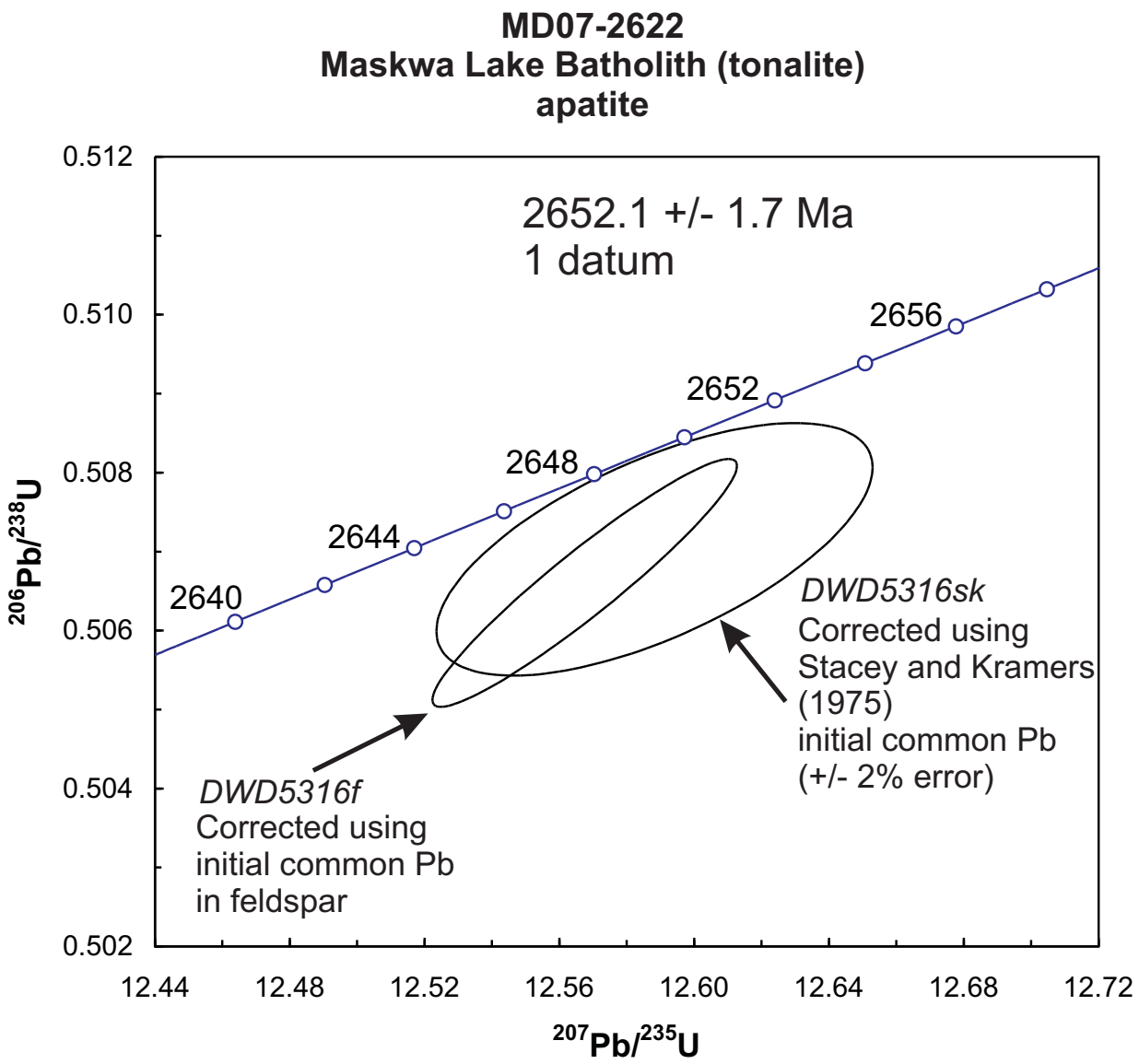

Figure 17: d) *U-Pb concordia diagram of isotope dilution–thermal ionization mass spectrometry (ID-TIMS) age data on apatite in tonalite from the Maskwa Lake Batholith (sample MD07-2622). Photomicrograph in lower part of figure shows apatite crystals selected for U-Pb isotopic analysis.*

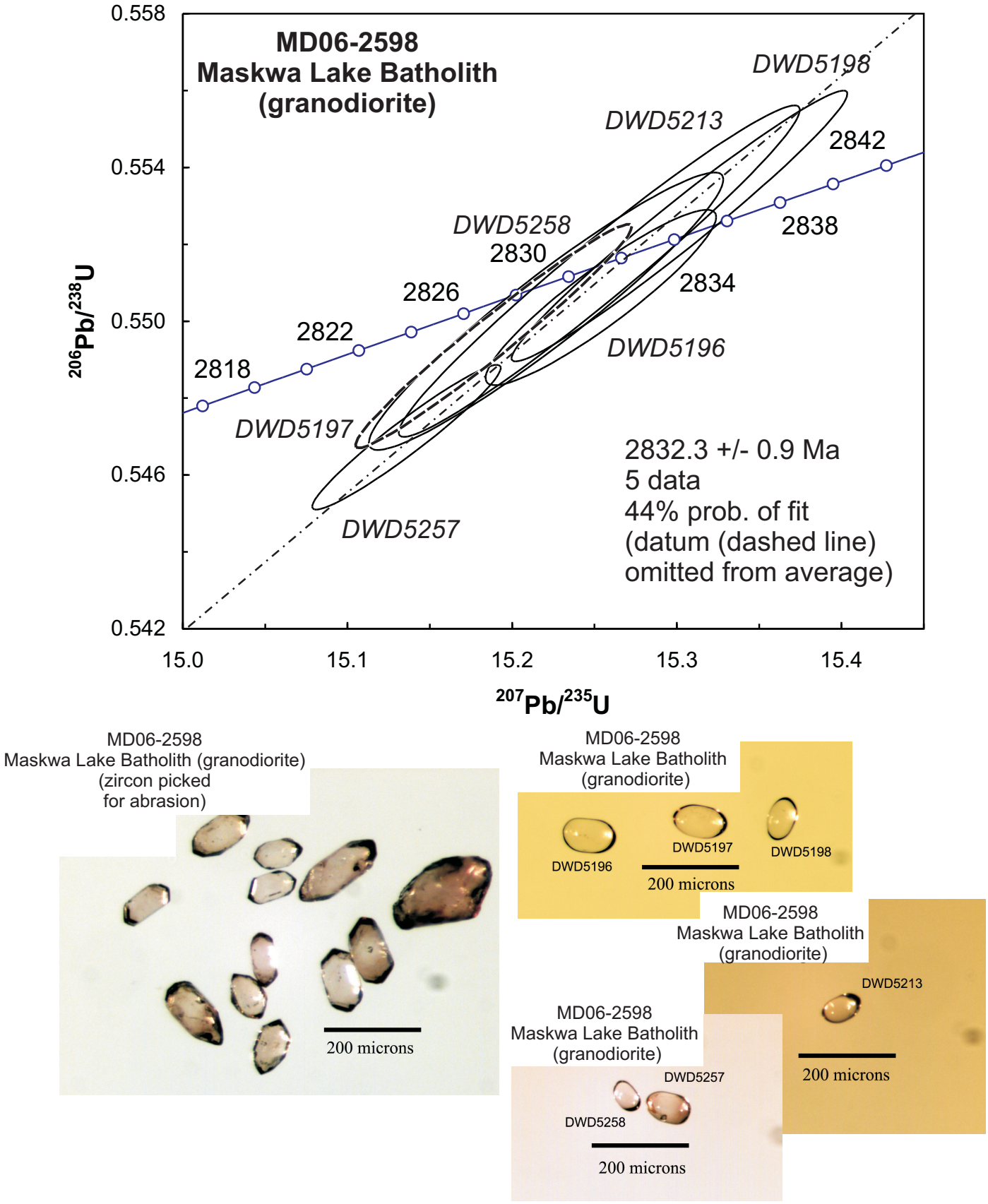

Figure 18: a) *U-Pb concordia diagram showing isotope dilution–thermal ionization mass spectrometry (ID-TIMS) age data on zircon in granodiorite from the Maskwa Lake Batholith (sample MD06-2598). Photomicrograph in lower left part of figure shows zircon crystals hand-picked for abrasion. Photomicrographs in lower right part of figure show six abraded zircon crystals selected for U-Pb dating.*

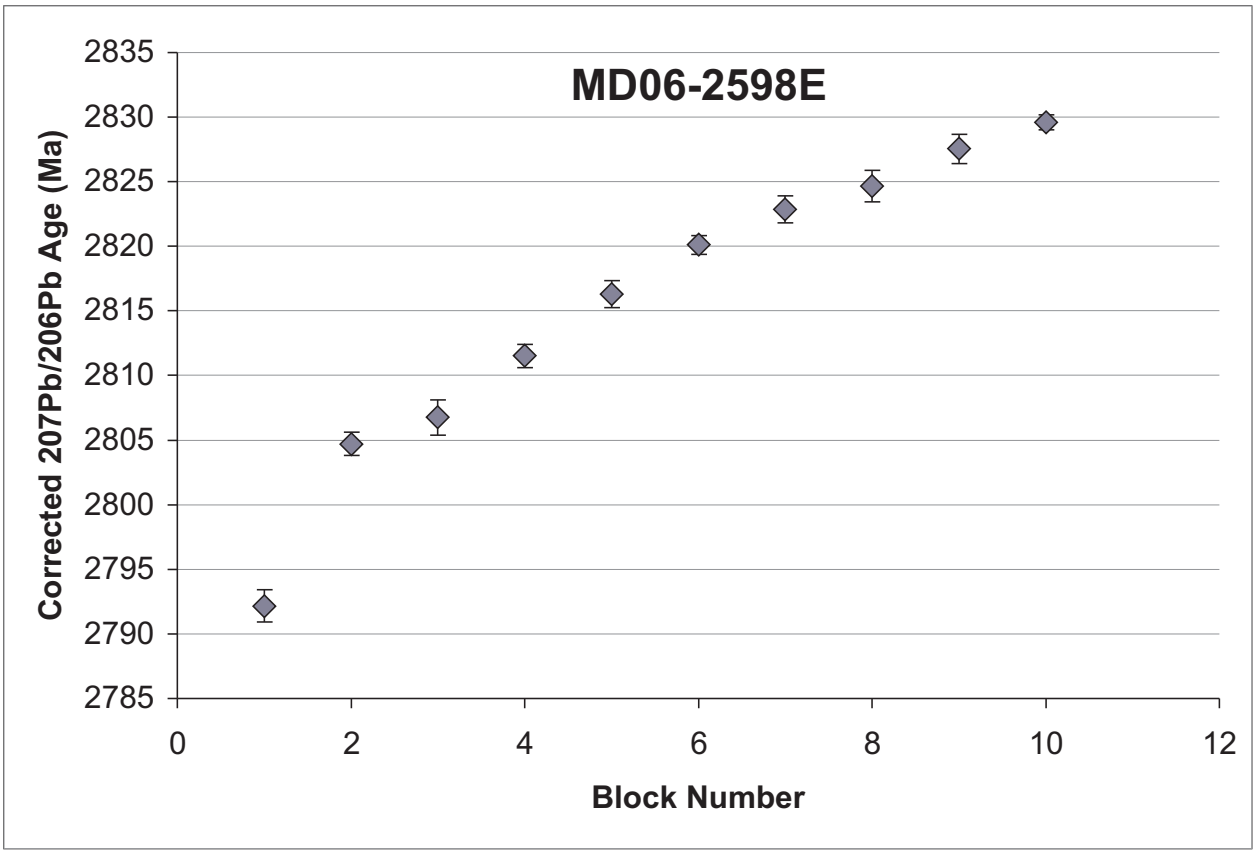

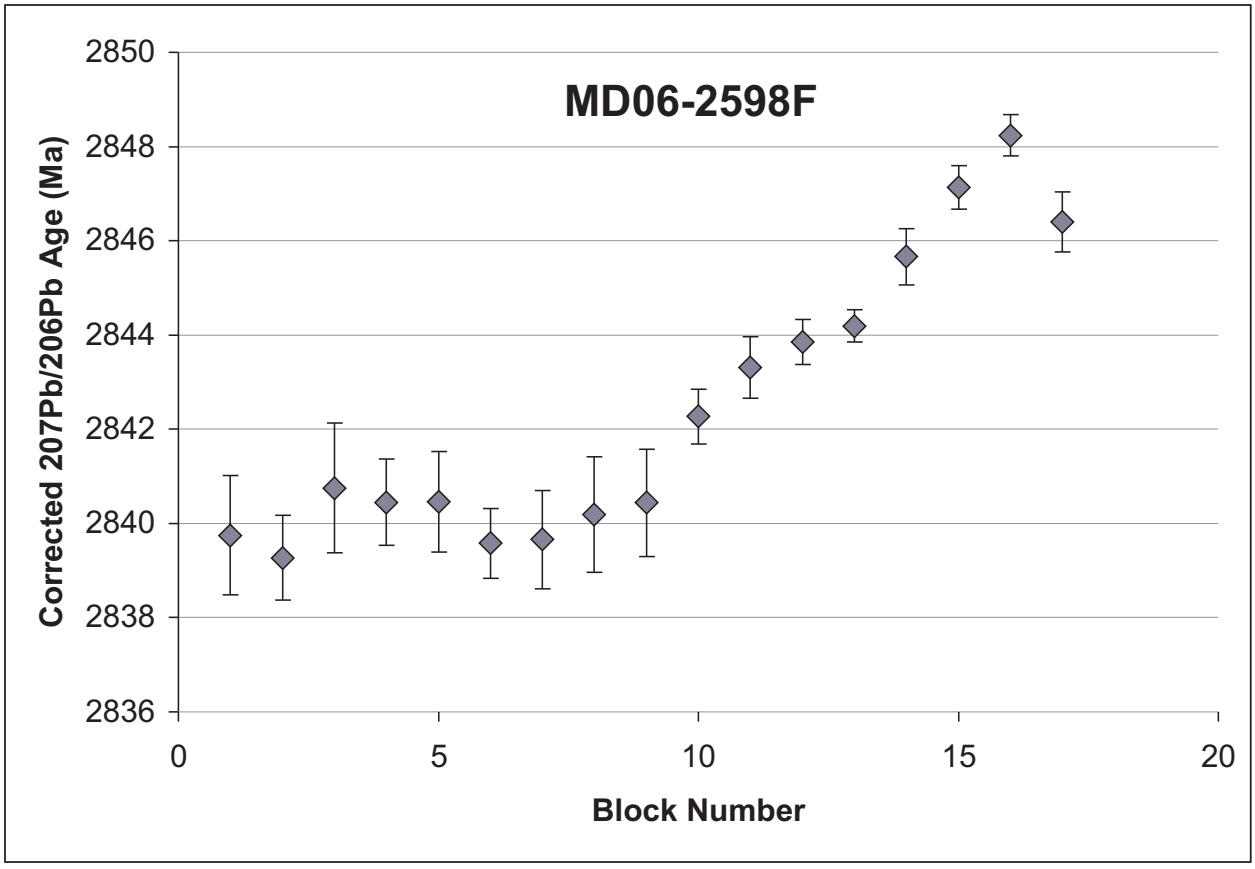

Figure 18: b) *Progression of corrected $^{207}Pb/^{206}Pb$ ages during TE-TIMS data collection on zircon in granodiorite from the Maskwa Lake Batholith (sample MD06-2598).*

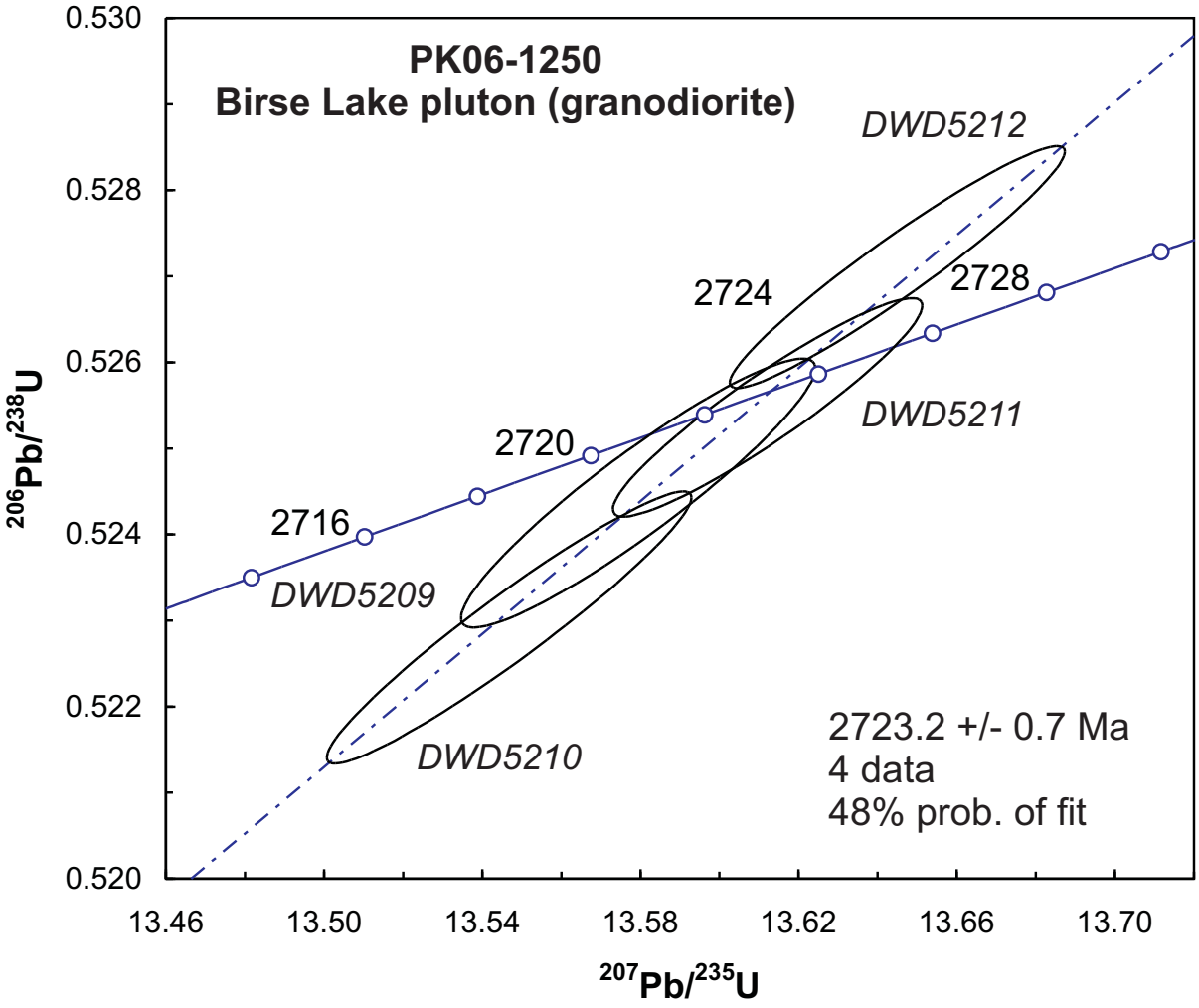

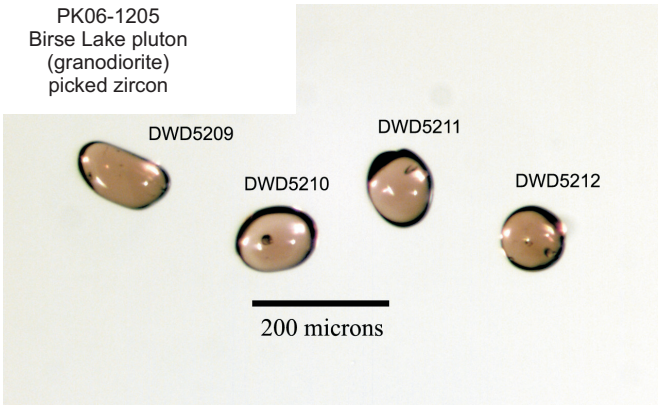

Figure 19: a) *U-Pb concordia diagram showing isotope dilution–thermal ionization mass spectrometry (ID-TIMS) age data on zircon in granodiorite from the Birse Lake pluton (sample PK06-1250). Photomicrograph in lower left part of figure shows zircon crystals hand-picked for abrasion. Photomicrograph in lower right part of figure shows four abraded zircon crystals selected for U-Pb dating.*

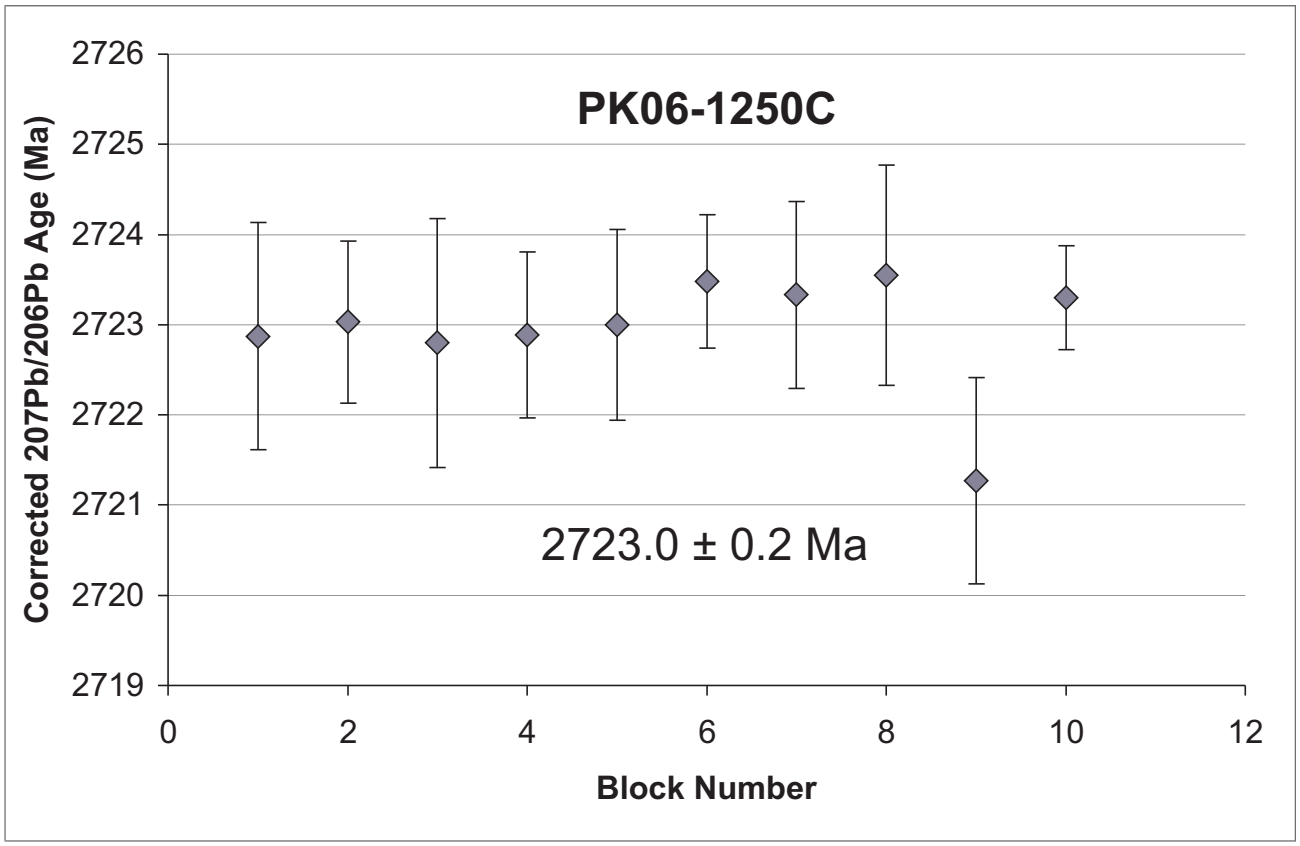

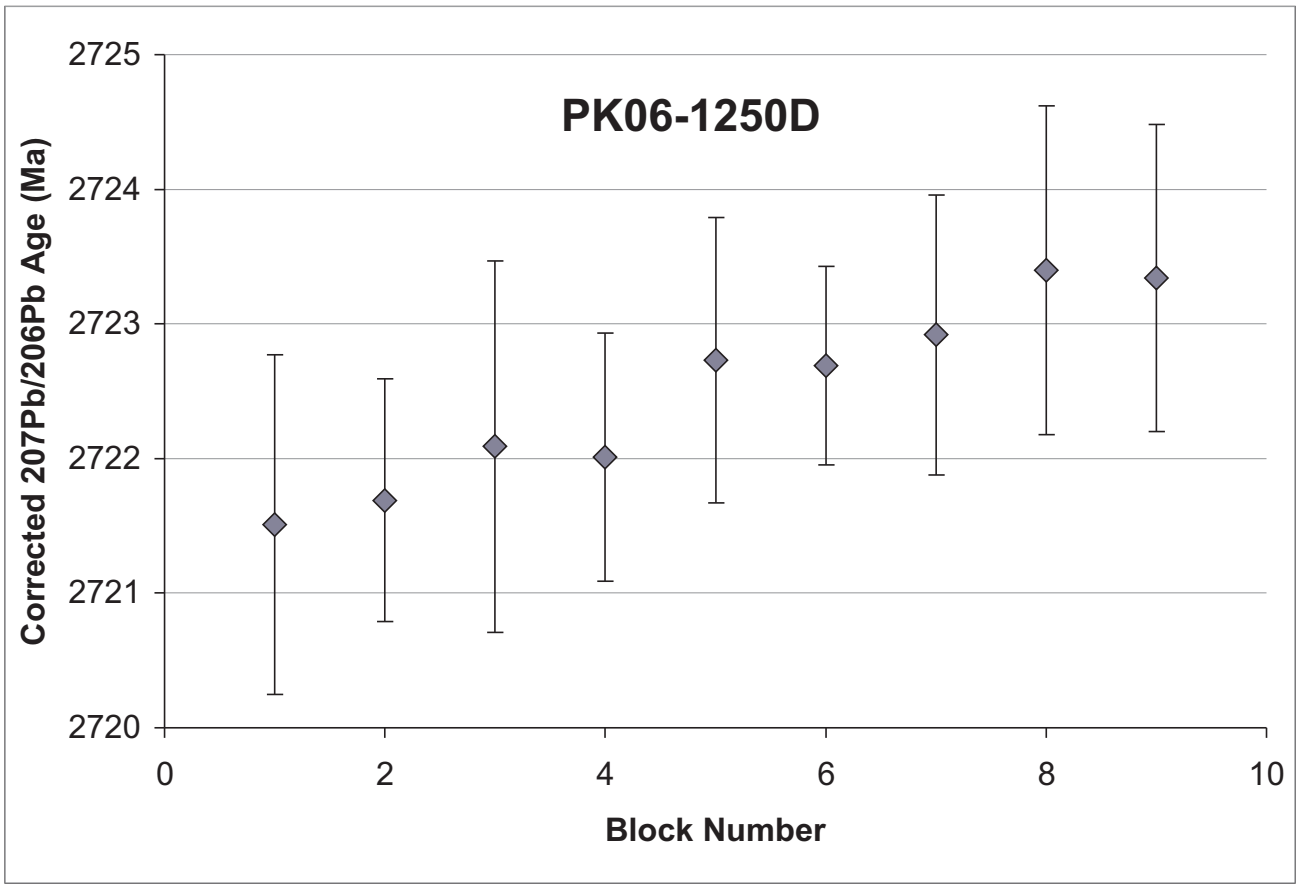

Figure 19: b) *Progression of corrected $^{207}Pb/^{206}Pb$ ages during TE-TIMS data collection on zircon in granodiorite from the Birse Lake pluton (sample PK06-1250).*

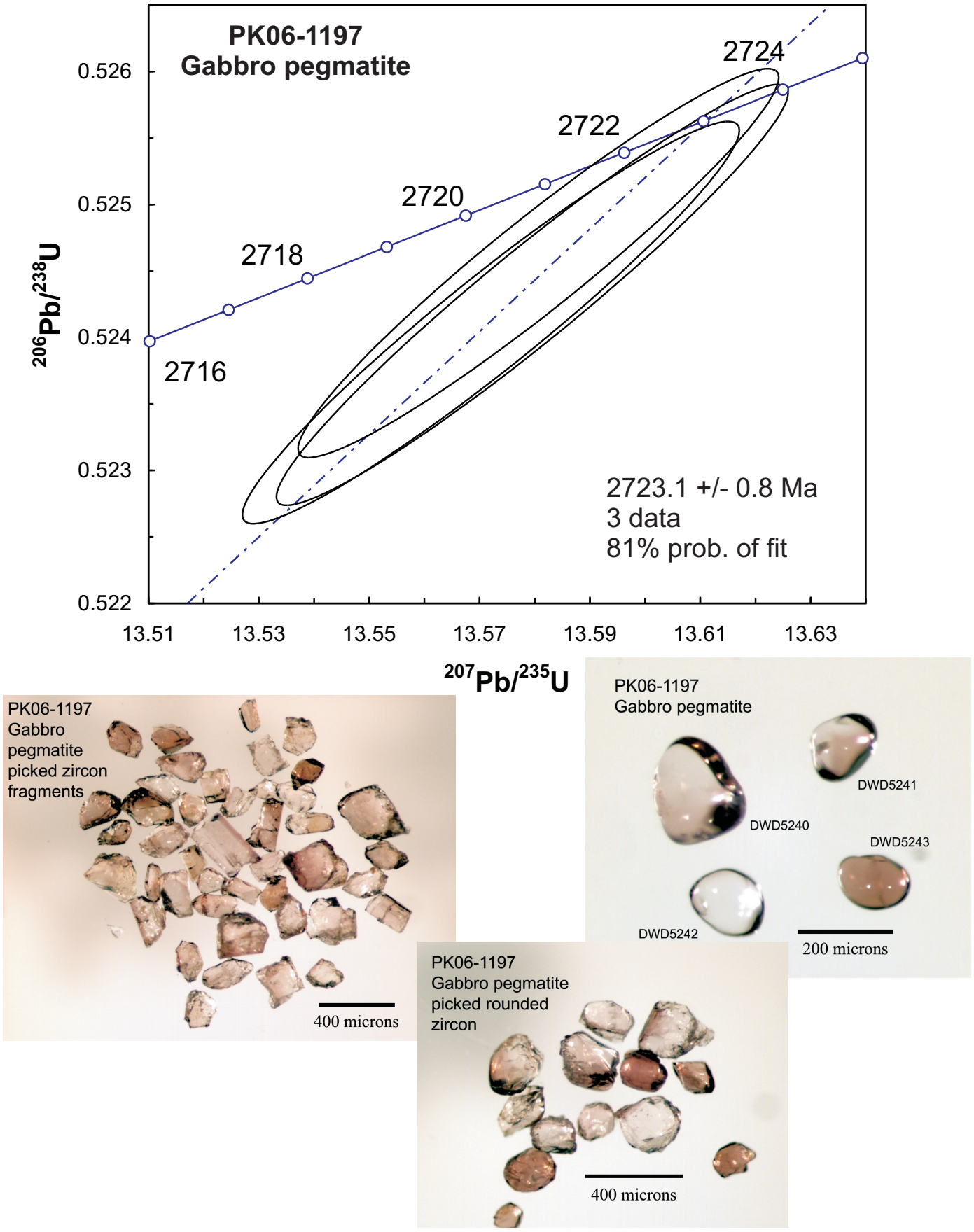

Figure 20: *U-Pb concordia diagram showing isotope dilution–thermal ionization mass spectrometry (ID-TIMS) age data on zircon in gabbro pegmatite (sample PK06-1197). Photomicrograph in lower left part of figure shows hand-picked zircon fragments, some of which were selected for abrasion and U-Pb dating (photomicrographs in lower right part of figure).*

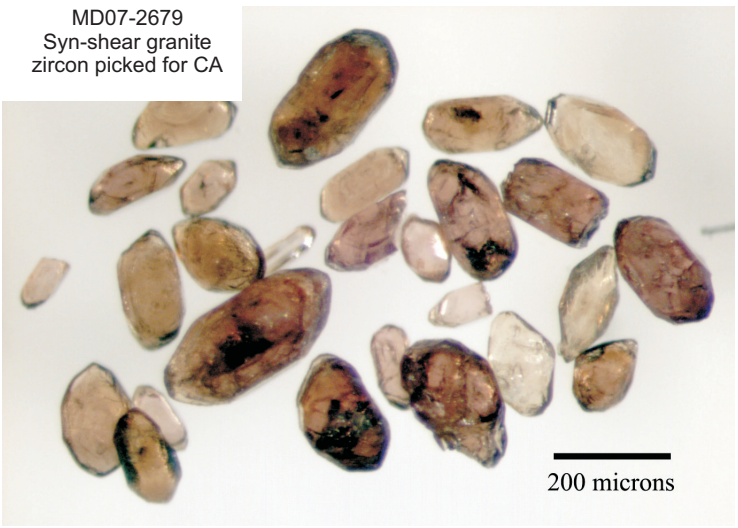

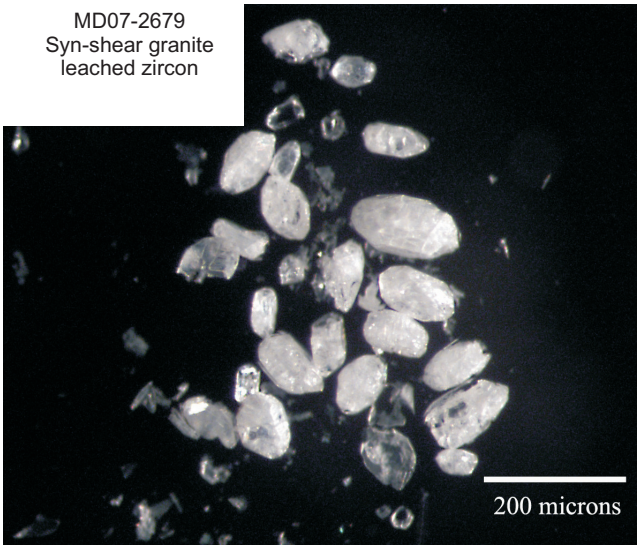

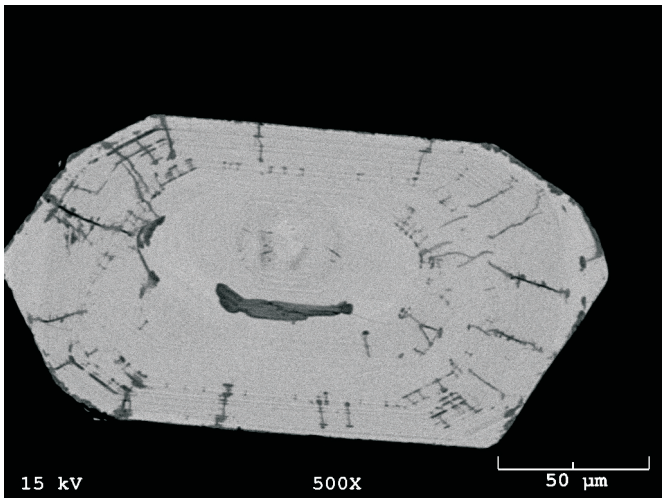

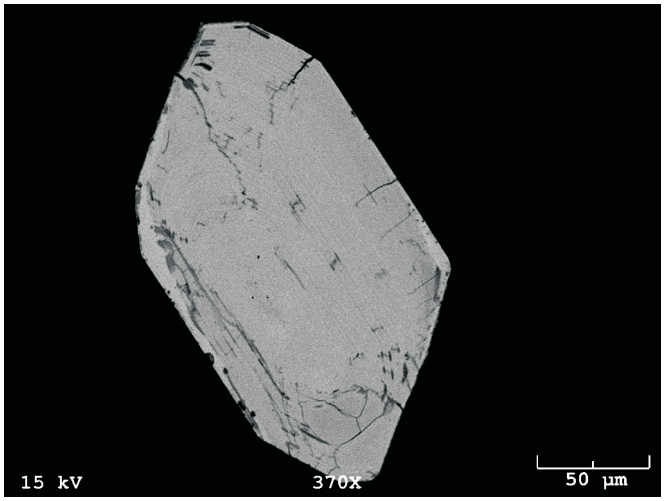

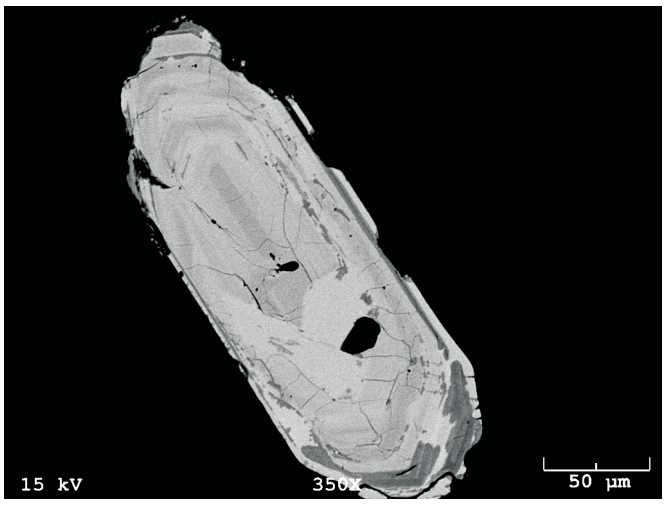

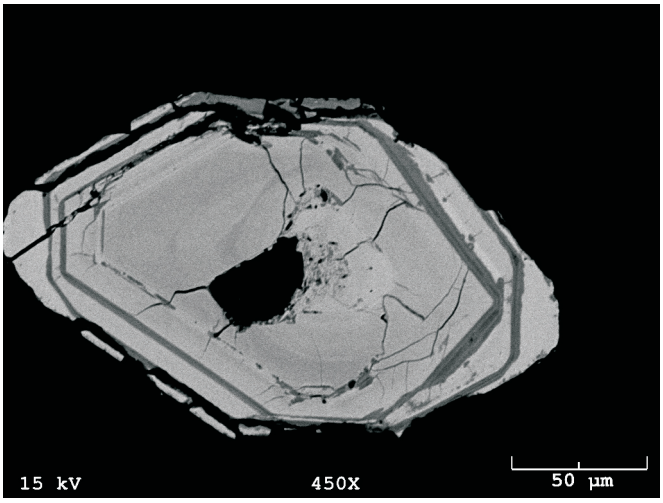

Figure 21: a) *Photomicrographs of picked zircon before and after annealing followed by HF leaching along with electron-microprobe backscatter images of unannealed zircon from the syn-shear granite (sample MD07-2679).*

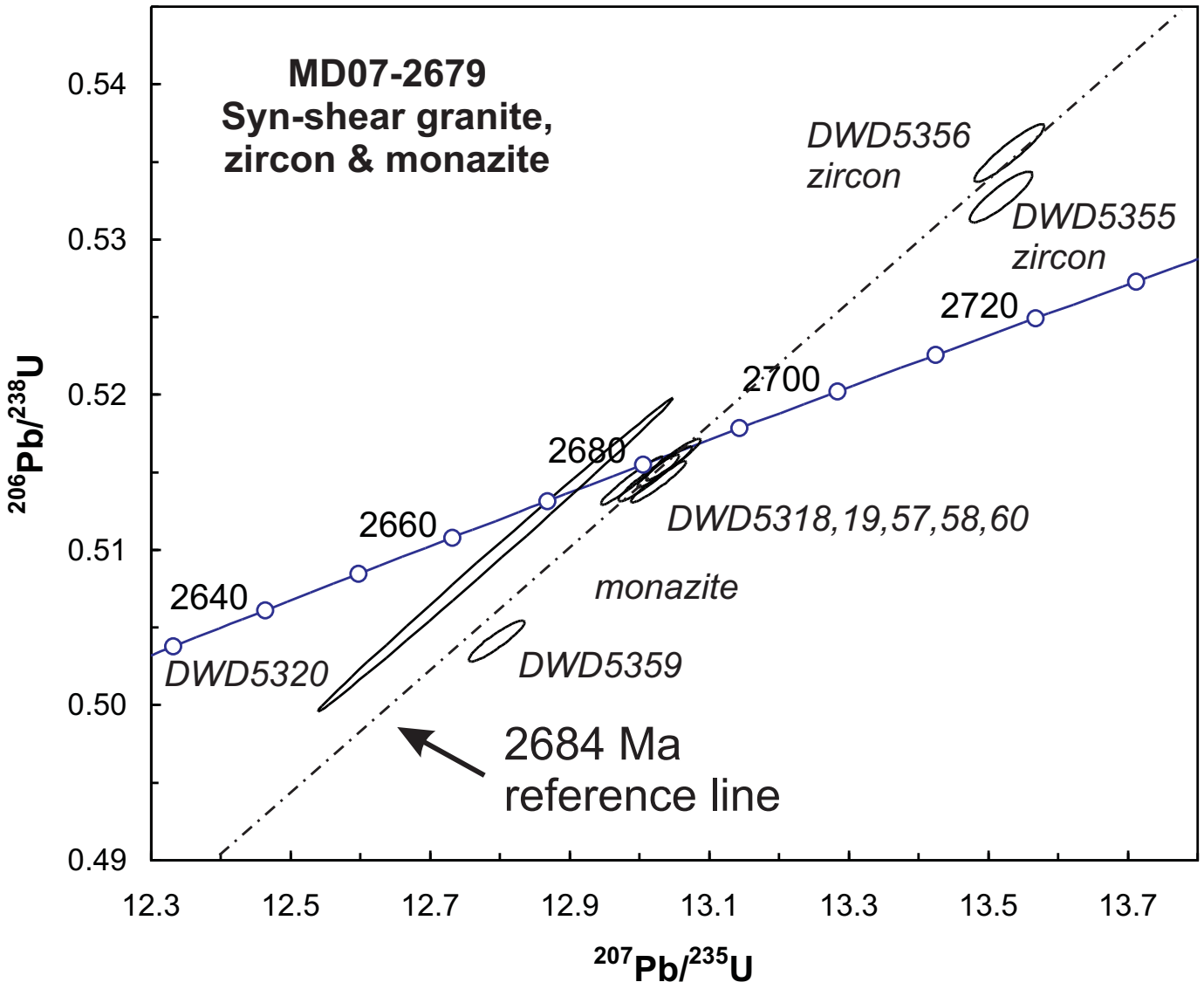

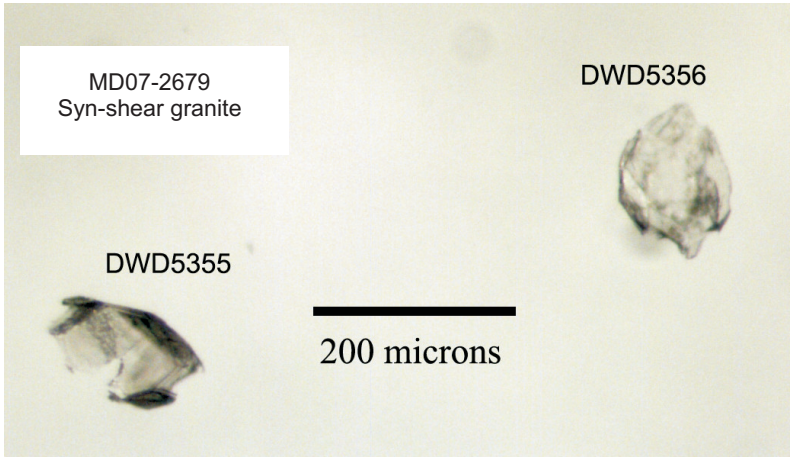

Zircon shells from leached-out zones

Figure 21: b) *U-Pb concordia diagram showing isotope dilution–thermal ionization mass spectrometry (ID-TIMS) age data on zircon and monazite from the syn-shear granite (sample MD07-2679). Photomicrograph in lower part of figure shows leached zircon shells that produced reversely discordant U-Pb data.*

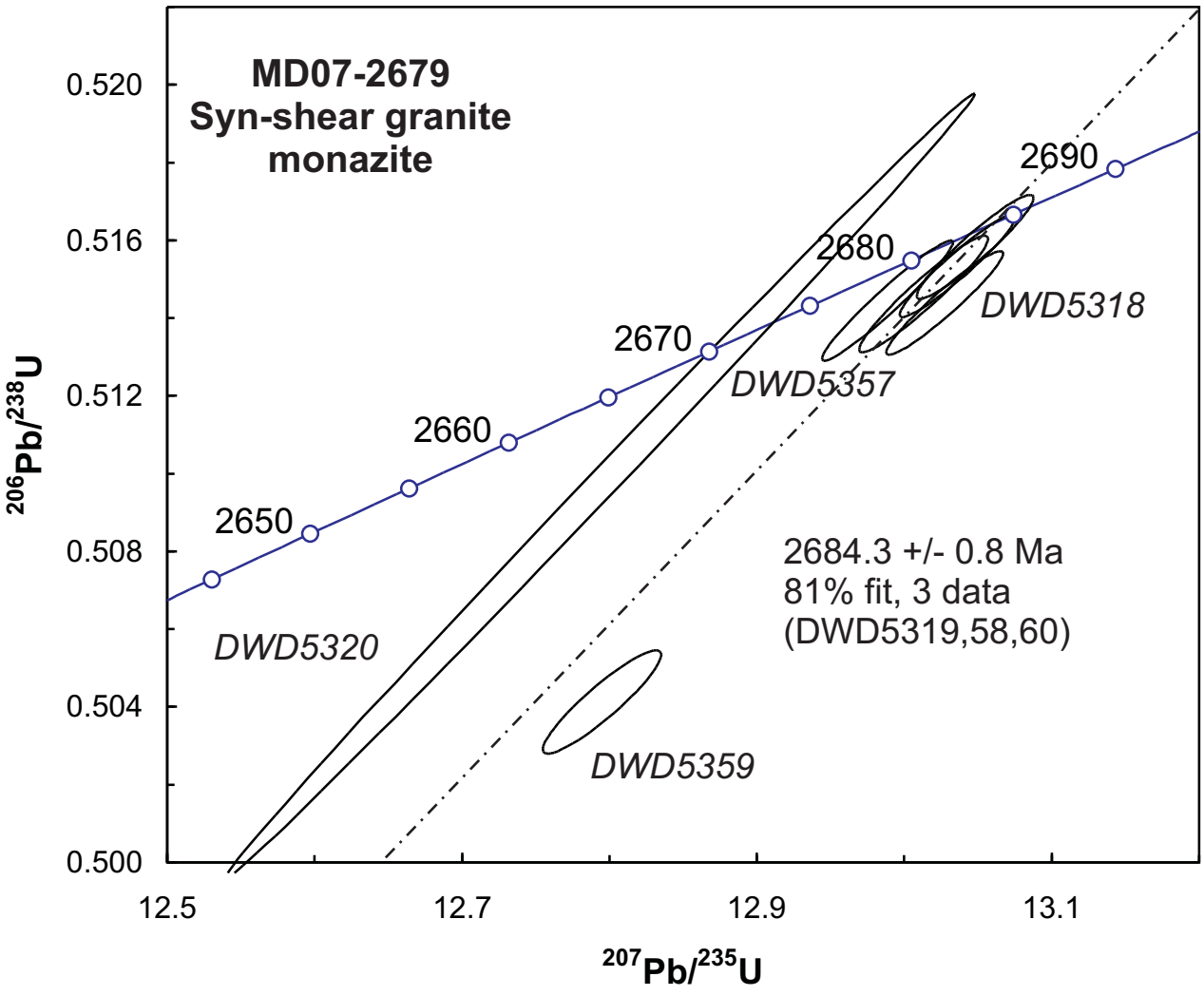

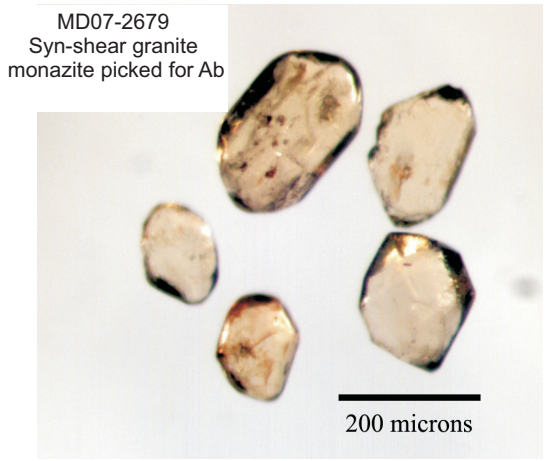

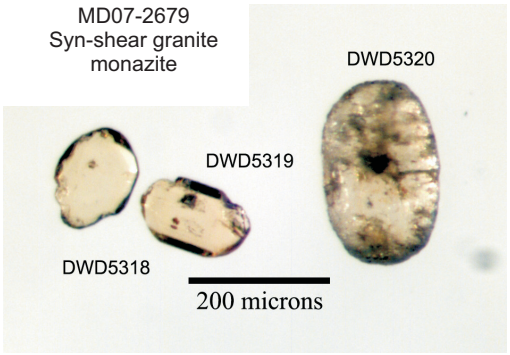

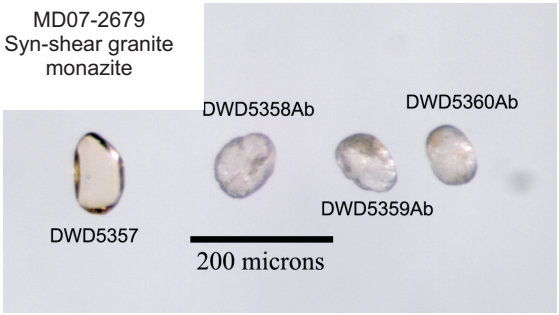

Figure 21: c) *U-Pb concordia diagram showing isotope dilution–thermal ionization mass spectrometry (ID-TIMS) age data on monazite from the syn-shear granite (sample MD07-2679). Photomicrographs in lower part of figure show monazite crystals selected for U-Pb isotopic analysis.*

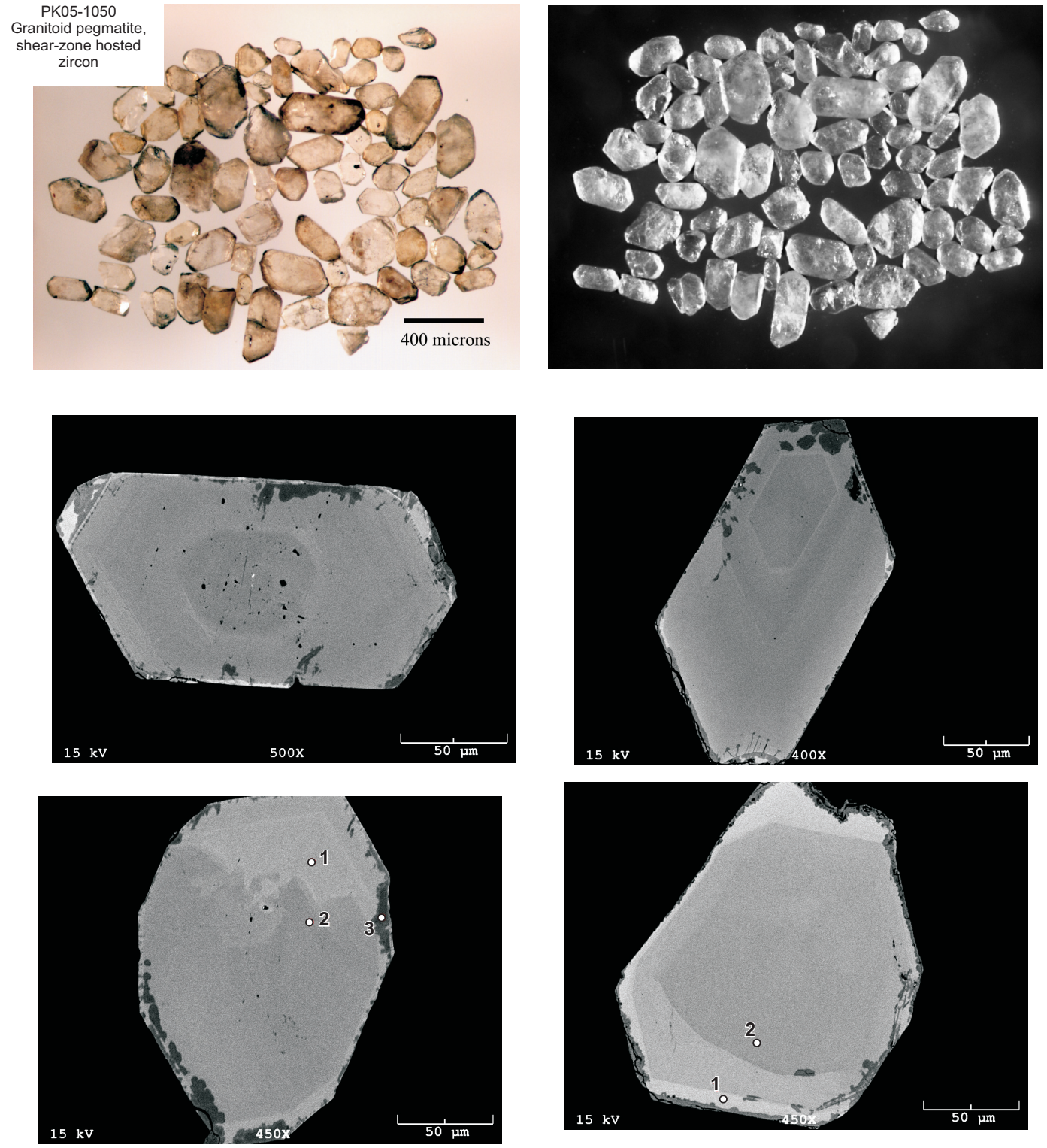

Figure 22: a) *Photomicrographs and electron-microprobe backscatter images of zircon from the shear-zone–hosted granitoid pegmatite (sample PK05-1050).*

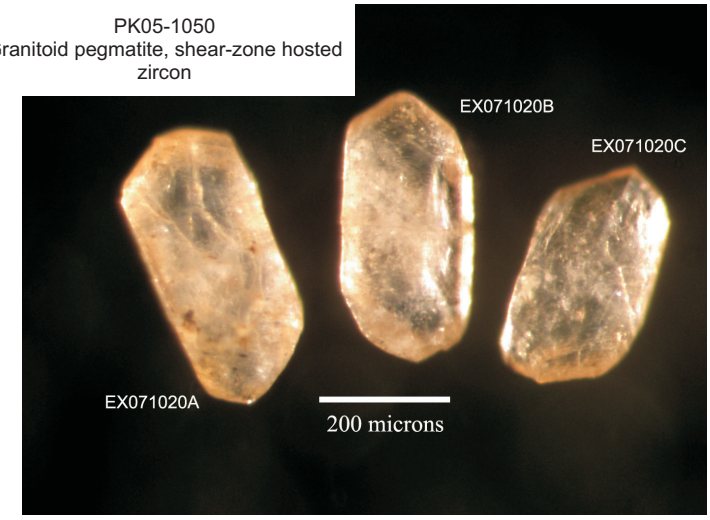

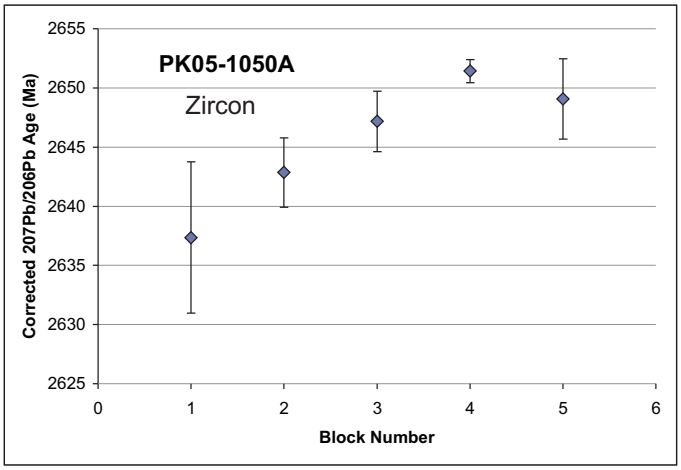

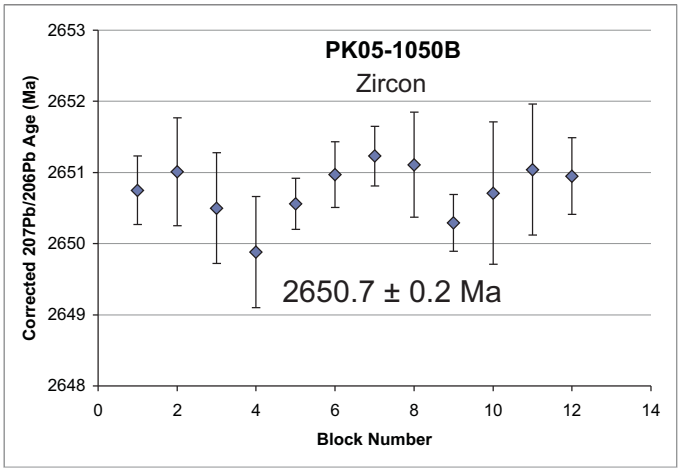

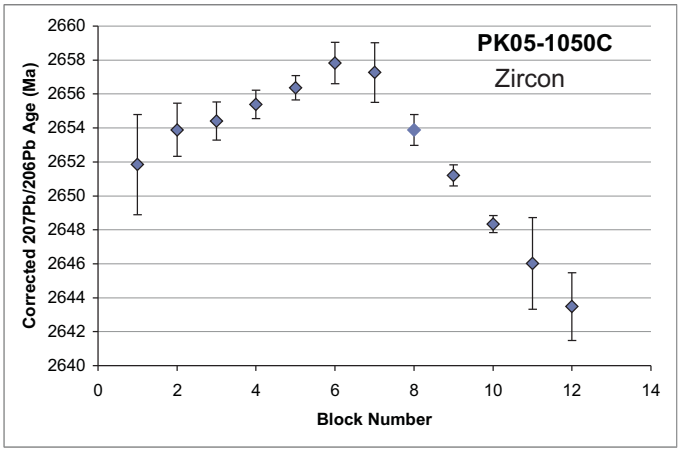

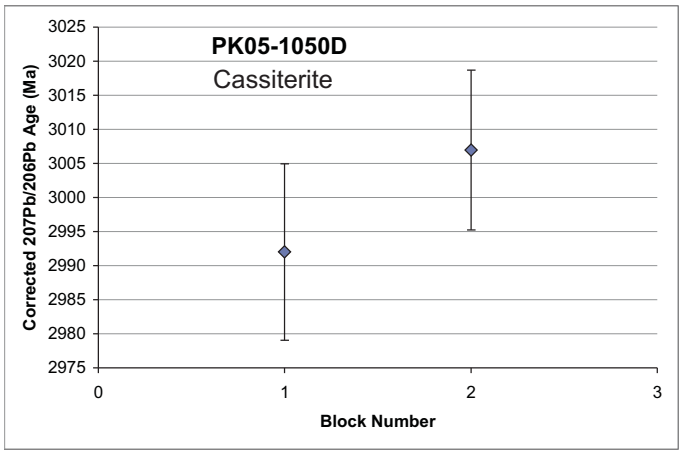

Figure 22: b) *Thermal extraction–thermal ionization mass spectrometry (TE-TIMS) age data on zircon and cassiterite from the shear-zone–hosted granitoid pegmatite (sample PK05-1050). Photomicrograph shows three zircon crystals selected for Pb/Pb dating.*

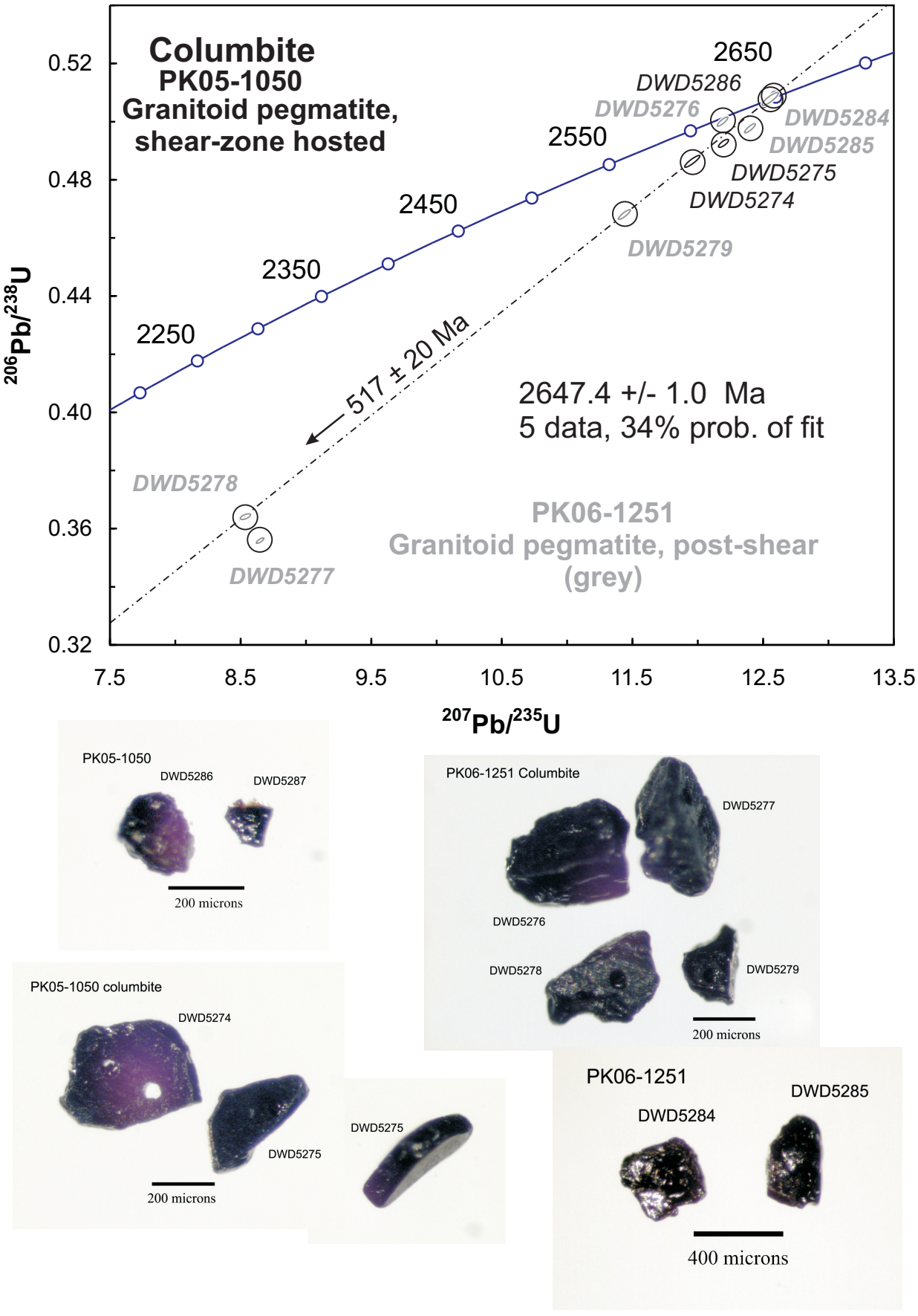

Figure 22: c) *U-Pb concordia diagram showing isotope dilution–thermal ionization mass spectrometry (ID-TIMS) age data on columbite from the shear-zone–hosted and post-shear granitoid pegmatites (samples PK05-1050 and PK06-1251, respectively). Photomicrographs in lower part of figure show columbite crystals selected for U-Pb isotopic analysis.*